A MECHANISTIC STUDY OF ATLANTIC MERIDIONAL OVERTURNING CIRCULATION CHANGES ON TROPICAL ATLANTIC CLIMATE

A Dissertation

by

CAIHONG WEN

Submitted to the Office of Graduate Studies of
Texas A&M University
in partial fulfillment of the requirements for the degree of

DOCTOR OF PHILOSOPHY

August 2009

Major Subject: Oceanography

A MECHANISTIC STUDY OF ATLANTIC MERIDIONAL OVERTURNING CIRCULATION CHANGES ON TROPICAL ATLANTIC CLIMATE

A Dissertation

by

CAIHONG WEN

Submitted to the Office of Graduate Studies of
Texas A&M University
in partial fulfillment of the requirements for the degree of

DOCTOR OF PHILOSOPHY

Approved by:

Chair of Committee,	Ping Chang
Committee Members,	Benjamin Giese
	R. Saravanan
	Achim Stössel
	Fuqing Zhang
Head of Department,	Piers Chapman

August 2009

Major Subject: Oceanography

ABSTRACT

A Mechanistic Study of Atlantic Meridional Overturning Circulation Changes on Tropical Atlantic Climate. (August 2009)
Caihong Wen, B.S., Nanjing University, China;
M.S., Nanjing University, China
Chair of Advisory Committee: Dr. Ping Chang

An eddy-permitting 2-1/2-layer Reduced Gravity Ocean (RGO) model is developed. Compared with the conventional 2-1/2-layer RGO models, the new model has improvements in subsurface thermodynamics, vertical mixing scheme and open boundary conditions. Using this new 2-1/2-layer RGO model as a dynamical tool, a systematic investigation of the role of oceanic processes in controlling tropical Atlantic sea-surface temperature (SST) response to Atlantic Meridional Overturning Circulation (AMOC) changes is carried out by varying the strength of northward mass transport at the open boundaries. It is found that the North Brazil Undercurrent (NBUC) reverses its direction in response to a shut-down of the AMOC. Such circulation change allows warm waters of the northern subtropical gyre enter the equatorial zone, giving rise to a prominent warming in the Gulf of Guinea and off the coast of Africa. Sensitivity experiments further show that the SST response behaves nonlinearly to AMOC changes. The rate of SST changes increases dramatically when the AMOC strength is below a threshold value. This nonlinear threshold behavior depends on the position of subsurface temperature gradient. The new RGO is coupled to an atmosphere general circulation model (AGCM) (CCM3.6). The coupled model is capable of capturing major features of tropical Atlantic variability. With the aid of this coupled model, a series of experiments with different combinations of oceanic and atmospheric processes are carried out to elucidate the relative importance of the oceanic processes and atmospheric processes in AMOC-induced tropical Atlantic variability/change. It is found that the

oceanic processes are a primary factor contributing to the warming at and south of the equator and the precipitation increase over the Gulf of Guinea, while atmospheric processes are responsible for the surface cooling of the tropical north Atlantic and southward displacement of ITCZ. The sensitivity of the coupled system to different strength of the AMOC is further investigated. It is found that equatorial SST and precipitation response also behaves nonlinearly to AMOC changes. The impact of AMOC changes on Tropical Instability Waves (TIWs) is assessed. It is found that the activity of TIWs is reduced in response to the AMOC-induced equatorial SST warming. Correlation analysis suggests that AMOC may affect TIW activities by modifying SST gradient north of the equator.

ACKNOWLEDGEMENTS

I would like to give my most grateful thanks to my advisor, Dr. Ping Chang, for his inspirational ideas and expert suggestions during the course of my Ph.D. program. He always kept his door open for discussing any interesting idea or problem in hand and made this period an enjoyable and valuable experience.

I would also like to thank Dr. R. Saravanan, Dr. Achim Stössel, Dr. Benjamin Giese and Dr. Fuqing Zhang for serving on my committee. Their suggestions and comments greatly improved the dissertation.

I would like to extend my deepest gratitude to my family and family-in-law for their unconditional support. Finally, I would specially like to thank my husband, Zhibo Zhang, for serving as my honest reading and writing assistant in preparing this manuscript.

TABLE OF CONTENTS

CHAPTER Page

CHAPTER Page

LIST OF FIGURES

FIGURE Page

FIGURE Page

FIGURE Page

FIGURE Page

FIGURE Page

LIST OF TABLES

CHAPTER I
INTRODUCTION

1.1 Motivation

Paleo proxy evidence is mounting that a substantially weakened Atlantic Meridional Overturning Circulation (AMOC) is concurrent with global-scale abrupt climate changes on centennial to millennial timescales during glacial and interglacial periods (e.g.,Broecker et al., 1985; Haug et al., 2001). A popular hypothesis explaining the AMOC change is that rapid freshening of the North Atlantic due to melting of continental ice sheets during deglaciation leads to a significant reduction in strength or even a collapse of the AMOC. Inspired by this hypothesis, the so-called water hosing experiments have been extensively conducted in the framework of coupled ocean-atmosphere general circulation models (GCMs) to investigate impact of AMOC changes on climate. In these experiments, a freshwater source is artificially added to high-latitude North Atlantic of climate models to mimic the melt water input. The modeling studies reveal a robust climate response to a weakened AMOC in the tropical Atlantic. The response is characterized by a dipole like SST pattern with cooler (warmer) temperature over the north (south) tropical Atlantic and a southward shift in the Intertropical Convergence Zone (ITCZ) accompanied with C-shape wind anomalies (Figure 1.1) (e.g. Stouffer et al. 2006; Timmermann et al. 2007). The response of the ITCZ suggests drier conditions over the Cariaco basin (Peterson et al. 2000) and wetter conditions over northeastern Brazil during Heinrich events (Wang et al 2004). The consistency between models and paleo observations implies the existence of a tight linkage between AMOC changes and Tropical Atlantic climate. It is important to understand this linkage, as it may help us to understand and predict potential abrupt climate change.

This dissertation follows the style of *Journal of Climate*.

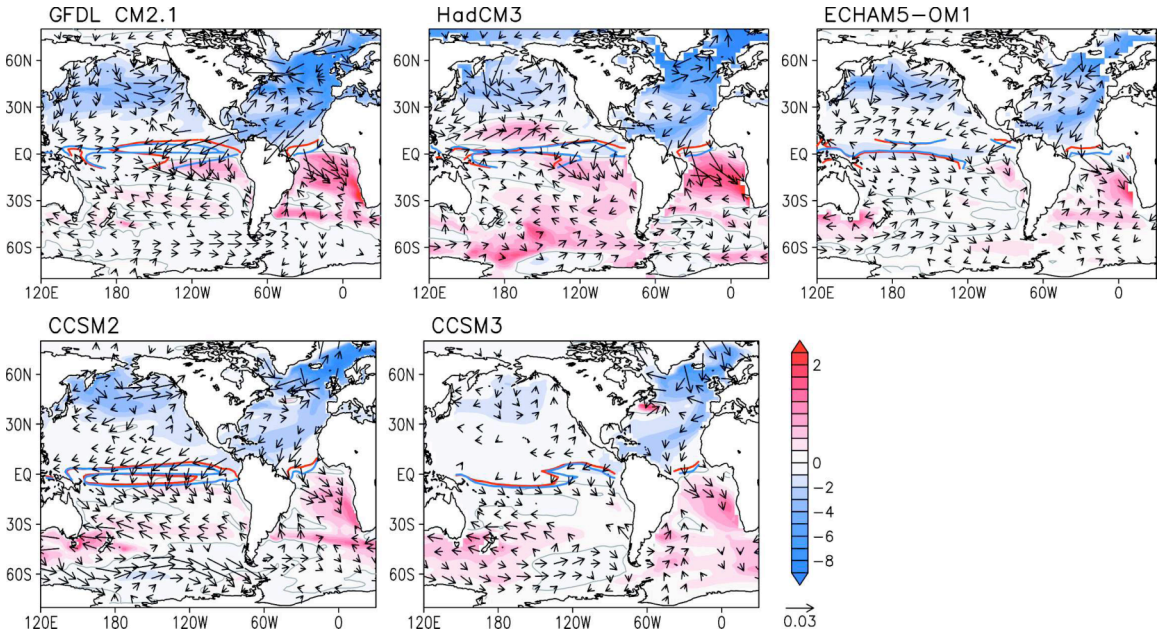

Figure 1.1 SST anomaly (K) and wind stress anomaly (Nm^2) generated by the shutdown of the AMOC for the (top left) GFDL CM2.1, (top middle) HadCM3, (top right) MPIO-M1, (bottom left) CCSM2, and (bottom right) CCSM3. The red and blue lines represent the annual mean zero lines of meridional wind stress in the control and water hosing experiments, respectively. Note the asymmetric temperature scale (From Timmermann et al., 2007).

Despite considerable progress that has been made over the past few decades, our understanding of mechanisms by which the AMOC affects tropical Atlantic remains incomplete. Current understanding can be largely divided into two categories. One focuses on the role of ocean dynamics, while the other focuses more on the importance of atmospheric processes. In the first category, many studies focus on how the AMOC modulates oceanic meridional heat transport. For example, Yang (1999) proposed that a change of AMOC can affect the interhemispheric SST gradient by modulating cross-equatorial heat transport through planetary wave adjustment (Kawase, 1987). Following

Yang's reasoning, Johnson and Marshall (2002) suggested an equatorial buffer mechanism. It is argued that southern hemispheric response to a sudden change in deep-water formation at northern high latitudes lags northern hemispheric response. This asynchronous response between the two hemispheres results in convergence or divergence of heat transport, producing SST changes in the equatorial region.

Recently, Chang et al. (2008) proposed an alternative oceanic teleconnection mechanism. They showed that a substantially weakened AMOC can induce a tropical SST response by modifying the pathway of subtropical cells (STCs). In a coupled GCM water-hosing experiment, they observed that the warming in south equatorial Atlantic develops in two stages: a weak warming within the first two decades followed by a more dramatic warming. The initial warming is caused by planetary wave adjustment, while the second warming has a different dynamic origin. It occurs when the AMOC is weakened below a threshold, causing the North Brazil Undercurrent (NBUC) to reverse its direction and carry warm northern subtropical gyre water to the south equatorial region. The NBUC region has been previously shown to be a region where interactions between return branch of the AMOC and wind-driven STCs are particularly strong (Fratantoni et al., 2000; Jochum and Malanotte-Rizzoli, 2001). Chang et al. (2008) argue that these interactions play an important role in equatorial Atlantic SST response to AMOC changes.

In the second category, Chiang and Bitz (2005) suggested that a cooling in high latitudes can be readily transmitted to the tropics through the wind-evaporation-SST (WES) feedback. It operates through intensifying northeasterly trade winds that leads to an increase in the latent heat loss and a cooling in the north tropical Atlantic, resulting in a southward shift of ITCZ. In a follow-up study, Chiang et al. (2008) showed that the WES feedback plays a more important role than the oceanic dynamical adjustment in the equatorward progression of SST anomalies induced by the weakening of AMOC.

1.2 Issues to be addressed

Although the above-mentioned mechanisms have shed some light on the underlying dynamics linking changes in high latitudes to changes in the tropical Atlantic, more detailed work is needed to improve our understanding of these mechanisms. In particular, it is important to understand whether the ocean plays an active or passive role in the connection between AMOC changes and tropical Atlantic climate. If the role of the ocean is active, it is then important to know how dynamics control SST response in the tropical Atlantic and where the oceanic control is prominent. Note that the oceanic mechanism involving meridional heat transport (Yang, 1999; Johnson and Marshall, 2002) may explain the redistributed heat content after the climate system reaches a new equilibrium state, but it may not explain exactly how oceanic dynamical processes operate to impact SST response during the transient state.

The hypothesis proposed by Chang et al. (2008) offers a plausible dynamical explanation. However, many details need to be examined and explored. Previous studies suggest that both the AMOC (Fratantoni et al., 2000) and potential vorticity barrier created by Ekman suction associated with north Atlantic ITCZ (Chepurin and Carton, 1996; Jochum and Malanotte-Rizzoli, 2001) are two dominant factors in determining the structure of the northern STC. In Chang et al's mechanism, the change in the pathway of the northern STC is mainly attributed to the AMOC change. As the wind stress over the tropical Atlantic is subject to significant change in response to a slowdown of AMOC (Figure 1.1), it is possible that wind stress anomalies also affect the pathway of the northern STC. Chang et al.'s analysis was based on a fully coupled GCM simulation where both the atmospheric processes and oceanic processes are included. It is thus difficult to isolate oceanic influence from air-sea interaction processes and identify areas that are most vulnerable to oceanic processes. Moreover, it is not clear how the mechanism could operate under different strengths of the AMOC as Chang et al.'s study was based on the results of a substantial weakened AMOC.

It needs to be emphasized that oceanic processes alone cannot fully explain the response of the tropical Atlantic. Chang et al. (2008) articulates the importance of the

oceanic role in leading surface warming on and south of the equator. The atmospheric teleconnection proposed by Chiang and Bitz (2005) offers an explanation of the cooling. This mechanism, however, cannot explain the strong subsurface warming observed in the water hosing experiment (e.g. Dahl et al., 2005; Chang et al., 2008). Here, we hypothesize that both oceanic and atmospheric processes contribute to the response in the tropical Atlantic. Validating this hypothesis will help us understand how these processes together modulate the response of tropical Atlantic to changes of the AMOC that may cause abrupt climate change.

The tropical Atlantic Ocean is a region where mesoscale oceanic variability is highly active. One prominent phenomenon is tropical instability waves (TIWs), appearing as westward-propagating wavelike oscillations of the temperature front between cold upwelling equatorial water and warmer water to the north (Duing et al., 1975; Legeckis et al., 1983). TIWs generally occur in June and decay in January of the following year. This life cycle is closely connected with the seasonal cycle of SST. Previous studies suggested that the effect of the AMOC on SST seasonal cycle is strongest during boreal summer and fall. To the best of our knowledge, the issue concerning how this change in the background state has an effect on TIW activity has not been explored.

1.3 Objectives and approaches

The primary goal of this study is to improve our understanding of the potential impact of the AMOC on tropical Atlantic variability (TAV). The main objective is to use a simplified ocean-atmosphere coupled model to study in detail the relevant oceanic and atmospheric teleconnection mechanisms. Particularly, we will focus on the oceanic teleconnection mechanism put forward by Chang et al. (2008). The following is a list of specific questions that will be addressed in this study:

(1) Can the change of the northern STC pathway due to AMOC changes produce an SST response as hypothesized by Chang et al. 2008? What are the key conditions

that must be satisfied in order that the oceanic teleconnection mechanism can have a significant impact on tropical Atlantic SST?

(2) What is the annual cycle of the SST response and associated rainfall of the tropical Atlantic to a shutdown of AMOC?

(3) What is the relative significance of atmospheric and oceanic processes in determining the behavior of the SST response to changes in the AMOC? Is there any threshold behavior of the tropical SST response to AMOC changes as proposed by Chang et al.(2008)?

(4) What is the impact of large-scale climate change in the tropical Atlantic on oceanic mesoscale activities? In particular, how may large-scale SST change affect TIW activities?

The above questions will be addressed within a framework of a newly developed regional coupled model. This regional coupled model consists of an atmospheric global circulation model and a reduced gravity ocean model. Merits of this model are its relative simple ocean dynamics, computational efficiency and the flexibility to be run as an ocean-alone or a fully coupled model. The simple yet effective dynamic ocean model makes it easy to identify the essential dynamics of interest. An open boundary condition is implemented in the ocean model so that the strength of AMOC can be modulated by the prescribed mass transport at the northern and southern boundaries of the model domain. The ocean model alone allows us to explore whether and to what extent the oceanic processes are responsible for the SST response pattern as suggested in coupled GCMs. When fully coupled, the model can be used to study the relative importance of the atmospheric processes versus the oceanic processes in AMOC-induced tropical Atlantic variability.

1.4 Organization of the chapters

Chapter II introduces the newly developed 2-1/2-layer reduced gravity ocean model. Chapter III is devoted to a study of the oceanic mechanisms that link AMOC changes to tropical Atlantic SST changes. Using the 2-1/2-layer RGO, the sensitivity of

SST response to changes in the AMOC is examined and the oceanic processes contributing SST response is also investigated. The dependence of SST response on oceanic parameters important to the oceanic mechanism is further explored in Chapter III. The primary objective of Chapter IV is to elucidate the relative importance of the atmospheric processes versus the oceanic processes in AMOC-induced TAV change. Chapter IV starts with an introduction of the coupled model and a description of numerical experiment design. Then, the influence of AMOC changes on TAV and relative contribution of atmospheric and oceanic processes are discussed. The sensitivity of tropical Atlantic response to changes in the AMOC is presented at the end of Chapter IV. In Chapter V, the impact of AMOC changes on oceanic mesoscale activities is explored using various statistical methods. Chapter VI summarizes the major findings and outlines future work.

CHAPTER II
A 2-1/2-LAYER REDUCED GRAVITY OCEAN MODEL

2.1 Introduction

Most of previous studies of the AMOC utilize sophisticated ocean global circulation models (OGCMs) to investigate its impact on global climate. However, it can be challenging to explore mechanistic details using a highly complex and computationally expensive GCM integrations. One goal of this study is to develop an ocean model that is dynamically simple yet capable of simulating the salient circulation features of the upper tropical Atlantic Ocean. In particular, the model needs to be dynamically rich enough to encompass the oceanic pathway mechanism proposed by Chang et al. (2008).

The simplest dynamic ocean model including all the dynamic processes mentioned above is perhaps a 2-1/2-layer reduced gravity ocean model(RGO). The ability of such a model to represent the upper-ocean dynamics has been demonstrated by many studies (e.g. Schopf and Cane, 1983; McCreary and Yu, 1992). Lee and Csanady (1999) show that a 2-1/2-layer reduced gravity model is capable of capturing major features of the upper tropical Atlantic circulation and seasonal variation of SST. Unfortunately, subduction processes and the oceanic pathway mechanism by which the AMOC can exert its influence on the tropical Atlantic are ignored in their model.

To enhance the model's capability, three major modifications were made based on the numerical code developed by Lee and Csanady (1999): (1) A new open boundary condition (OBC) developed by Marchesiello et al. (Marchesiello et al., 2001) is implemented. The OBC not only allows the perturbations generated by the model to propagate out of the domain, but also is capable of incorporating external forcing (i.e. AMOC) into the model. (2) A new vertical mixing scheme is adopted. Both entrainment and detrainment processes are included. The former is estimated using a modified version of KT (Krauss and Turner, 1967) model. The latter is parameterized following

McCreary et al. (1993). (3) A prognostic subsurface temperature equation is incorporated to allow the model to simulate subsurface temperature changes.

This chapter is organized as follows. The governing equations are described in Section 2.2. A special heat flux correction term added in the thermocline layer temperature equation is introduced in Section 2.3. Section 2.4 describes the vertical mixing scheme. The open boundary condition is introduced in Section 2.5. The model configuration and numerical method are summarized in Section 2.6.

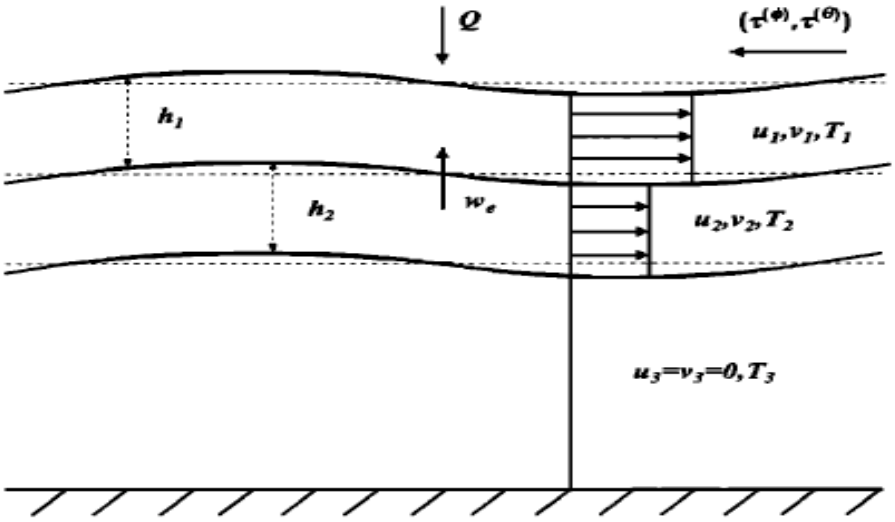

Figure 2.1 Schematic vertical structure of the 2-1/2-layer ocean model.

2.2 Governing equations

The 2-1/2-layer model consists of two active layers, the mixed layer and the thermocline layer as illustrated in Figure 2.1. The infinitely deep water below the thermocline layer is assumed to be motionless. The governing equations for the mixed layer are as follows (the symbols used begins explained on page 16):

$$\frac{\partial u_1}{\partial t}+\frac{1}{a\cos\theta}\frac{\partial u_1^2}{\partial \phi}+\frac{1}{a\cos\theta}\frac{\partial}{\partial\theta}(u_1v_1\cos\theta)-\frac{u_1v_1}{a}\tan\theta-2\Omega\sin\theta v_1= \\ -\frac{1}{a\cos\theta}\frac{\partial P_1}{\partial\phi}+\frac{\tau^{\phi}}{\rho_1 h_1}+\frac{\omega H(\omega)}{h_1}(u_2-u_1)+F_1^{\phi} \quad , \tag{1}$$

$$\frac{\partial v_1}{\partial t}+\frac{1}{a\cos\theta}\frac{\partial}{\partial\phi}(u_1v_1)+\frac{1}{a\cos\theta}\frac{\partial}{\partial\theta}(v_1^2\cos\theta)+\frac{u_1^2}{a}\tan\theta+2\Omega\sin\theta u_1 \\ =-\frac{1}{a}\frac{\partial P_1}{\partial\theta}+\frac{\tau^{\theta}}{\rho_1 h_1}+\frac{\omega H(\omega)}{h_1}(v_2-v_1)+F_1^{\theta} \quad , \tag{2}$$

$$\frac{\partial h_1}{\partial t}+\frac{1}{a\cos\theta}\left[\frac{\partial}{\partial\phi}(u_1h_1)+\frac{\partial}{\partial\theta}(v_1h_1\cos\theta)\right]=\omega\,, \tag{3}$$

$$\frac{\partial T_1}{\partial t}+\frac{u_1}{a\cos\theta}\frac{\partial T_1}{\partial\phi}+\frac{v_1}{a}\frac{\partial T_1}{\partial\theta}=\frac{Q_0-Q_{-h_1}}{\rho_1 C_p h_1}-\frac{\omega H(\omega)}{h_1}(T_1-T_2)+K_t\nabla^2T_1+K_z\frac{\partial^2T_1}{\partial z^2}\,, \tag{4}$$

and for the thermocline layer:

$$\frac{\partial u_2}{\partial t}+\frac{1}{a\cos\theta}\frac{\partial u_2^2}{\partial\phi}+\frac{1}{a\cos\theta}\frac{\partial}{\partial\theta}(u_2v_2\cos\theta)-\frac{u_2v_2}{a}\tan\theta-2\Omega\sin\theta v_2 \\ =-\frac{1}{a\cos\theta}\frac{\partial P_2}{\partial\phi}+\frac{\omega H(-\omega)}{h_2}(u_2-u_1)+F_2^{\phi} \quad , \tag{5}$$

$$\frac{\partial v_2}{\partial t}+\frac{1}{a\cos\theta}\frac{\partial}{\partial\phi}(u_2v_2)+\frac{1}{a\cos\theta}\frac{\partial}{\partial\theta}(v_2^2\cos\theta)+\frac{u_2^2}{a}\tan\theta+2\Omega\sin\theta u_2 \\ =-\frac{1}{a}\frac{\partial P_2}{\partial\theta}+\frac{\omega H(-\omega)}{h_2}(v_2-v_1)+F_2^{\theta} \quad , \tag{6}$$

$$\frac{\partial h_2}{\partial t}+\frac{1}{a\cos\theta}\left[\frac{\partial}{\partial\phi}(u_2h_2)+\frac{\partial}{\partial\theta}(v_2h_2\cos\theta)\right]=-\omega\,, \tag{7}$$

$$\frac{\partial T_2}{\partial t}+\frac{u_2}{a\cos\theta}\frac{\partial T_2}{\partial\phi}+\frac{v_2}{a}\frac{\partial T_2}{\partial\theta}=\frac{Q_{-h_1}}{\rho_2 C_p h_2}+Q_{cre}-\frac{\omega H(-\omega)}{h_2}(T_1-T_2)+K_t\nabla^2T_2+K_z\frac{\partial^2T_2}{\partial z^2}$$

Based on the hydrostatic assumption, the pressure gradient terms are given by

$$\langle\nabla P_1\rangle=ga\nabla\left[h_1(T_1-T_3)+h_2(T_2-T_3)\right]-\tfrac{1}{2}gah_1\nabla T\,, \tag{8}$$

$$\langle \nabla P_2 \rangle = ga\nabla\left[(h_1 + h_{2)}(T_2 - T_{3})\right] - ga(h_1 + {}^{h_2}\!/_2)\nabla T_2\,, \tag{9}$$

The horizontal momentum friction terms for the i[th] layer are (Wajsowicz, R. C., 1993):

$$F_i^{\phi} = \frac{1}{a\cos\theta}\frac{\partial(A_i D_{Ti})}{\partial\phi} + \frac{1}{a\cos^2\theta}\frac{\partial(A_i\cos^2\theta D_{S_i})}{\partial\theta}, \tag{10}$$

$$F_i^{\theta} = \frac{1}{a\cos\theta}\frac{\partial(A_i D_{S_i})}{\partial\phi} - \frac{1}{a\cos^2\theta}\frac{\partial(A_i\cos^2\theta D_{T_i})}{\partial\theta}, \tag{11}$$

where horizontal tension is given by:

$$D_{Ti} = \frac{1}{a\cos\theta}\left(\frac{\partial u_i}{\partial\phi} - \frac{\partial(v_i\cos\theta)}{\partial\theta} - v_i\sin\theta\right), \tag{12}$$

and horizontal shearing strain $D_{Si} = \frac{1}{a\cos\theta}\left(\frac{\partial v_i}{\partial\phi} + \frac{\partial(u_i\cos\theta)}{\partial\theta} + u_i\sin\phi\right)$, (13)

The viscosity A_i is determined as (Smagorinsky, J., 1963: Smagorinsky, J., 1993) :

$$A_i = C\Delta x\Delta y\sqrt{(D_{T_i}^2 + D_{S_i}^2)}\,, \tag{14}$$

where C is the Smagorinsky dimensional scaling coefficient and is empirically determined based on details of the model. The advantages of the Smagorinsky scheme are that A_i is enhanced (reduced) in the regions of large (small) horizontal velocity shear, and A_i decreases with finer model resolution. Compared with constant viscosity used in many numerical models, this non-constant viscosity approach is essential to make our model capable of simulating multiple spatial-temporal varying flows. In our model, it is required to set the constant viscosity higher than $1500\,m^2/s$ in order to maintain the vigorous Yucatan current. However, this value is too large to allow energetic eddies, such as tropical instability waves and North Brazil rings, in the model.

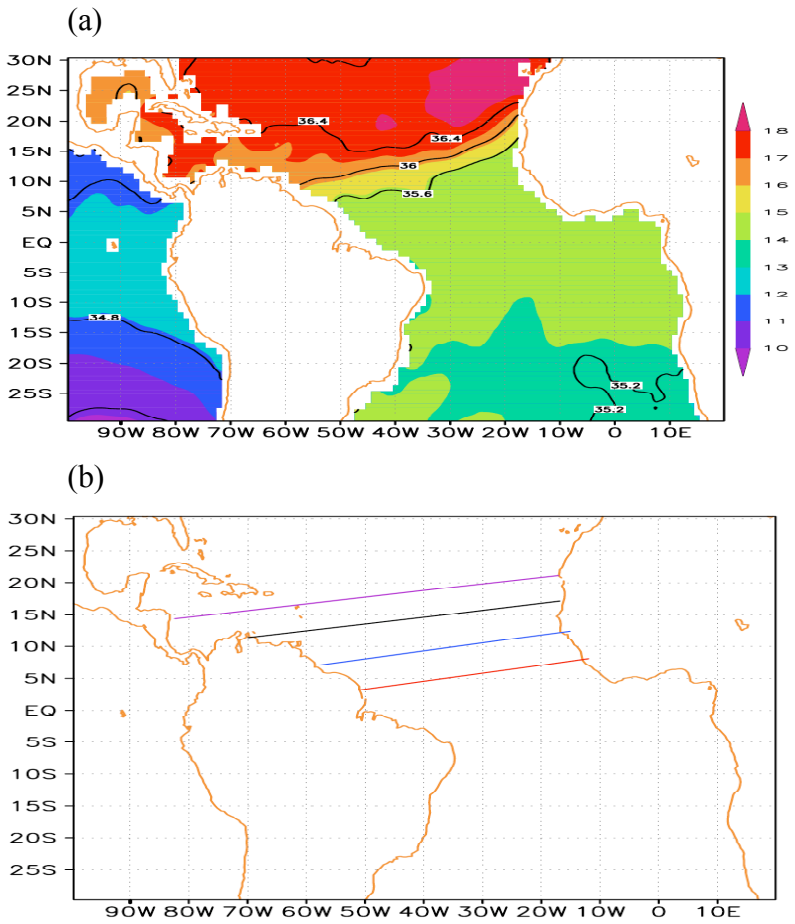

Figure 2.2 (a) Temperature (color) and salinity (contour) changes on 1026.45 kg m^{-3} density surface derived from the Levitus dataset (Levitus, 1994). (b) Idealized temperature front used in the thermocline of the model with temperature variation from 14°C in the southern edge to 21°C in the northern edge of the front. The purple, black, blue and red lines show the location of front in Experiment L15NG7C, L10NG7C, L7NG7C and L3NG7C, respectively. Black line also presents the front position of the CTRL run.

2.3 Heat flux correction in the thermocline layer

One special treatment of our model is the temperature in the thermocline layer, as the mechanism proposed by Chang et al. (2008) is sensitive to the subsurface temperature distribution. In the observations, there is a salient front forming along the boundary between the north Atlantic subtropical gyre and the tropical gyre in the

subsurface, separating the saltier and warmer subtropical gyre water from the fresher and colder tropical gyre water. As can be seen from Figure 2.2a, the temperature along the 1026.45 kg m^{-3} density surface increases from 14ºC south of 6ºN to 17ºC north of 10ºN across the front. The formation of the front is likely attributed to the subduction process that injects the saltier and warmer surface water in the northeastern subtropical Atlantic into the ocean interior along isopycnal surfaces. The subducted water flows southwestward to the western boundary, where it bifurcates into a westward branch and an equatorward branch (the return branch of the northern STC). The latter is counteracted by the northward flowing NBUC as a part of AMOC return flow. Since the NBUC is stronger than the STC return flow under the current climate condition, the equatorward pathway is blocked (Fratantoni et al., 2000; Zhang et al., 2003), keeping the warmer and saltier water to the north of the front. This is a key aspect of the mechanism proposed by Chang et al. (2008) and must be treated carefully in the model in order to test this mechanism.

Given that the model used in this study has only two active layers and salinity changes in each layer are not explicitly computed, subduction processes cannot be fully accounted for by the simplified physics. We, therefore, adopt a simple approach to maintain an idealized temperature front around 10°N in the thermocline layer of the model. Across the idealized temperature front, the temperature increases from 14°C near the equator to 21°C north of 15°N (Figure 2.2b). The temperature front is maintained by adding a specified heat source term to the thermocline layer temperature equation, i.e.,

$$Q_2 = Q_{-h1} + Q_{cre},$$

where Q_{-h1} is the downward flux at the mixed layer base and Q_{cre} is the source term which is determined by first restoring the model thermocline temperature to the temperature front during a spin-up run and then taking an average over the last 10 years of the spin-up run. This correction term is computed prior to the start of the model experiments described below and does not depend on the model solutions once

determined. This approach is essentially similar to the anomaly flux correction method, widely used in climate modeling studies (e.g. Seager et al., 2001).

2.4 Vertical mixing scheme

The total exchange rate (ω) of water mass across the base of the upper layer can be represented as sum of entrainment rate and detrainment rate (McCreary et al., 1993):

$$\omega = \omega_k H(\omega_k) + \omega_d . \tag{15}$$

The entrainment rate (ω_k) is estimated using a modified version of KT (Krauss and Turner, 1967) model, which is based on the turbulent kinetic energy budget. The net production of turbulent kinetic energy (P) in the mixed layer is parameterized as:

$$P = m_s u_*^3 - \varepsilon h_1 - 0.25 h_1 \left[(1-n)\left|B(h_1)\right| + (1+n)B(h_1) + 2m_f \left|\Omega \sin(\phi)\right| u_*^2 \right], \tag{16}$$

where u_* is the friction velocity($u_* = (\tau/\rho_1)^{1/2}$); ε is a coefficient associated with background dissipation and taken to be $5\times10^{-9} m^2 s^{-3}$; n is the turbulent mixing coefficient due to convection, and m_f is introduced to get the correct neutral (zero surface heat flux) equilibrium mixed layer depth (Wallcraft et al., 2003). m_s is the wind-stirring coefficient and is function of latitude with strong mixing near the equator (Chang, 1994):

$$m_s = m_{so}(1 + e^{-y^2/L_m^2} h_m / h_1), \tag{17}$$

where h_m is the depth of the mixed layer at rest and L_m is taken to be 300 km.

Following Chang (1994), the buoyancy flux $B(h_1)$ is given by

$$B(h_1) = \frac{\alpha g}{\rho_1 C_p} \left\{ Q_o + Q_{sol} \left| R_p e^{(-\gamma_1 h_1)} + (1-R_p) e^{(-\gamma_2 h_2)} - \frac{2}{h_1} \left(\frac{R_p (1 - e^{(-\gamma_1 h_1)})}{\gamma_1} + \frac{(1-R_p)(1-e^{(-\gamma_2 h_1)})}{\gamma_2} \right) \right| \right\} \tag{18}$$

where Q_{sol} is the downward solar radiation flux at the ocean surface, R_p , γ_1 and $\gamma_2$denote the solar radiation penetration coefficient and the attenuation coefficient of the penetrated solar radiation.

When the effect of wind stirring exceeds that of the thermal forcing and background dissipation (P>0), the entrainment rate of water mass into the mixed layer is given by:

$$\omega_k = \frac{P}{\frac{1}{2}\alpha g h_1 (T_1 - T_2)}. \tag{19}$$

In KT-type bulk models, detrainment is often treated in a simple way: when the stabilizing effect of a negative buoyancy flux outweighs that of the wind mixing (P<0), the mixed layer shallows until it reaches the equilibrium depth (e.g., Krauss and Turner, 1967; Schopf and Cane, 1983). The mixed layer at the equilibrium state is determined by setting P equal to zero. This approach may be suitable to estimate one-dimension mixed layer thickness as proposed by Kraus and Turner. However, it is not appropriate to determine two-dimension mixed layer thickness field, because mixed layer thickness is not only influenced by local processes but also by large scale factors, such as divergence of the mean flow and distribution of surface heat fluxes. Accordingly, the detrainment rate is parameterized as (McCreary et al., 1993):

$$\omega_d = -\frac{Q_o H(Q_o)}{Q_r} \frac{(h_1 - h_r)^2}{t_d h_1} H(h_1 - h_r), \tag{20}$$

where h_r is equilibrium depth, which is set as observed annual mean mixed layer depth computed from the National Oceanographic Data Center (NODC) and from the World Ocean Circulation Experiment (WOCE) database (http://www.locean-ipsl.upmc.fr/~cdblod/mld.html). t_d is an arbitrary detrainment time scale and Q_r is a scaling parameter with the same order of the mean net heat flux at tropical Atlantic Ocean. Detrainment occurs whenever ocean absorbs heat from the air and mixed layer is thicker than the specified equilibrium depth h_r. Note that entrainment rate ω_k contributes to the total exchange rate ω only when ω_k is positive, otherwise the mixed layer retreats to the equilibrium depth h_r.

Variables used in the above equations are defined as follows:

u_i, v_i	zonal and meridional components of velocity for layer i
h_i	thickness of layer i
T_i	temperature of layer i
a, ϕ, θ	radius, longitude and latitude of the Earth
Ω	angular velocity of rotation of the Earth
ρ_i	density of layer I
g	acceleration of gravity
α	thermal expansion coefficient
C_p	specific heat of water
K_t	horizontal heat diffusion coefficient
K_z	vertical heat diffusion coefficient
$\tau^{\phi}, \tau^{\theta}$	zonal and meridional components of surface wind stress
Q_o	downward net heat flux at the surface
Q_{-h_1}	downward heat flux at the base of the mixed layer
Q_{cre}	heat flux correction term for the thermocline layer
H(x)	Heaviside step function(H(x)= 1 if x>=0, H(x)= 0 if x<0)

2.5 Open boundary condition (OBC) algorithm

One of the problems often encountered by regional ocean models is the treatment of open boundaries. The ideal OBC is that the open boundaries are transparent to motion and model solutions are consistent with external large-scale climatology. Generally, the OBCs that have been used in layered models can be categorized into two groups: the local type and the global type. The local approach determines OBC by the local solution from the model governing equations. The global approach provides OBC by restoring prognostic variables to a prescribed state within specified regions. Both of these two approaches have advantages and disadvantages. The local approach is consistent with model physics, while it is can lead to system drift to an unrealistic state without external information. On the contrary, the global approach tends to overspecify the solution at the

boundaries. In this study, we utilize an open boundary condition (OBC) developed by Marchesiello et al. (Marchesiello et al., 2001) which combines the advantages of the two approaches.

The radiation equation for a prognostic model variable ϕ is given by

$$\frac{\partial \phi}{\partial t} + c_x \frac{\partial \phi}{\partial x} + c_y \frac{\partial \phi}{\partial y} = -\frac{1}{\gamma}(\phi - \phi^{ext}), \tag{21}$$

with

$$\gamma = \gamma_{out} \qquad \text{if } c_x > 0,$$

$$\gamma = \gamma_{in} \qquad \text{if } c_x < 0,$$

where ϕ^{ext} denotes the external information and γ is the time scale for nudging. The phase speeds (c_x, c_y) are projections of the oblique radiation and are calculated as follows:

$$c_x = -\frac{\partial \phi}{\partial t} \frac{\frac{\partial \phi}{\partial x}}{(\partial \phi^2 / \partial^2 x) + (\partial \phi^2 / \partial^2 y)}, \tag{22}$$

and

$$c_y = -\frac{\partial \phi}{\partial t} \frac{\frac{\partial \phi}{\partial y}}{(\partial \phi^2 / \partial^2 x) + (\partial \phi^2 / \partial^2 y)}. \tag{23}$$

The main idea of these OBCs is that when the radiation phase moves outward of the region (C_y>0), the boundary solution is determined by the interior solution. When the phase propagation is inward (C_y<0), the boundary is determined by external information. Thus, this technique not only allows perturbation generated in the interior model propagate out of the domain, but also make the model solution consistent with large-scale information.

In order to maintain the total mass of the model during the integration, a volume constraint is applied. The basic idea of the constraint is that the total volume transport

across the open boundary is adjusted to balance external source/sink of the sea water (M) by uniformly subtracting/adding a velocity correction (V_c). The V_c is defined as

$$V_c = \frac{1}{S_b}\left(\int_{L_b} (h_1 v_1 + h_2 v_2)\, dL - M\right), \tag{24}$$

where S_b and L_b are the total intersection surface and total perimeter of the open boundary respectively.

This volume constraint approach, which is applied at each time step, only involves in small correction and does not modify the flow pattern at the open boundaries since velocity at each grid point is subtracted by the same value. The merits of such constraint are not only to guarantee mass conservation of the system in long-term integration, but also to incorporate external effect into the model by the specified volume transport (M). The latter is useful since we can investigate the impact of various strength of the AMOC on the upper tropical Atlantic by simply tuning adjusting prescribed volume transport M.

2.6 Model configuration and numerical method

The model covers the tropical Atlantic basin from 100ºW to 20ºE in longitude and from 30ºS to 30ºN in latitude with realistic coastal lines. The northern and southern boundaries are open. No-flux conditions are applied for temperature and layer thicknesses at all boundaries. For flow velocities, no-slip boundary conditions are employed only at wall boundaries. SST at the open boundaries is relaxed to a climatological annual cycle within a sponge layer with a damping timescale of 5 days.

The numerical equations were discretized using a 2^{nd} order entropy-conserving finite difference scheme on Arakawa C-grid in space and a leapfrog scheme in time. The model resolution is 0.25° in both longitude and latitude. In order to remove the computational mode produced by the leapfrog scheme, an averaging scheme proposed by Shuma (1957) is applied twice consecutively every 48-time step.

CHAPTER III

EFFECT OF ATLANTIC MERIDIONAL OVERTURNING CIRCULATION CHANGE ON TROPICAL ATLANTIC SEA SURFACE TEMPERATURE VARIABILITY – A 2-1/2-LAYER REDUCED GRAVITY OCEAN MODEL STUDY

3.1 Introduction

Recent coupled model studies suggest that substantial changes in the strength of the AMOC have far-reaching impact on tropical Atlantic climate. Vellinga and Wood (Vellinga and Wood, 2002) showed that a weakened AMOC results in a dipole-like SST response over the Atlantic, with cooling in the North Atlantic and warming in the South Atlantic. Similar results were obtained by Zhang and Delworth (2005). Through an intercomparison of a set of climate models ranging from intermediate complexity coupled models to sophisticated GCMs, Stouffer et al., (2006) show that the dipole-like SST pattern is a rather robust tropical Atlantic response to a weakening in the AMOC. The numerical model results are consistent with paleo proxy records. Reconstructed paleo-SST records suggest the occurrence of similar dipole-like SST response to a substantially weakened AMOC during the Younger Dryas event (Boyle, 2000; Hughen et al., 2004; McManus et al., 2004) and Heinrich events (Wang et al., 2004). A question that begs an answer is: why is there such a strong linkage between the tropical Atlantic and the AMOC change?

Attention has been drawn to oceanic pathways in search of teleconnection mechanisms, because the upper tropical Atlantic Ocean is located right above the return flow of the AMOC. This unique connection makes the tropical Atlantic ocean circulation one of most complex circulation systems in the world. The upper circulation of the tropical Atlantic Ocean is connected to extratropical circulations via STCs. Oceanic pathways carry water subducted in the subtropics during winter into the equatorial

thermocline and then to the surface via equatorial upwelling. Unlike its counterpart in the Pacific Ocean, the Atlantic STCs are highly asymmetric about the equator with most of the equatorial thermocline water supplied from the southern hemisphere STC. This unique feature makes the Atlantic the only ocean where net heat transport is everywhere northward (e.g., Trenberth and Caron, 2001; Ganachaud and Wunsch, 2003).

Many previous studies focus on how the AMOC changes modulate oceanic meridional heat transport. For example, Yang (1999) proposed that a change of AMOC can affect the interhemispheric SST gradient by modulating cross-equatorial heat transport through planetary wave adjustment (Kawase, 1987). On the other hand, Chang et al. (2008) articulate the importance of interactions between the AMOC and the wind-driven STCs. In a coupled GCM water-hosing experiment, they found a substantial warming occurs when the AMOC is weakened below a threshold. The weakened AMOC causes the North Brazil Undercurrent (NBUC) to reverse direction and carry warm northern subtropical gyre water to the equatorial region. The NBUC region has been shown to be a region where interactions between return branch of the AMOC and the wind-driven STCs are particularly strong (Fratantoni et al., 2000; Jochum and Malanotte-Rizzoli, 2001). Chang et al. (2008) thus hypothesize that these interactions play an important role in modulating equatorial Atlantic SST response to the AMOC changes.

In contrast with above-mentioned studies, other investigations focus on the importance of atmospheric teleconnection mechanisms. Chiang and Bitz (2005) showed that cooling in the high latitude can be readily transmitted to the tropics through intensifying northeasterly trade winds and their thermodynamic interactions with the oceanic mixed layer. The latter is often referred to as the wind-evaporation-SST (WES) feedback (Chang et al., 1997; Xie, 1999). In a follow-up study, Chiang et al. (2008) suggest that atmospheric processes are the primary cause for cooling in the high-latitude North Atlantic induced by a weakened AMOC to spread into the tropics.

The relative importance of oceanic versus atmospheric processes in transmitting changes in the high-latitude North Atlantic to the tropics deserves further study, as the

issue has a potential bearing on abrupt climate change prediction. In particular, it is important to understand whether the ocean plays an active or passive role in tropical SST response to high latitude oceanic changes. If the ocean's role is active, it is then important to know how oceanic dynamics control SST responses in the tropical Atlantic and where the oceanic control is most prominent. Although Chang et al. (2008) elucidated an oceanic teleconnection mechanism, it is not clear how the mechanism could operate under different strengths of the AMOC. Moreover, their analysis was based on a fully coupled GCM simulation where both atmospheric and oceanic processes were at work. Thus, it was difficult to isolate oceanic influence from air-sea interaction processes and identify areas that are most influenced by oceanic processes.

The primary objective of this chapter is to further advance oceanic processes in linking tropical SST response to the AMOC changes with a particular emphasis on examining the mechanism proposed by Chang et al. (2008). This mechanism builds on the finding of earlier modeling studies that the pathway of the northern STC to the equatorial zone is blocked by the AMOC return flow along the western boundary under the present climate condition (Fratantoni et al., 2000; Jochum and Malanotte-Rizzoli, 2001; Zhang et al., 2003). Chang et al. (2008) hypothesized that if during a major climatic event, such as Younger Dryas, AMOC strength would decrease beyond a critical value, the pathway could then open, leading to warming in the equatorial Atlantic. In this chapter, we shall take a systematic look at the dependency of the pathway on AMOC strength and its effect on SST response. We shall examine whether there is a threshold behavior of the tropical SST response to the AMOC changes, as proposed by Chang et al. (2008). We shall also explore the sensitivity of the mechanism on oceanic parameters that affect the water mass exchange between subtropical gyre and tropical gyre.

We shall conduct our investigation within a framework of a 2-1/2-layer reduced gravity ocean (RGO) model introduced in Chapter II. Such model is perhaps the simplest and yet most effective dynamic ocean model that is capable of resolving interactions between the return flow of the AMOC and the wind-driven circulation. This ocean-along

model will allow us to explicitly demonstrate the extent to which the oceanic processes are responsible to the SST response pattern as suggested in coupled GCMs.

The simplicity of the ocean model and its computational efficiency make it easy to carry out a large suite of numerical experiments to obtain a clear mechanistic understanding of the oceanic processes. A similar model has been successfully used by Fratantoni et al. (2000) to study the dynamic aspects of the interaction between the AMOC and the wind-driven circulation. In this study, we shall extend their work to include thermodynamic effect and focus our investigation on the effect of AMOC and STC interactions on tropical Atlantic SST variability. As in Fratantoni et al. (2000), our model does not directly simulate the AMOC. We simply prescribe mass transport at the northern and southern boundaries of the model domain to mimic the return flow of AMOC. This modeling approach provides us a simple control of the strength of the AMOC return flow in the model. We believe that this is a viable approach to gain mechanistic understanding of the role of the AMOC in Atlantic climate variability. We also discuss potential drawbacks of the approach.

The remainder of this chapter is organized as follows: Section 3.2 gives an overview of the model performance. In section 3.3, we examine the sensitivity of SST response to changes in AMOC and explore the oceanic processes contributing SST response. In section 3.4, the dependence of SST response on subsurface thermal condition will be discussed. Our major results will be summarized and discussed in section 3.5.

3.2 Model validation

Before using the newly developed ocean-modeling tool to investigate oceanic processes contributing the linkage between the AMOC changes and the tropical Atlantic SST, it is necessary to validate the model to see whether it is capable of capturing the key features of upper ocean circulation and variability of the tropical Atlantic. Since the major objective of this study is to examine the mechanisms proposed by Chang et al. (2008) which involves the interaction between the wind-driven circulation and the

AMOC, it is essential that the model has the ability to simulate SST, entrainment, and circulation patterns in the upper tropical Atlantic. For this reason, we will focus on validating these variables in this section.

For the control run (CTRL), the ocean model is driven by ECMWF ERA-40 reanalysis monthly mean wind stress climatology (Uppala et al., 2005). The surface heat flux forcing consists of shortwave radiation, longwave radiation, latent heat flux and sensible heat flux. Shortwave and longwave radiation are specified and taken from the Southampton Oceanographic Centre (SOC) data set (Josey et al., 1998; Josey et al., 1999). Latent heat flux and sensible heat flux are computed from air temperature and wind speed based on the standard bulk formulas described by Lee and Csanady (1999). The air temperature is derived from the NCEP reanalysis product (Kalnay et al., 1996) and the wind speed is derived from ECMWF ERA-40 product. Schmitz and Richardson (1991) found that almost one-half of the Florida Current transport is of South Atlantic origin, necessitating an interhemispheric and intergyre upper-ocean transport of about 14 Sv. According to this, a 14 Sv mass transport is specified at the northern boundary and the southern boundary to mimic the return flow of AMOC. The model is integrated for 20 years and approaches a steady solution after 8-years simulation. The model climatology is computed from the last 10 years of the simulation.

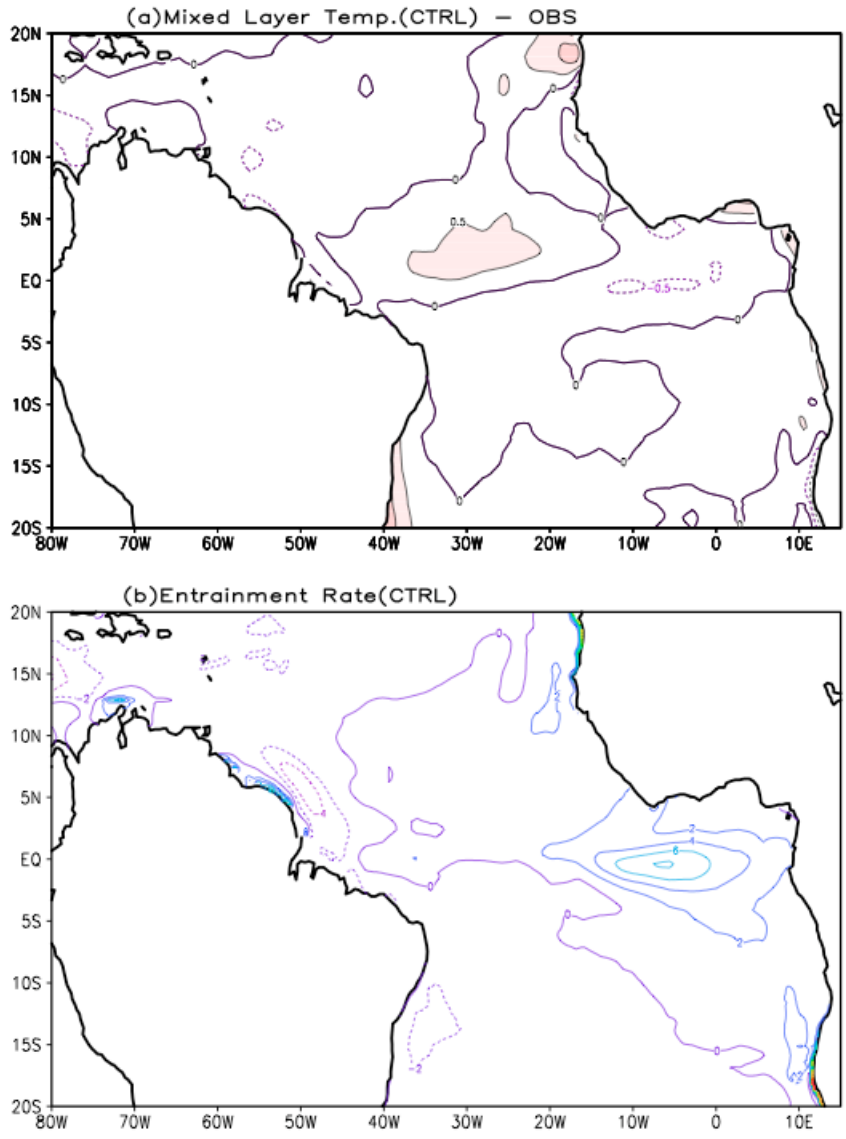

Figure 3.1 Annual mean mixed layer temperature biase (a) and entrainment rate (b) from the CTRL run. The contour interval is 0.5°C for SST errors and $2x10^{-6}$ m/s for entrainment rate.

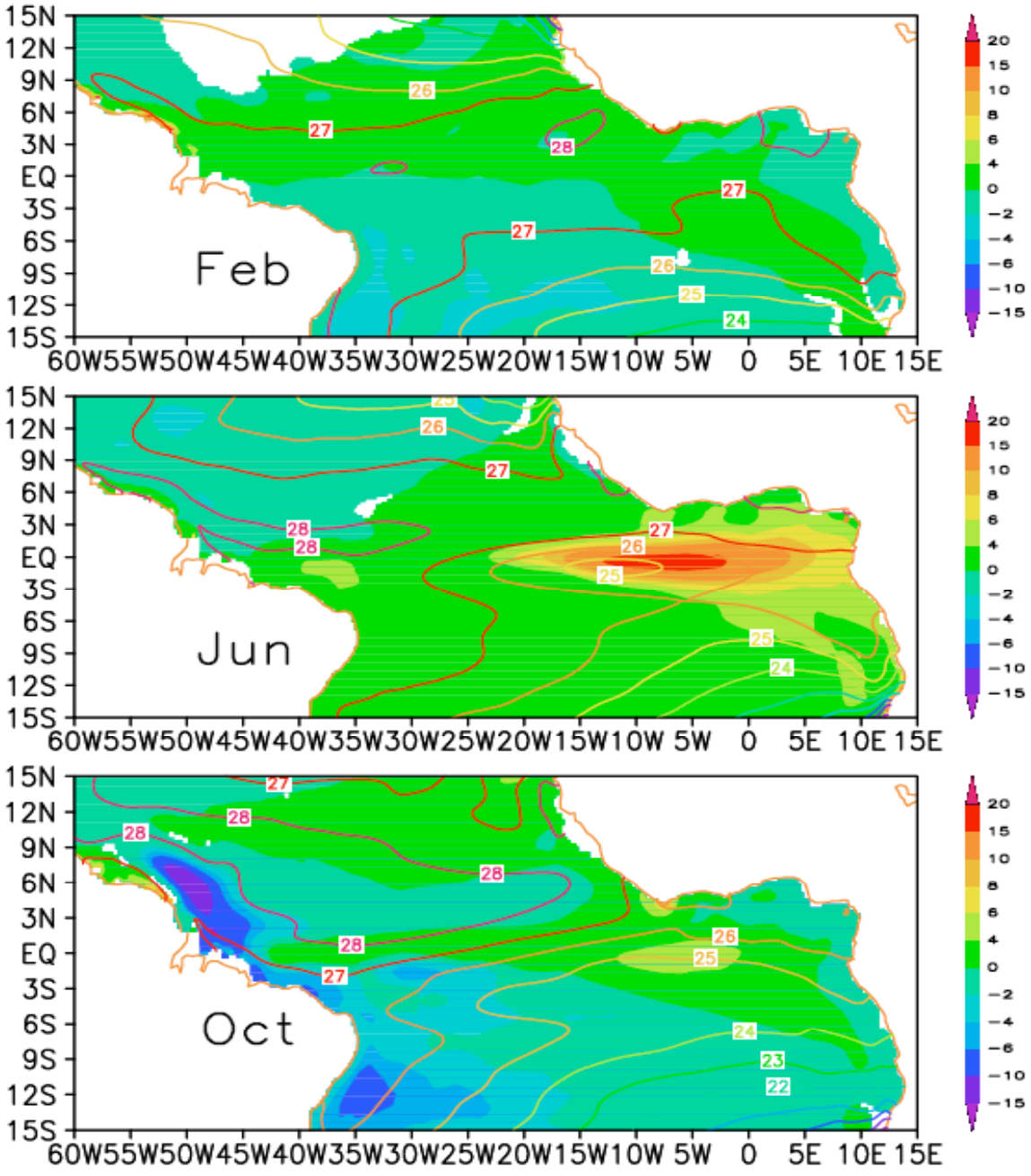

Figure 3.2 Monthly averaged SST (contours in °C) and entrainment rate (color in 10^{-6} m/s) in February, June and October from the control simulation.

The annual mean mixed layer temperature resembles closely the observed SST. For convenience, the SST solution is displayed in Figure 3.1 in terms of the difference between the model SST and observations. In most regions, SST error is less than 0.5°C. Entrainment mainly occurs in the eastern tropical Atlantic with a maximum center in the eastern of equatorial region. In the subtropical regions, detrainment dominates.

The simulated annual cycle of entrainment and SST are shown in Figure 3.2. The entrainment starts to increase after February in the eastern tropical Atlantic. Then, within a couple of months, it extends to the center of the basin and strengthens rapidly. After reaching its peak in June, the entrainment begins to decrease and its center retreats back to the eastern basin. Following the entrainment, a cold water tongue quickly developed in June and reaches its maximum in August. The development of the pronounced annual cycle of SST in the eastern equator agrees well with observations (e.g. Philander, 1990).

The model reproduces a quite realistic seasonal circulation pattern in the upper tropical Atlantic, as shown in Figure 3.3. The NBUC overshoots into the Northern Hemisphere along the western boundary and then retroflects at about 5ºN, turning southeastward to feed the Equatorial Undercurrent. The simulated retroflection latitude varies seasonally from 4ºN in March to 9ºN in September, which is consistent with observations (Molinari and Johns, 1994). The EUC water is entrained into the mixed layer and then flows westward as part of the South Equatorial Current (SEC). A majority of the SEC water mass merges with the North Brazil Current (NBC) at the western boundary and flows northward. The NBC continues to 5Nº-9ºN where it retroflects seasonally into the North Equatorial Counter Current (NECC) during May to December. The simulated seasonal variation of the NBC/NECC system is consistent with observations (Richardson and McKee, 1984; Richardson and Walsh, 1986). Overall, the model successfully captures the major features of SST and circulation pattern in the upper tropical Atlantic.

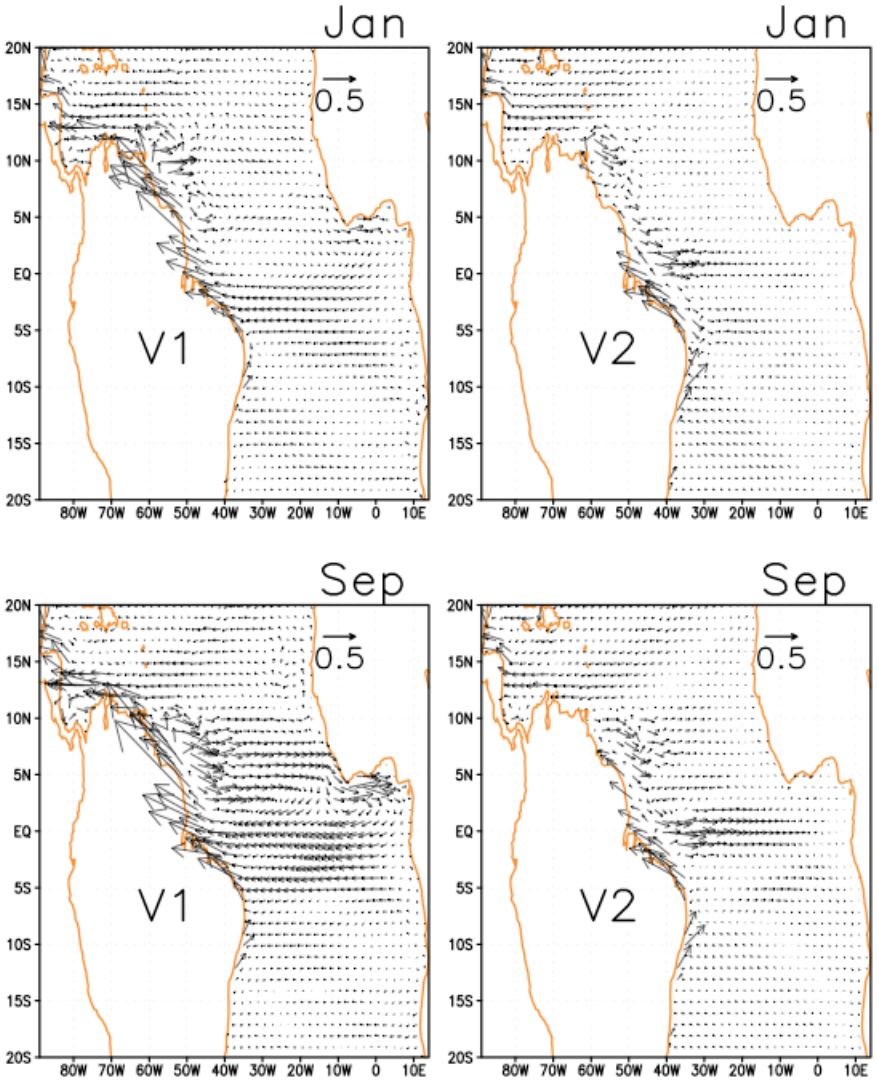

Figure 3.3 Monthly averaged currents in the mixed layer (left panel) and the thermocline layer (right panel) in January and September from the control simulation. Unit is in m/s.

3.3 Sensitivity of SST response to changes in AMOC

In this section, we perform a set of sensitivity experiments to test the hypothesis that changes in AMOC strength can have an effect on tropical Atlantic SST response by modifying the pathway of the STCs. First, we will simulate the response of the tropical Atlantic to a total shutdown of AMOC. Then, we will systematically explore the sensitivity of the tropical Atlantic circulation and SST to changes in the northward mass transport imposed at the open boundaries. As will be demonstrated below, the equatorial SST responds nonlinearly to changes in AMOC strength. A prominent equatorial warming occurs when AMOC is weakened below a threshold value. Note that we name all the experiments conducted in this study, except for the above-mentioned CTRL run, according to the latitude of the subsurface temperature front, temperature gradient and the strength of AMOC. For example, "L10NG7C_0Sv" indicates that in the experiment the subsurface temperature front is located at 10^0N, the temperature difference across the front is 7 ^{0}C and the strength of the AMOC, i.e., the imposed transport at the open boundaries, is zero.

3.3.1 SST response to a shutdown of AMOC

As noted previously, in the tropical Atlantic Ocean, wind-driven circulation interacts with the return flow of the AMOC. In this section we test the possibility that a substantially weakened AMOC may trigger SST warming in the equatorial South Atlantic by reorganizing the pathways of the STCs as suggested by Chang et al. (2008). We first describe the results of the experiment L10NG7C_0Sv, where everything is kept identical to the CTRL simulation described in section 3.2, except that the northward mass transport is set to zero at the open boundaries. The configurations of the experiment are summarized in Table 3.1. We assume that the CTRL run, which is forced by 'realistic' combination of wind stresses and the AMOC, represents the 'current climate state'. In contrast, the L10NG7C_0Sv run is only driven by the winds and gives a representation of the climate state when the AMOC is totally shutdown. A comparison of the two experiments allows us to assess the extent to which tropical ocean circulation

system can be modified by the absence of the AMOC and how these circulation changes affect SST.

Both experiments were integrated from the same initial conditions and ran for 20 years. The climatology of both experiments is constructed from the last 10 years of the model integrations. Unless stated otherwise, all the anomalies shown below are defined as the difference between the mean state of the L10NG7C_0Sv run and the CTRL run. Figure 3.4 compares annual mean current and temperature of the L10NG7C_0Sv run and the CTRL run. In the presence of a full strength AMOC, the model captures many of the salient features of the observed upper tropical Atlantic circulation (top panel). In the thermocline layer, a major portion of subducted water in the subtropical north Atlantic flows westward to the western boundary, where it feeds directly into the western boundary current. A small portion flows equatorward, but it is weaker than the northward western boundary current resulted from the AMOC return flow. Therefore, the return branch of the northern STC is invisible in the thermocline layer and the Atlantic STCs are highly asymmetric about the equator with water mass supplying the EUC mainly from the Southern Hemisphere (right top panel) (Zhang et al., 2003). When the AMOC is disabled, the STCs become more symmetric about the equator.

Table 3.1 List of sensitivity experiments

Integration name	Experiment design
CTRL	Thermal front is located around 10°N; Cross-front temperature difference is 7°C; Northward mass transport is set to 14Sv at the northern boundary.
L10NG7C_0Sv	Thermal front is located around 10°N; Cross-front temperature difference is 7°C; Northward mass transport is set to zero at the northern boundary.
L10NG7C	Thermal front is located near 10°N off the coast of South America; Cross-front temperature difference is 7°C; Northward mass transport at the open boundaries is decreased systematically from 14Sv to 0Sv.
L15NG7C	Thermal front is located around 15°N off the coast of South America; Other setting is the same with L10NG7C.
L7NG7C	Thermal front is located around 7°N; Cross-front temperature difference is 7°C; Other setting is the same with L10NG7C.
L3NG7C	Thermal front is located around 3°N near the equator; Other setting is the same with L10NG7C.
L10NG4C	Cross-front temperature difference is 4°C; Other setting is the same with L10NG7C.
L10NG2C	Cross-front temperature difference is 2°C; Other setting is the same with L10NG7C.

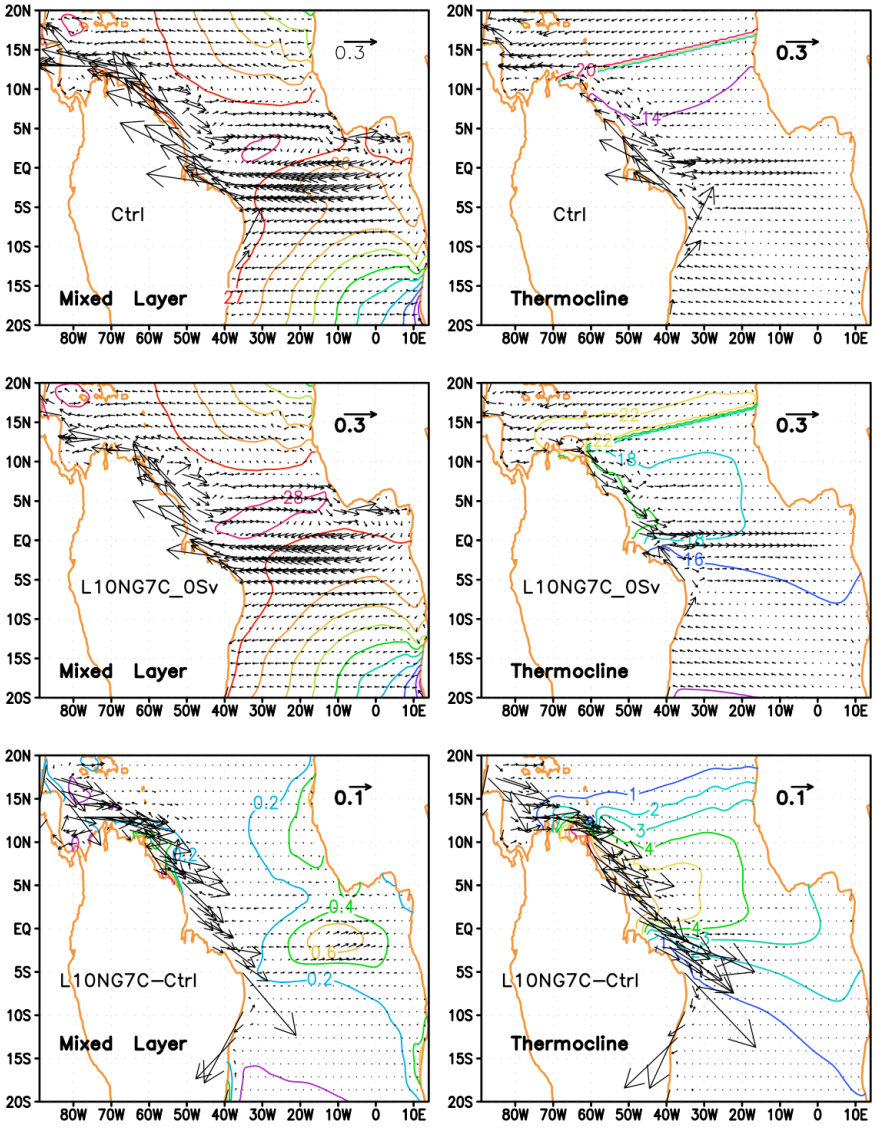

Figure 3.4 Simulated annual mean currents (vectors in unit of m s-1) and temperature (contours in unit of °C) in the mixed layer (left panels) and in the thermocline layer (right panels). Top panel: CTRL (wind-driven + AMOC). Middle panel: L10NG7C_0Sv (wind-driven only). Bottom panel: L10NG7C_0Sv - Ctrl. Note that the bottom panels are plotted in a different scale.

This is particularly evident in the northern STC where the southward western boundary current just north of the equator is intensified substantially (right middle

panel), allowing a portion of the subducted water to feed the EUC via the western boundary current pathway from the Northern Hemisphere. This result is consistent with the previous findings by Fratantoni et al. (2000) and Jochum and Malanotte-Rizzoli (2001). Near the surface the NBC is reduced as a result of the absence of the AMOC (left middle panel). The difference of the annual-mean circulation between the L10NG7C_0Sv run and the CTRL run is shown in the bottom panels. As expected, the dominant feature of the difference is a narrow and continuous southward-western boundary current that is associated with the upper return flow of AMOC (Fratantoni et al., 2000).

We next explore how the circulation change affects the SST response. As described above, the removal of the interhemispheric flow causes the western boundary current along the northeastern coast of South America (the return branch of the northern STC) to reverse its direction from poleward to equatorward. As shown in Figure 3.5, this change of circulation gives rise to a rapid increase in subsurface temperature near the strong temperature gradient front. The warm anomaly is then carried equatorward along the western boundary. A portion of the warm water is advected by the North Equatorial Undercurrent (NEUC), while the other portion enters the equatorial zone and then propagates easterward. To explore what processes are responsible for the easterward propagation, we draw a time-longitude section of subsurface temperature anomalies along 1°N (Figure 3.6). It shows that temperature anomaly front propagates in a range of speed. For example, it is observed that sometimes temperature anomaly front rapidly propagates from 35°W to 5°W within two months (red lines). The speed is about 1.1m/s, which is close to Kelvin wave speed. It also shows that sometimes temperature anomaly front propagates slowly. It takes about 7 months for the anomaly propagating from 35°W to 5°W (yellow lines). The speed is about 0.18m/s, which is close to the EUC speed in this model. It indicates that the temperature movement along the equator is achieved through a combination of seasonal Kelvin wave propagation and advection along the equator.

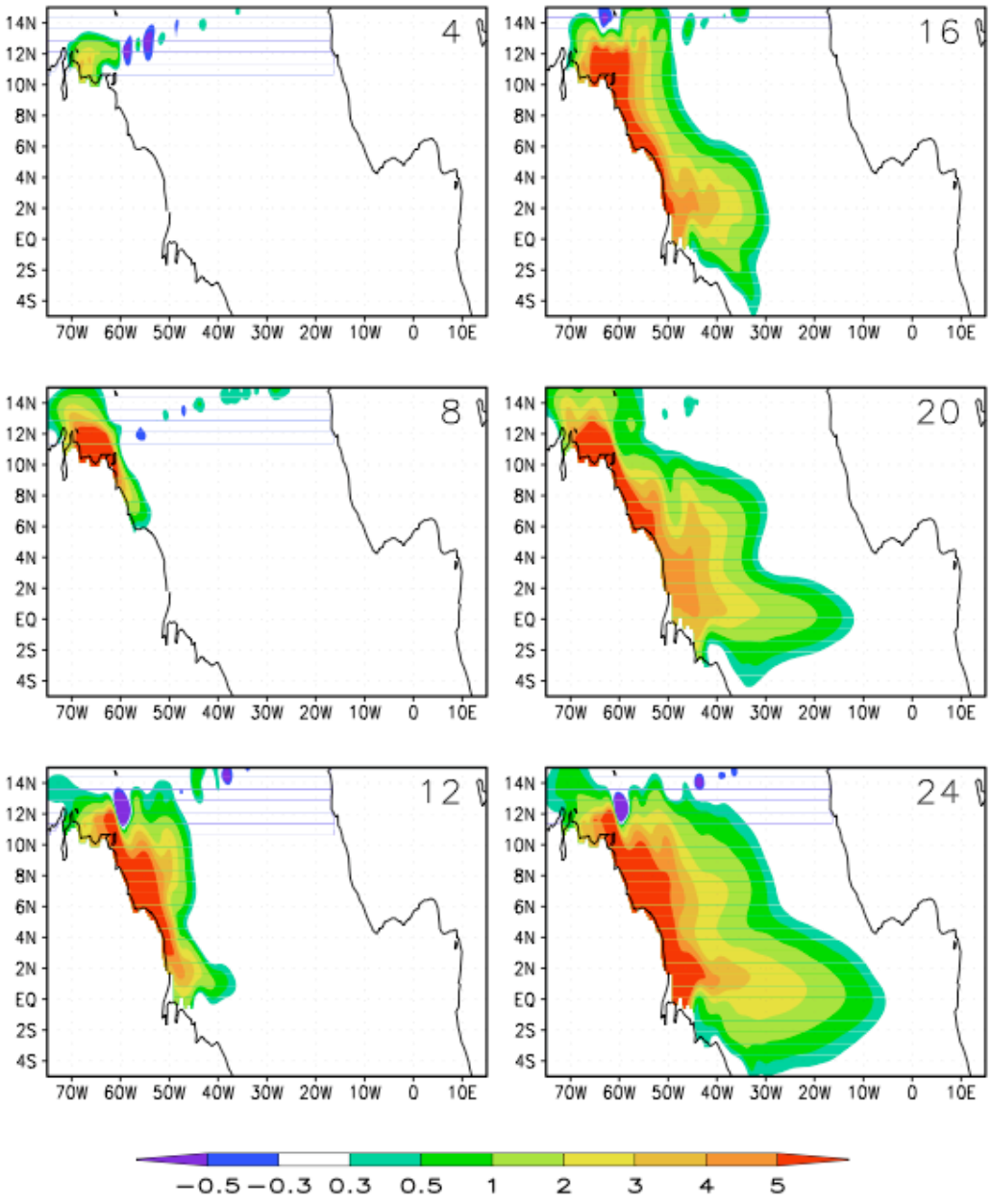

Figure 3.5 Evolution of subsurface temperature anomalies at the first 24 months (L10NG7C_0Sv and CTRL). Numbers at the right top of each panels correspond to model months after the shutdown of AMOC.

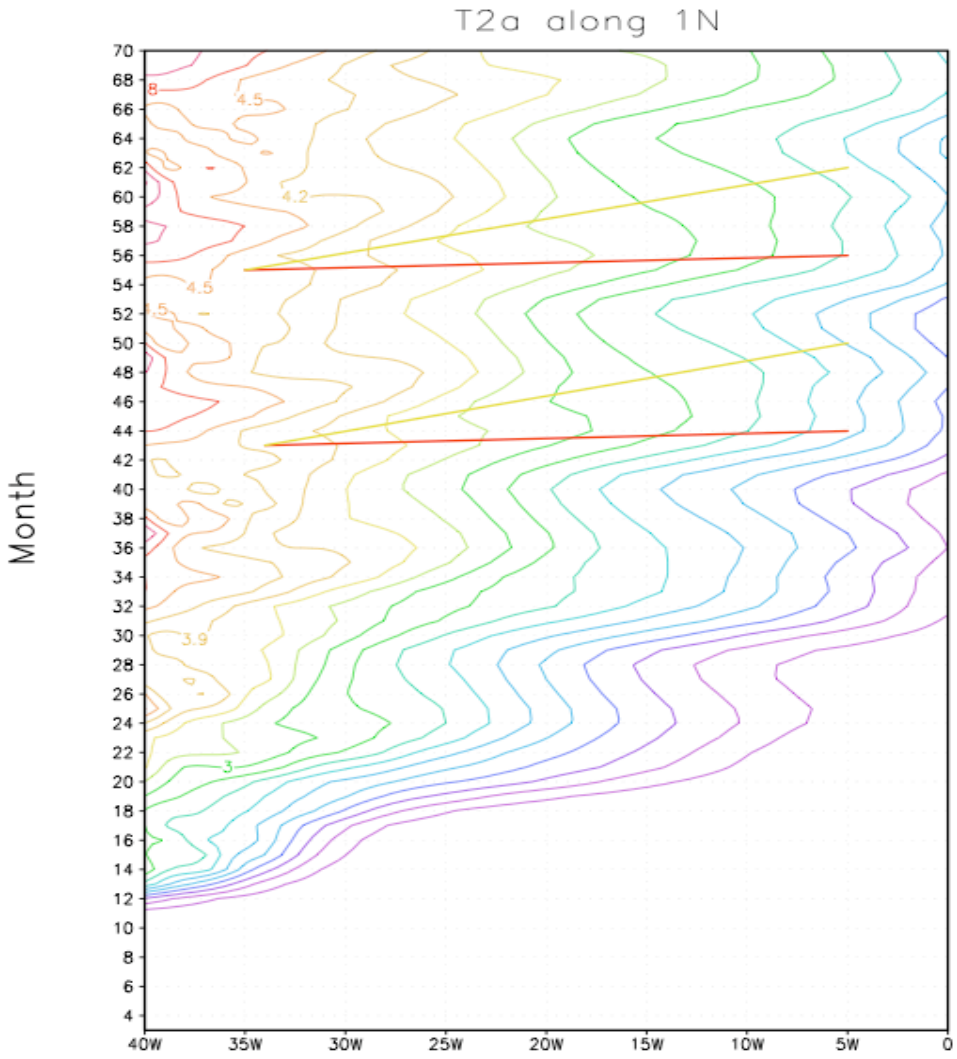

Figure 3.6 Time-longitude plot of subsurface temperature anomalies along 1°N. Red lines represent the propagation of Kelvin waves. Yellow lines indicate the speeds at which mean current propagate.

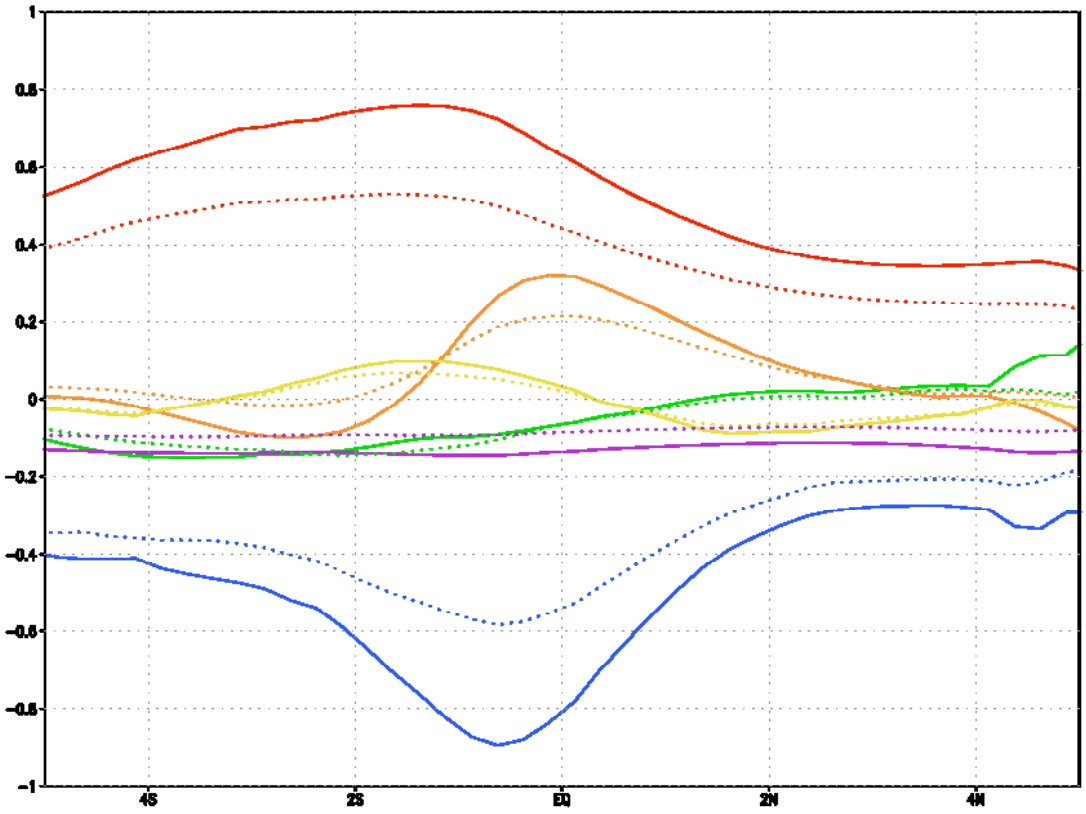

Figure 3.7 Annual mean heat budget (°C mon^{-1}) of the mixed layer in the CTRL run (solid line) and L10NG7C_0Sv (dot line) in the vicinity of the equator (5°S to 5°N). All the quantities shown in the figure are zonally averaged across the Atlantic basin. The net surface heat fluxes are in red; Entrainment cooling in blue; Zonal advection in green; Meridional advection in yellow; Horizontal diffusion in orange; Vertical diffusion in purple.

A heat budget analysis reveals that the SST warming is primarily due to the reduction of the upwelling cooling in the equatorial Atlantic. Figure 3.7 shows the mean mixed layer heat budget in the vicinity of equator. In the CTRL run, the dominant balance is between the heat input from the atmosphere (solid red line) and the entrainment cooling by the ocean (solid blue line). When AMOC is disabled (L10NG7C_0Sv), the entrainment cooling decreases substantially owing to the reduction of the vertical temperature gradient (dot blue line). As a result, the oceanic heat uptake from the atmosphere is reduced (dot red line). Further analysis shows that the reduction of entrainment cooling is attributed to the mean upwelling acting on the reduced vertical temperature gradient ($\bar{\omega}\frac{\partial T'}{\partial Z}$) and the reduction of upwelling ($\omega'\frac{\partial \bar{T}}{\partial Z}$) as result of the deepened mixed layer (Figure 3.8).

The large subsurface warming along the boundary between the subtropical and tropical gyres and the surface warming along the equator and the African coast in response to a shut-down AMOC are consistent with coupled GCM water-hosing simulations (Dahl et al., 2005; Stouffer et al., 2006; Chang et al., 2008; Wu et al., 2008). In contrast, the strong surface cooling in the Northern Hemisphere simulated by the GCMs is absent in our stand-alone ocean model simulation, suggesting that the surface cooling is largely attributed to atmospheric processes, which are excluded in this study. Therefore, the direct influence of the AMOC induced circulation change on SST is confined in the equatorial South Atlantic Ocean. This finding is consistent with the results of previous modeling studies that atmospheric boundary layer processes and their interaction with the ocean mixed layer are mainly responsible for transmitting the surface cooling from the high-latitude North Atlantic to the tropics (Chiang et al., 2003; Chiang et al., 2008), whereas the oceanic teleconnection is responsible for the warming in equatorial South Atlantic (Chang et al., 2008; Wu et al., 2008).

As in the GCM studies, we find that the substantial subsurface warming has a major effect on the equatorial SST seasonal cycle. The effect on the SST seasonal cycle

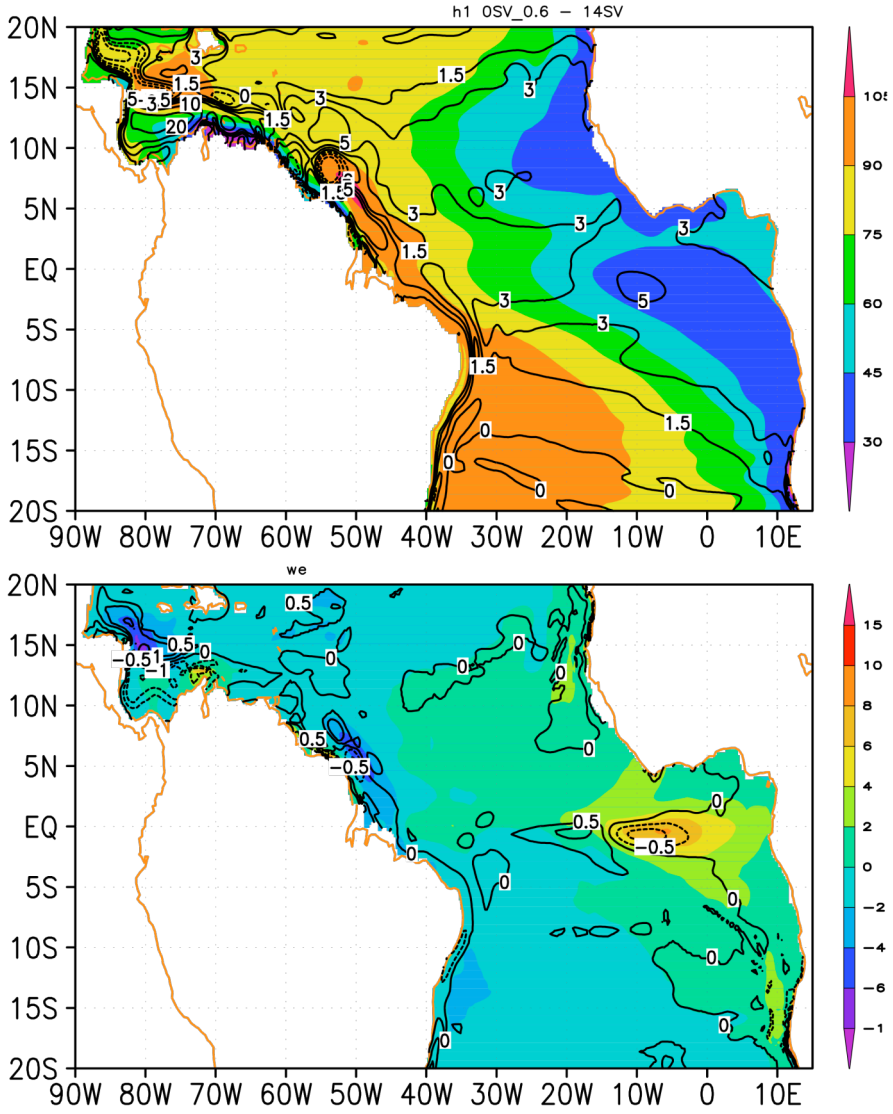

Figure 3.8 (a) Difference of mixed layer thickness (contour, unit in m) and (b) entrainment (contour unit in 10^{-6}m/s) between the L10NG7C_0Sv run and the CTRL run. Values from the CTRL run are shaded.

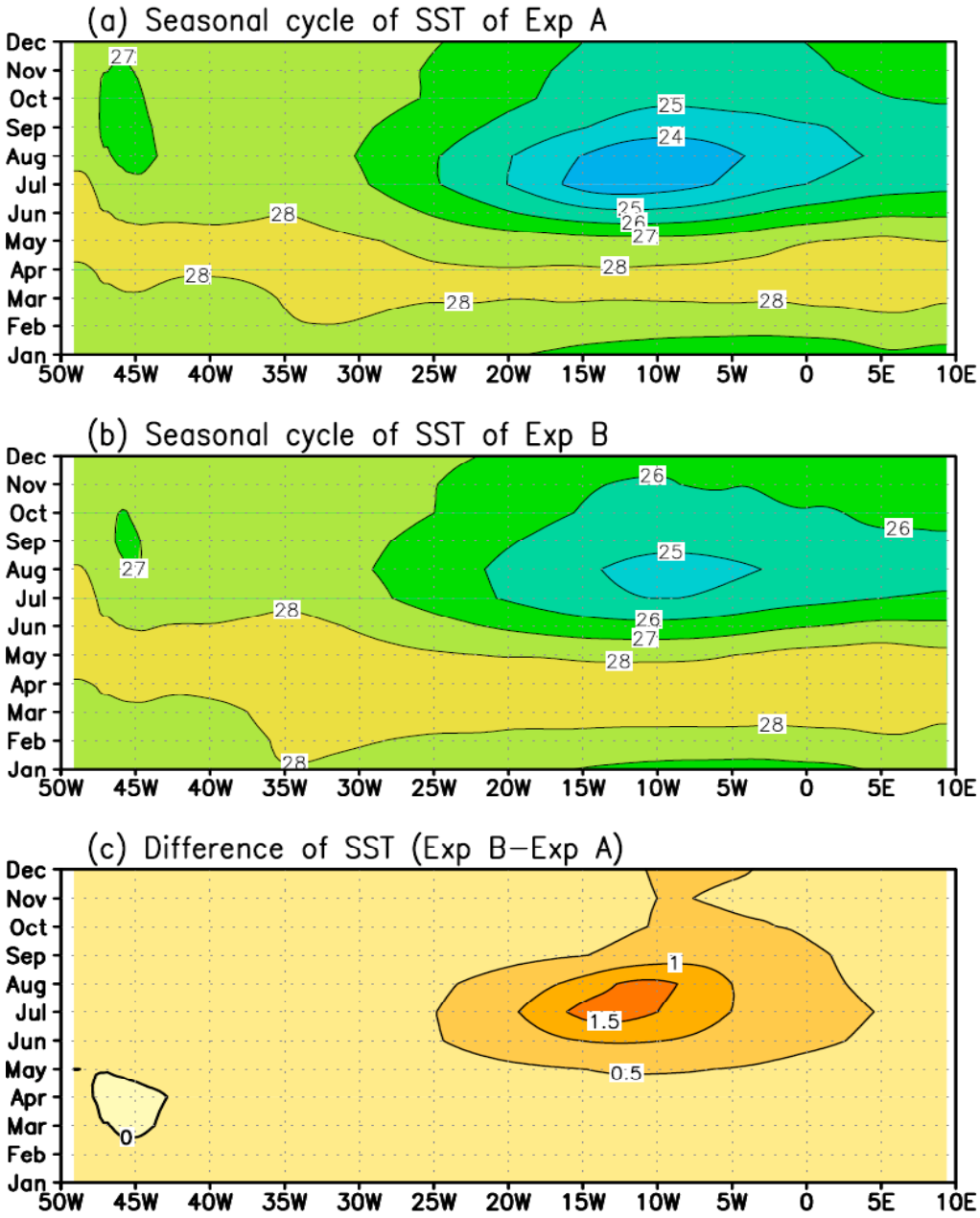

Figure 3.9 Simulated seasonal variation of SST along the equator in (a) CTRL (wind-driven + AMOC), (b) L10NG7C_0Sv (wind-driven only), (c) Difference of SST between L10NG7C_0Sv and CTRL.

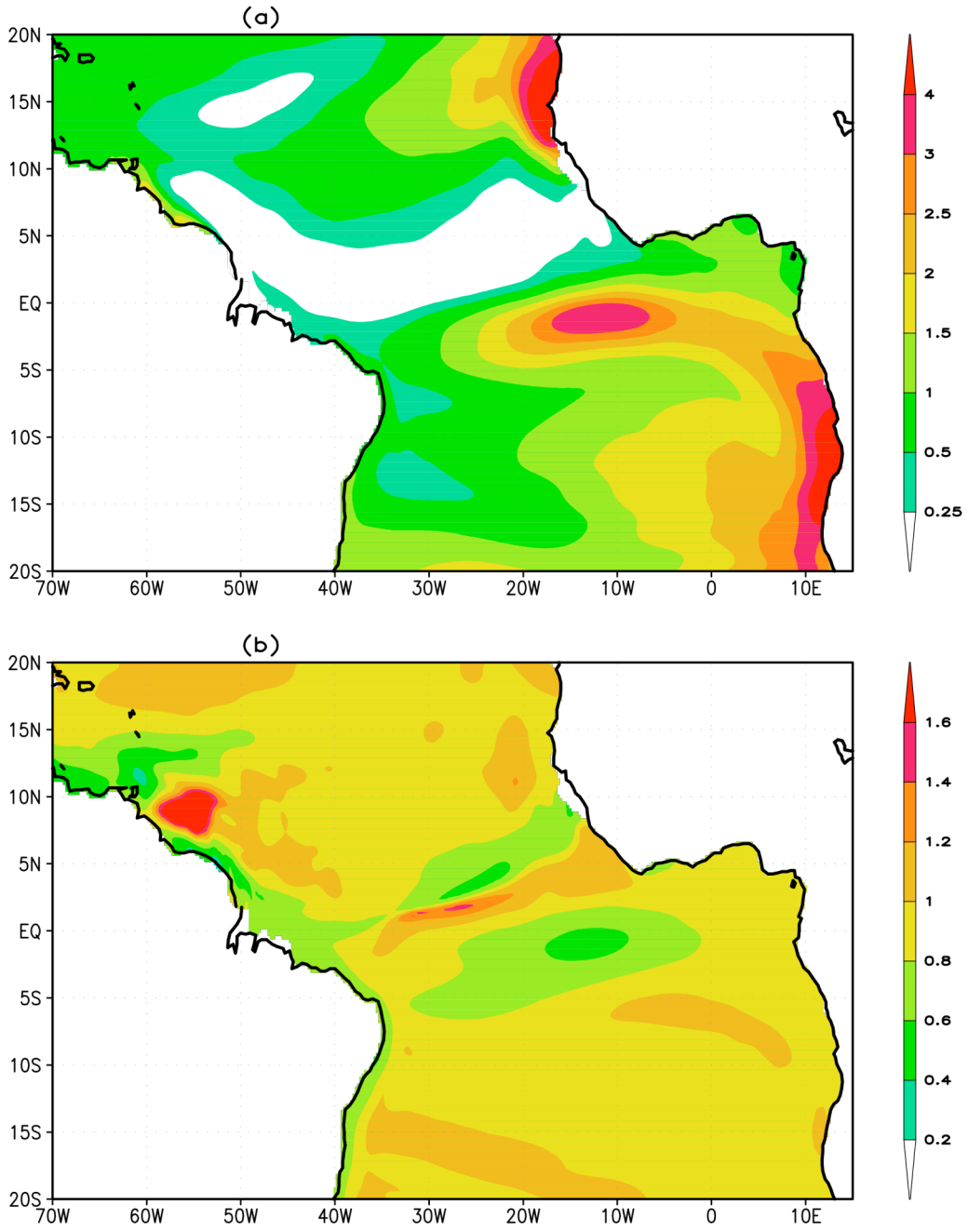

Figure 3.10 (a) The spatial structure of the seasonal variance of SST from the CTRL run. (b) Ratio of seasonal variance in the L10NG7C_0Sv (wind-driven only) to the CTRL run.

is strongest during boreal summer and fall (Figure 3.9). This is because the SST change is mainly forced by the mean upwelling acting on the reduced vertical temperature gradient. The upwelling-induced cooling is most effective during boreal summer and fall when the equatorial cold tongue develops in the Gulf of Guinea. Figure 3.9 shows that the equatorial cold tongue SST increases by more than 1.5°C during July to September in response to a total shutdown of the AMOC. As a result, the seasonal variation is substantially reduced (Figure 3.10). As shown in Figure 3.10, the seasonal variation of SST is reduced by about 50% in response to a shutdown of AMOC. This change in the equatorial SST seasonal cycle can have an important influence on the African Monsoon (Vizy and Cook, 2002; Chang et al., 2008). The change in the upper ocean stratification can also have an important impact on 'Atlantic Nino' activity during the boreal summer (Haarsma and Hazeleger, 2007; Chang et al., 2008).

3.3.2 SST response to different strength of AMOC

To explore the sensitivity of the SST response to changes in the AMOC, we carried out a set of sensitivity experiments, L10NG7C, where the imposed northward mass transport at the open boundaries is decreased systematically from 14Sv to 0Sv (See Table 3.1 for details of the experiment configurations). We are particularly interested in examining questions, such as, does the SST respond linearly or nonlinearly to the AMOC changes? Is there a threshold value in the AMOC strength below which the SST response becomes more sensitive? The CTRL run with 14 Sv imposed interhemispheric flow (CTRL), serves as a reference for all other sensitive experiments.

Figure 3.11 displays the annual mean temperature response to different strength of AMOC in the mixed layer and the thermocline layer. It shows that SST responds nonlinearly to different strengths of AMOC. There are mostly negligible SST anomalies over the whole tropical Atlantic basin for slight decreases in the AMOC strength (L10NG7C_12Sv, L10NG7C_10Sv). When AMOC strength decreases to 6Sv, weak

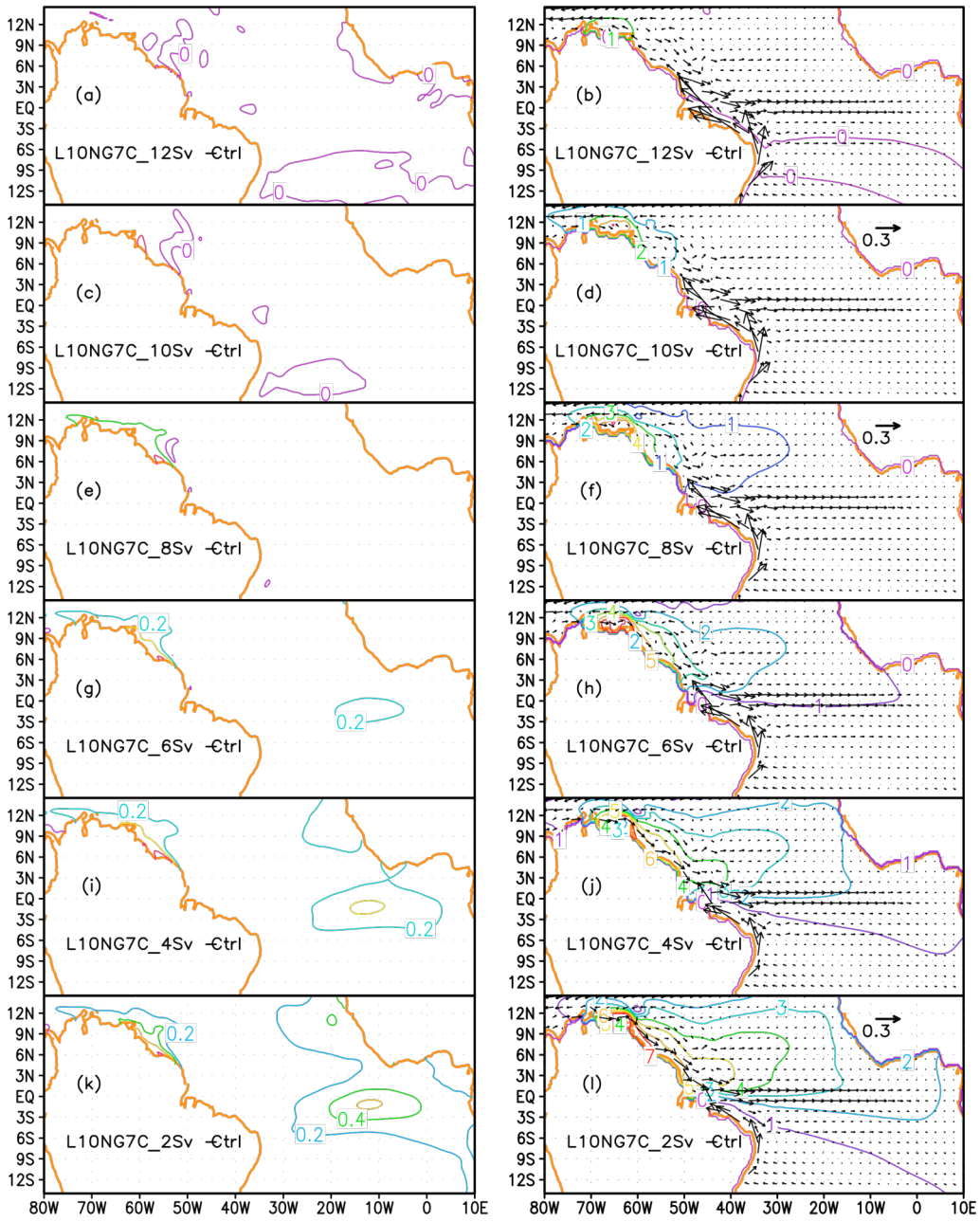

Figure 3.11 Simulated annual mean currents (vectors in unit of m s-1) and temperature response (contours in unit of °C) to different strength of AMOC in the mixed layer (left panels) and in the thermocline layer (right panels).

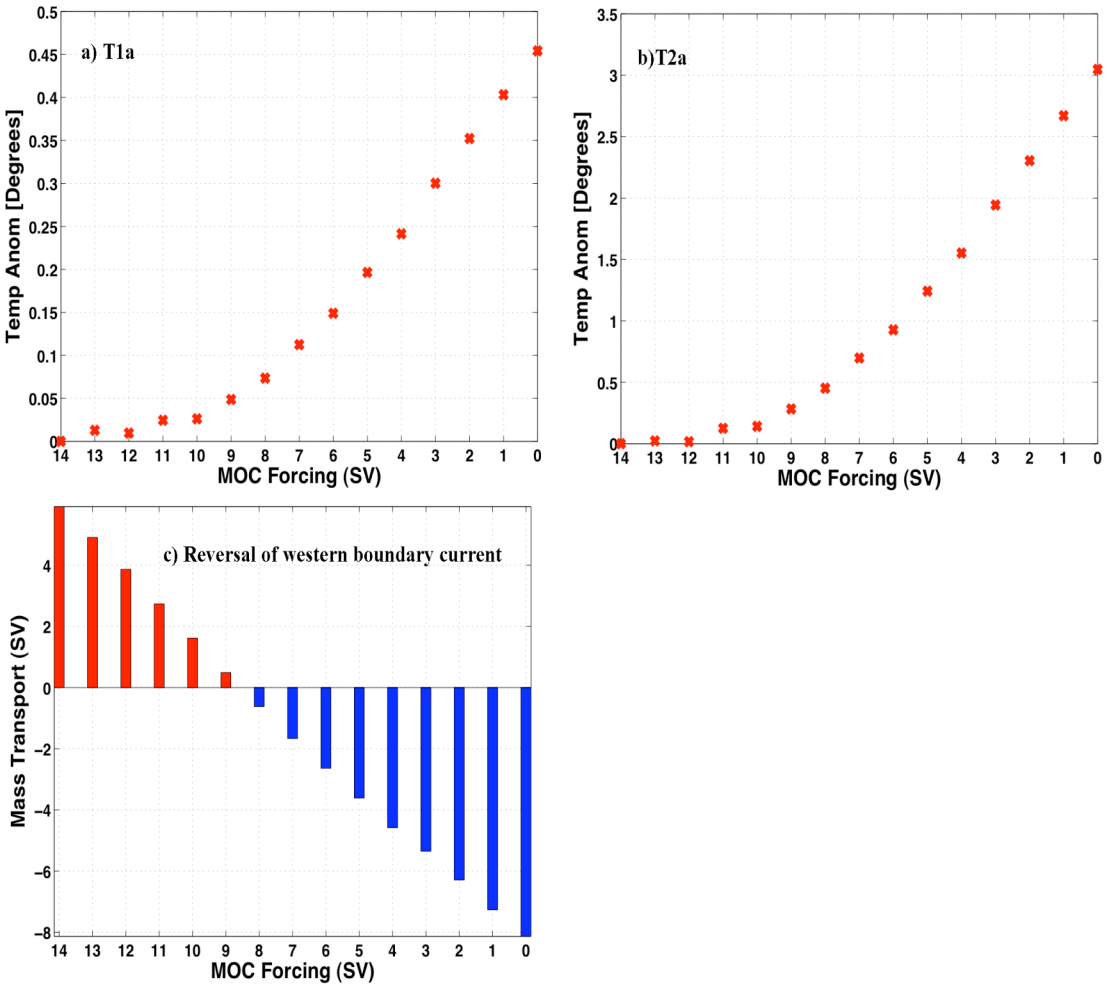

Figure 3.12 Changes in (a) SST index T1a, (b) thermocline temperature index T2a, (c) the western boundary current transport across 5°N in the thermocline layer as a function of AMOC strength for the L10NG7C experiment. T1a and T2a are defined as SST anomaly and thermocline temperature anomaly averaged over 20°W-5°W, 3°S-3°N, respectively. Black circle indicates the AMOC threshold value (8Sv) that marks the increase of the sensitivity of the temperature response to AMOC changes. In (c) the northward transport takes a positive value.

SST anomalies on the magnitude of 0.2°C begin to emerge along the northern coast of the south Atlantic and equatorial cold tongue. As the AMOC continues to decrease, the warm anomaly spreads over the eastern side of the basin along the upwelling zones with increasing strength. Figure 3.11 suggests that the nonlinear response of the SST is related to subsurface temperature response. For a slightly weakened AMOC, significant subsurface temperature response only occurs near the temperature front. As the AMOC strength decreases below 8Sv, substantial warming anomaly spreads further to the equatorial South Atlantic.

To further illustrate the sensitivity of temperature response, we define two indices: T1a is taken as the SST averaged over an equatorial box of 20°W-5°W and 3°S-3°N from each experiment and then subtracted by the SST from the control run; T2a is the same as T1a except that it is taken from the thermocline layer. Figure 3.12 shows the two indices in response to different strengths of the AMOC. Both T1a and T2a indicate clear nonlinear behavior. For small decreases in AMOC strength (13Sv-10Sv), the subsurface and surface temperature response is weak and is insensitive to the change in AMOC strength. As AMOC strength continues to weaken, the temperature response becomes more sensitive. If we define the response sensitivity as temperature change per unit change in AMOC strength measured in °C/Sv, i.e., the slope of T1a and T2a, then one finds that the sensitivity of the temperature response increases drastically when the AMOC strength is decreased below a threshold value of about 8 Sv.

What mechanism is responsible for such nonlinear behavior in SST response and what oceanic conditions determine the threshold value? As shown in Figure 3.11, the extent to which subsurface temperature anomalies accumulated near the temperature front spreads toward to the equator is associated with the NBUC penetration. As the AMOC decreases to 12Sv, the NBUC penetrates into the Northern Hemisphere to about 10°N. The warm/cold water exchange is prohibited by the NBUC. As the AMOC continues to decrease, the penetration of NBUC retreats toward the equator. The warm water extends along the path of retreat of the NBUC. To make this point more clear, we draw the integrated western boundary current transport at 5°N in the thermocline layer

for different strength of AMOC (Figure 3.12). It reveals that the NBUC starts to reverse its direction from northward to southward when AMOC is weakened below 8 Sv. The fact that the critical AMOC value for NBUC reversal coincides with that of the temperature sensitivity change suggests that the nonlinear temperature response is associated with the interplay between the wind-driven northern STC and the AMOC.

As illustrated in Figure 3.4 (right bottom panel), the AMOC return flow interacts with wind-driven circulation mainly via the western boundary current. The net transport of the NBUC is given by the superposition of the equatorward return flow of the northern STC and the northward western boundary current associated with the AMOC. When the AMOC is strong, the NBUC of the Southern Hemisphere origin penetrates into the Northern Hemisphere and essentially blocks the return branch of northern STC (Figure 3.12c). As the AMOC weakens, the strength of the northward western boundary current decreases. When the imposed AMOC strength is below 8Sv, the northward western boundary current becomes weaker than the northern STC return flow, causing the NBUC reverses its direction. The southward NBUC is strengthened as the AMOC strength continues to decrease. Mass transport analysis suggests that for our model 8 Sv is the threshold value at which the strength of the northern STC is approximately equal to the AMOC. Figure 3.13 sketches out the zonally integrated annual mean meridional circulation between 8°S and 8°N in three model simulations with the imposed northward transport of 0Sv, 8Sv and 14Sv. The dark pathways are the northern and southern STCs, which are wind-driven and self balanced with the same amount of water flowing poleward in the mixed layer as equatorward in the thermocline layer. The gray dashed pathways indicate the upper branch of the AMOC in the model. As shown in Figure 3.12c, the decrease of western boundary current transport is proportional to changes in AMOC strength. It shows that, in an annual mean sense, the upper circulation solution of our ocean model can be well approximated by a linear superimposition of the wind and the AMOC forced solutions. When the AMOC is disabled, the northern STC (6 Sv) is slightly stronger than the southern STC (4 Sv) in the model (Figure 3.13a). With 8 Sv imposed transport at the boundaries, the 6 Sv AMOC water enters the thermocline layer

is equal to the strength of the northern STC, leaving no mass transport across 8°N (Figure 3.13b) in that layer. When the imposed AMOC transport is set at 14 Sv, the

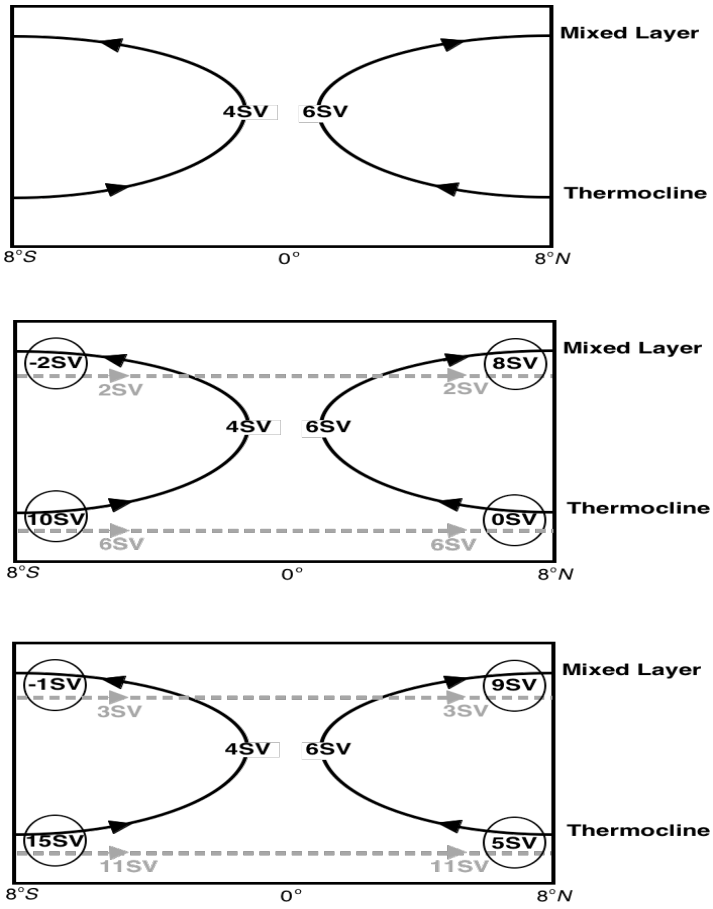

Figure 3.13 Schematic sketch of the zonally integrated mass transport in the upper tropical Atlantic Ocean with (a) 0Sv (wind-driven only), (b) 8Sv, (c) 14Sv imposed AMOC transport at the open boundaries for the L10NG7C experiment. Solid routes represent the wind-driven flows associated with the northern and southern STC. Light dished routes represent the return flow of the AMOC. Numbers marked on each route indicate the strength of the circulation component. Numbers in the black circle represent the total mass transport which is consist of the contributions from the wind-driven circulation and the AMOC in each layer. Note that the strength of the northern STC is equal to that of AMOC in the thermocline layer, resulting no mass transport across 8°N(b).

northward western boundary transport is much stronger than that of northern STC return flow, resulting in a net northward mass transport at 8°N (Figure 3.13c).

3.4 Sensitivity to subsurface temperature condition

The results described in the previous section suggest that there are two key elements controlling the tropical SST response to AMOC changes: 1) the western boundary current system along the northeastern coast of the South Atlantic, i.e., NBUC, and 2) the thermal front along the boundary of the subtropical and tropical gyres. In this section, we will examine how sensitive the SST response is to the properties of the thermal front, including its location and strength.

To test the effect of thermal front location on the SST response, besides the experiment L10NG7C discussed in Section 3.3.2 we carried out three sets of experiments where the center of the front was systematically displaced from a location near 15°N off the coast of South America to a location near the equator (see Figure 2.2b for the exact locations of the front). In each set of experiments, AMOC strength is systematically decreased from 14 Sv to 0 Sv. We refer to these sets of experiments as L15NG7C, L7NG7C and L3NG7C with L15NG7C having the front location furthest away from the equator (see Table 1 for experiments configurations). Note that the location of temperature front in the L10NG7C experiment is close to the observed subsurface temperature front derived from the Levitus dataset (Figure 2.2a). Admittedly, such an idealized setting is unrealistic because changes of thermal structure in reality are associated with changes in circulation structures as the two are dynamically linked through geostrophic constraint. In our simplified model, the thermal front is maintained by the heat flux correction as discussed in Chapter II. In a sense, we can view our model as an anomaly model where its mean temperature in the thermocline layer is specified and only departures from the mean temperature are simulated. Our purpose here is not to simulate realistic mean circulation of the ocean, but rather to

elucidate mechanisms governing changes of the ocean in response to AMOC changes. With these caveats in mind, we discuss the results of our sensitivity experiments.

Figure 3.14 shows the temperature response to different AMOC strengths in each set of experiments. When the temperature front is displaced furthest to the north (L15NG7C), the equatorial thermocline temperature response represented by T2a is very weak and the SST response T1a is almost non-existent. When the front shifts

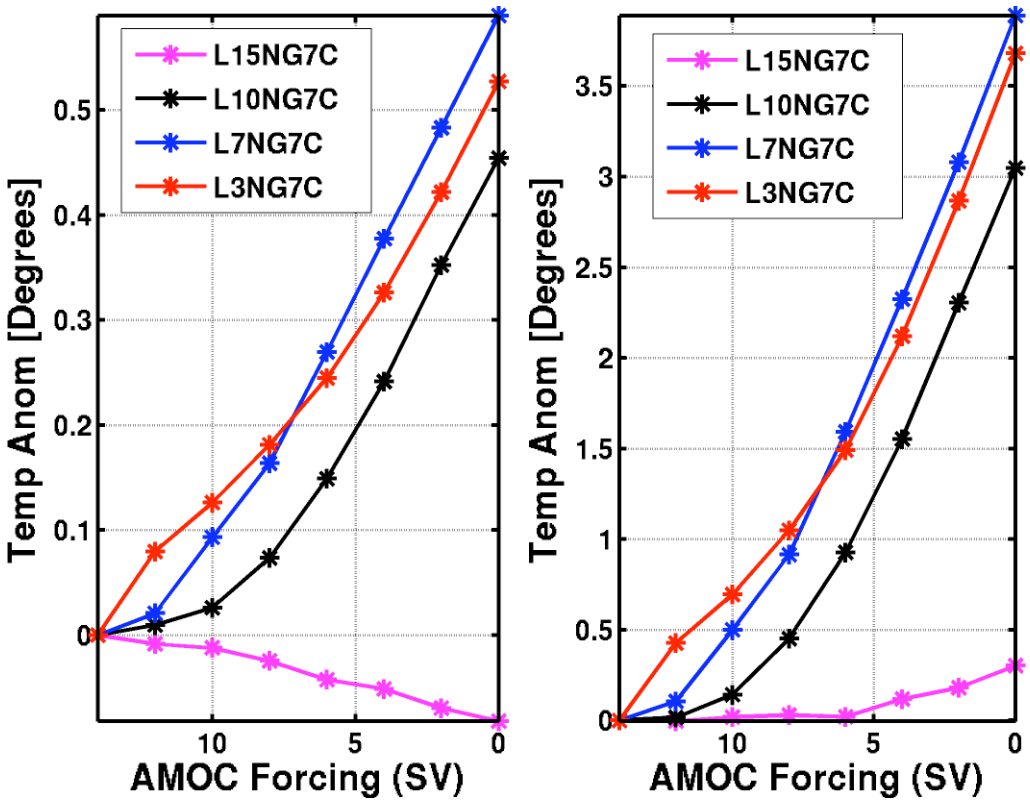

Figure 3.14 Equatorial temperature changes as a function of AMOC strength for L15NG7C (magenta), L10NG7C (black), L7NG7C (blue) and L3NG7C(red) where the subsurface thermal front location is varied. The positions of the thermal front in each experiment are displayed in Fig 3.1b. The definitions of the SST index T1a (left panel) and the subsurface temperature index T2a are the same as those in Fig 3.12.

equatorward to about 10°N (L10NG7C), it is evident that the temperature responds nonlinearly to changes in AMOC strength, as discussed in the previous section. With the location of the front moving closer to the equator (L7NG7C and L3NG7C), the nonlinear behavior of the temperature response appears to be weakened. This is seen more clearly in the L3NG7C experiment where the front location is very close to the equator (Red lines in Figure 3.14). These results suggest that the degree of nonlinearity in the temperature response is determined by whether the warm water is able to enter the equatorial zone along the western boundary. If subtropical/tropical gyre boundary is faraway from the equatorial zone, the warm water of the subtropical gyre must first be advected into the equatorial zone by the western boundary current before it can propagate eastward along the equatorial wave guide. To allow this to occur, the western boundary current along northeastern coast of South America, i.e., the NBUC, must flow equatorward. Therefore, the AMOC threshold behavior comes into play, giving rise to a nonlinear temperature response when the thermal front is located sufficiently far away from the equator. However, if the front is located too far northward as in the L15NG7C experiment, the temperature anomaly is caught in the path of the subtropical gyre and is swept away by the westward flowing Caribbean current, leaving little chance for the warm anomaly moving equatorward. Therefore, the temperature response in this case is very weak. In contrast, if the temperature front is very close to the equator as in the L3NG7C experiment, the warm anomaly is generated within the equatorial zone. In this case, even though the western boundary current does not reverse its direction, the anomaly can propagate quickly eastward along the equator, causing warming the equatorial South Atlantic. In this circumstance, the temperature responds linearly to AMOC changes.

We further examine the impact of the strength of the subsurface temperature front on the behavior of model temperature response. We repeated the sensitivity experiments by reducing the cross-front temperature difference from 7°C to 4°C and then to 2°C in the L10NG4C and the L10NG2C experiments, respectively (see Table 1 for experiment configurations). Results of these experiments are summarized in Figure

3.15. It shows that the temperature responses in both layers behave nonlinearly to AMOC changes, although the SST response is significantly weakened by the weak temperature front. Therefore, we conclude that the nonlinear behavior of the equatorial temperature response to AMOC changes depends more on the location of the thermal front than the strength of the front.

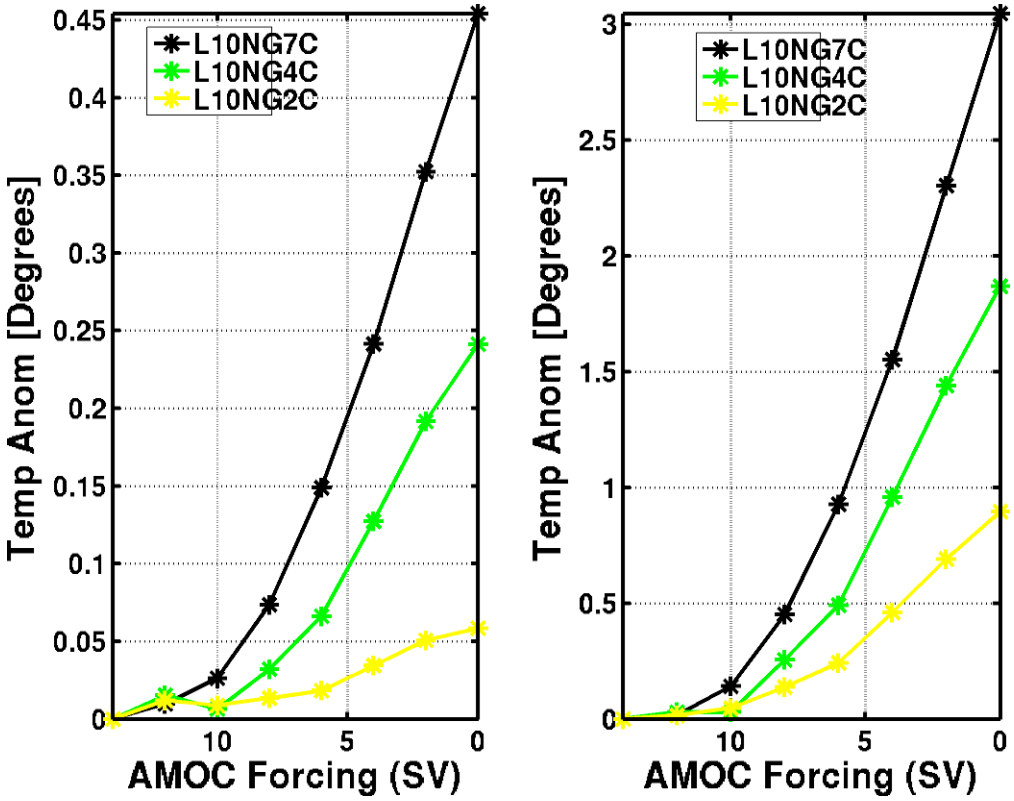

Figure 3.15 Same as in Fig. 3.12 except that the front location is fixed as in L10NG7C, but the cross-front temperature difference is reduced to 4°C (L10NG4C, green) and to 2°C (L10NG2C, yellow).

3.5 Summary and discussion

In this chapter, we advance an oceanic mechanism linking the AMOC changes to the tropical Atlantic SST changes proposed by Chang et al. (2008). Using a simple 2-1/2-layer RGO model that includes key dynamic and thermodynamic processes, we conducted a systematic investigation into the oceanic processes controlling the SST response to the AMOC changes. The modeling approach that we adopted is, in many ways, similar to that of Fratantoni et al. (2000) where a northward interhemispheric flow is specified at the northern and southern open boundaries of the model, mimicking the return flow of the upper limb of the AMOC. Different from Fratantoni et al. (2000), our emphasis is on the effect of AMOC changes on the tropical Atlantic SST response. By varying the strength of the imposed interhemispheric flow, we conducted a large number of numerical simulations to shed light on the detailed oceanic processes controlling the tropical Atlantic SST response and its sensitivity.

As in Fratantoni et al. (2000), we found that the most significant circulation change in the upper tropical Atlantic in response to a total shutdown of AMOC that occurs in the NBC/NBUC region. In the absence of the AMOC, the NBUC flows equatorward and the Atlantic STCs become more symmetric about the equator. We further show that this circulation change causes a pronounced subsurface warming that is initiated along the gyre boundary of the northern subtropical and tropical gyres and then spreads into the equatorial south Atlantic, giving rise to warm SST anomalies in the Gulf of Guinea and along the African coast. The surface warming is strongest during the boreal summer and fall when the upwelling is at its peak. This finding supports the hypothesis proposed by Chang et al. (2008). In contrast to the water hosing experiments carried out using coupled climate models, our ocean-only model simulation shows no prominent SST change in the northern tropical Atlantic. We speculate that the surface cooling in the Northern Hemisphere is primarily attributed to atmospheric processes and the oceanic teleconnection mechanism is mainly responsible for SST changes in the equatorial south Atlantic. In the next chapter, we will examine this speculation within a framework of a coupled model including both atmospheric and oceanic processes.

A major objective of this study is to assess the sensitivity of the tropical Atlantic SST to changes in AMOC strength through a set of sensitivity experiments where the imposed northward transport at the open boundaries is varied decrementally from 14 Sv to 0 Sv. An important finding that emerges from these experiments is that although interactions between the STC and AMOC can be essentially described as a linear superposition of two opposing western boundary currents driven by winds and thermohaline circulation off the northern Brazilian coast, as shown by Fratantoni et al. (2000), the tropical SST response to AMOC changes behaves nonlinearly. The sensitivity of the SST response increases drastically when the AMOC strength decreases below a threshold value of about 8 Sv. This threshold behavior is attributed to the reversal of the NBUC due to the weakened northward western boundary current associated with the AMOC. Sensitivity experiments reveal that the nonlinear threshold behavior depends primarily on the position of subsurface temperature front and is less sensitive to changes in the strength of the subsurface temperature gradient between the northern subtropical and tropical gyres. If the subsurface thermal front is located sufficiently close to the equator, nonlinear behavior is substantially weakened as the anomaly generated near the subsurface thermal front is readily able to excite equatorial Kelvin waves, propagating rapidly eastward along the equatorial wave guide and causing changes in the thermocline in the eastern equatorial Atlantic.

Our analysis suggests that in order for the oceanic teleconnection mechanism to operate, two conditions must be satisfied: 1) the AMOC reduction must be substantial enough to allow the NBUC to reverse direction and thus permit water mass exchange between the northern subtropical and tropical gyres, and 2) the gyre boundary where the subsurface thermal front is located must be situated in an optimal location. If the front is too far away from the equator, the subsurface temperature anomaly generated by the AMOC changes is unable to enter the equatorial zone and the SST response to AMOC changes is negligible. On the other hand, if the AMOC reduction is not strong enough, the subsurface warm anomaly will be trapped near the gyre boundary and not be able to enter the equatorial zone, consequently, no strong SST response will take place. This

implies that prominent equatorial warming can only occur during strong climatic events, such as Younger Dryas, when substantial AMOC reductions occurred. The result also suggests that climate models must accurately simulate the gyre boundary and the associated temperature gradient in order to simulate abrupt climate changes in the tropical Atlantic sector. If the gyre boundary and the temperature front are located too close to the equator, the warm anomaly can readily propagate along the equatorial wave guide even if the NBUC does not reverse its direction. In this case, models may overestimate the sensitivity of the tropical SST response to the AMOC changes.

It is worth pointing out that the tropical SST response to the AMOC changes studied here can not be simply attributed to changes in meridional heat transport that have been widely used as an explanation for warming (cooling) of South (North) Atlantic when the AMOC is reduced (e.g. Dahl et al., 2005; Fedorov et al., 2006; Barreiro et al., 2008). The meridional heat transport is a vertically integrated measure of oceanic heat fluxes, $\int VT\,dz$. If we simply divide the ocean into a warm upper layer where the AMOC return flow takes place and a cold lower layer where the North Atlantic Deep Water (NADW) outflow occurs, the meridional heat transport can be approximated as $V(T_u - T_b)$, where V is vertically integrated northward flow carried by the AMOC return flow which is equal but opposite in sign to the NADW outflow, T_u and T_b are the temperature of the upper and lower layer. An AMOC-induced meridional heat transport change can be simply due to a change in V, i.e., $\Delta V(T_u - T_b)$, but does not necessarily require an exchange of water masses between gyres. Furthermore, since the meridional heat transport change is in proportion to changes in V, any changes in SST produced by the meridional heat transport change should be linearly dependent upon changes in AMOC strength. In contrast, the oceanic mechanism studied here relies on water mass exchange between the northern subtropical and tropical gyres and the SST responds nonlinearly to AMOC changes. We argue that the tropical SST change is not simply governed by the meridional heat transport change $\Delta V(T_u - T_b)$. To illustrate this point further, we compare the meridional heat transport and temperature response

between two sets of simulations. In the first set (Case 1), we ran the model with 14 Sv(CTRL) and 0 Sv AMOC forcing(L10NG7C_0Sv) with a subsurface temperature front of 7°C . In the second set(Case 2), we ran the identical model but set the amplitude of the subsurface temperature front to zero. As shown in Figure 3.16, although the northward meridional heat transport in both cases is substantially reduced by an order of 1 PW in response to the AMOC shutdown, simulated temperature changes are very different. In Case 1, pronounced warming is spread over the deep tropics, whereas temperature change in the Case 2 is essentially absent.

The study presented here suggests that to understand how Atlantic SST responds to AMOC changes it is not sufficient to just study meridional heat transport changes. The SST response to AMOC changes is governed by a set of complex oceanic and atmospheric processes. A comprehensive understanding of this issue requires an understanding of interactions between the wind-driven and thermohaline circulations along the western boundary, as well as an understanding of ocean-atmosphere interactions.

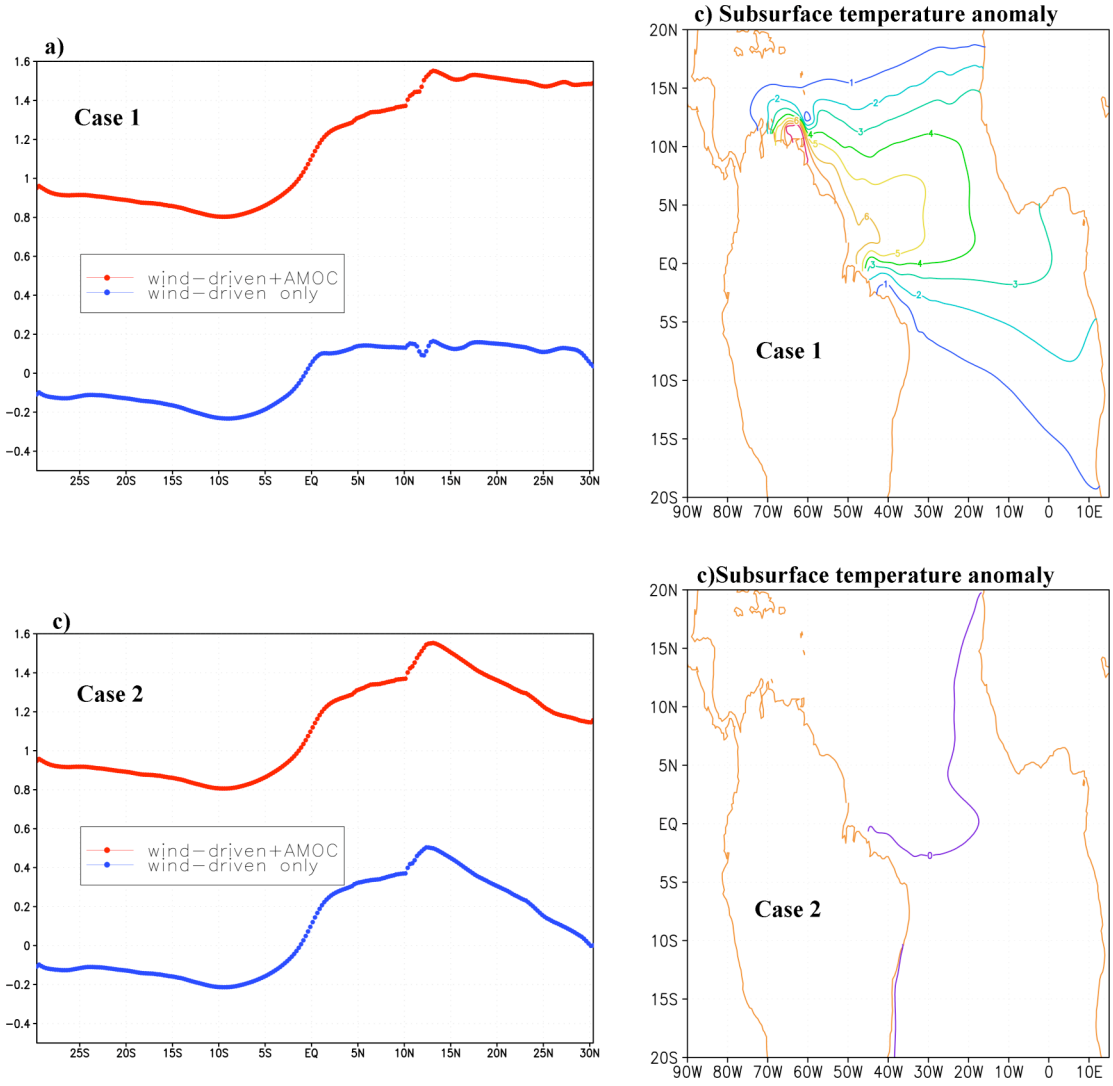

Figure 3.16 Simulated zonal annual mean heat transport (in unit of PW) in the upper ocean and subsurface temperature change (in unit of °C) in the presence of a subsurface front gradient of 7°C (Case 1, top panels) and in the absence of a subsurface front gradient (Case 2, bottom panels). In each case, the simulation with the AMOC forcing is contrasted to the simulation without the AMOC forcing (blue). Left panels show meridional heat transports for both cases. For both cases, the meridional heat transport without the AMOC forcing (blue) is decreased by about 1 PW compared to that with the AMOC forcing. Right panels show the subsurface temperature changes with and without the AMOC forcing for both cases.

CHAPTER IV
EFFECT OF ATLANTIC MERIDIONAL OVERTURNING CIRCULATION CHANGES ON TROPICAL ATLANTIC VARIABILITY: A REGIONAL COUPLED MODEL STUDY

4.1 Introduction

In Chapter III, we explored the oceanic teleconnection mechanism proposed by Chang et al. (2008) in details within a framework of a 2-1/2-layer reduced gravity ocean (RGO) model. The ocean-alone experiments show that a substantial warming in the Gulf of Guinea and off the coast of Africa occurs when the weakening of the AMOC causes a reversal of the direction of the North Brazil Undercurrent (NBUC). We thus concluded that this mechanism is mainly responsible for SST changes in the equatorial south Atlantic. On the other hand, Chiang and Bitz (2005, hereafter CB05), as previously mentioned, suggested that a cooling in high latitudes could be readily transmitted to the tropics through the wind-evaporation-SST (WES) feedback. It operates by intensifying northeasterly trade winds that leads to an increase in the latent heat loss and a cooling in the northern tropical Atlantic, resulting in a southward shift of ITCZ. In a follow-up study, Chiang et al. (2008) further argue that the WES feedback plays a more important role than the oceanic dynamical adjustment in the equatorward progression of SST anomalies induced by the weakening of the AMOC.

Although the previous studies have shed some light on the connecting mechanisms between changes in the high latitude and tropical Atlantic, more detailed studies are needed to fully explore the sensitivity of tropical Atlantic climate response to AMOC changes. This is because atmospheric and oceanic processes may exert competing influences on the tropical Atlantic and it is important to understand how the net response is controlled by these competing processes. As pointed out by Chiang et al. (2008), the ocean adjustment tends to counter surface cooling in the north Atlantic by warming up subsurface temperature. Wan et al., 2009 explicitly show that the competing atmospheric and oceanic processes give rise to a complex response of the Caribbean SST

to AMOC changes. Zhang (2008) also highlight the importance of atmosphere-induced surface cooling and ocean-induced subsurface warming in Atlantic decadal variability associated with the AMOC.

Using an ocean-only model, we show in Chapter III that a shutdown of the AMOC induces surface warming in the entire tropical Atlantic. This suggests that the ocean dynamical adjustment alone cannot explain the dipole-like SST pattern associated with AMOC changes. Thus, to fully explain the response of tropical Atlantic to AMOC changes, it is necessary to consider contributions from both oceanic and atmospheric processes. For this, we need a coupled ocean-atmosphere model. Although fully coupled global circulation models (CGCM) provide most comprehensive simulations of climate variability/change, it can be difficult to clearly delineate underlying dynamics in these models due to complexities of coupled air-sea interactions and teleconnection mechanisms. Therefore, it is sometime useful to use a reduced-physics coupled climate model to examine underlying dynamical processes.

In this study, we will present such a model. The new model is a regional coupled model (RCM) that consists of an AGCM coupled to a 2-1/2-layer reduced gravity ocean (RGO) model over the tropical Atlantic basin described in Chapter II. The model not only has the advantage of computational efficiency that permits a large number of sensitivity experiments, but also includes a number of novel features that are well suited for examining the relative importance of oceanic and atmospheric teleconnections. For example, the return limb of the AMOC can be controlled directly by varying the imposed mass transport at the open boundaries of the ocean model, as demonstrated in Chapter III. The use of regional coupling strategy also allows for an effective separation of AMOC's influence on tropical Atlantic variability (TAV) from other remote influences, such as El Niño-Southern Oscillation (ENSO). By forcing the atmosphere and ocean model independently, we can further isolate the effect of atmospheric processes on TAV from that of oceanic processes. Moreover, the simplified ocean dynamics make it easier and more straightforward to diagnose relevant dynamical processes.

The main objective of this Chapter is to elucidate the relative importance of atmospheric processes versus oceanic processes in AMOC-induced TAV change. In particular, we will focus on two specific scientific questions:

First, what is the role of the oceanic and atmospheric teleconnection in affecting the annual cycle of the Atlantic cold tongue/ITCZ complex (Mitchell and Wallace, 1992)? Coupled model experiments show that a shutdown of the AMOC has a significant impact not only on the climatological mean state of SST, but also on the equatorial SST seasonal cycle with the strongest change occurring during boreal summer and fall (Haarsma and Hazeleger, 2007; Chang et al., 2008; Wu et al., 2008). Both oceanic dynamics and atmospheric processes may contribute to the marked seasonal response of SST to AMOC changes. Chapter III is devoted to testing the former. The later, however, has not been systematically explored. It is widely recognized that there is a close linkage between tropical Atlantic SST and rainfall variability over the Nordeste region of Brazil and the Sahel region of West Africa based on numerous observational and modeling studies (Moura and Shukla, 1981; Hastenrath, 1984; Nobre and Shukla, 1996; Fontaine et al., 1999). A question we will be addressing in this Chapter is how changes in the SST seasonal cycle induced by AMOC changes affect the seasonal variation of the precipitation in these regions. We will conduct numerical experiments to investigate the annual cycle response of the SST and associated rainfall of the tropical Atlantic to a shutdown of the AMOC and the relative role of atmospheric and oceanic processes in this response.

Second, what is the role of oceanic and atmospheric processes in determining the behavior of the SST response to changes in the AMOC? In Chapter III, sensitivity experiments show that tropical Atlantic SST response to AMOC changes behaves nonlinearly in an ocean-alone model. The warming rate of the SST increases dramatically when the AMOC strength is below a threshold value of about 8 Sv. At this threshold the equatorward transport carried by the northern STC is approximately equal to the northward transport carried by the NBUC. The study, however, did not take into consideration ocean-atmosphere feedbacks and atmospheric processes. It is not clear

whether the nonlinear behavior of the SST response will hold in a coupled system. In this Chapter, we will conduct sensitivity experiments to investigate the behavior of the SST response and the associated atmospheric response in the tropical Atlantic by varying AMOC strength systematically.

The chapter is organized as follows. Section 4.2 provides an introduction of the RCM and a description of the experiment design. Section 4.3 gives an evaluation of model simulation of tropical Atlantic climate. Section 4.4 discusses the influence of AMOC change on tropical Atlantic climate and relative contribution of atmospheric and oceanic processes. In Section 4.5, we examine the sensitivity of tropical Atlantic response to changes in AMOC. Our major results will be summarized and discussed in Section 4.6.

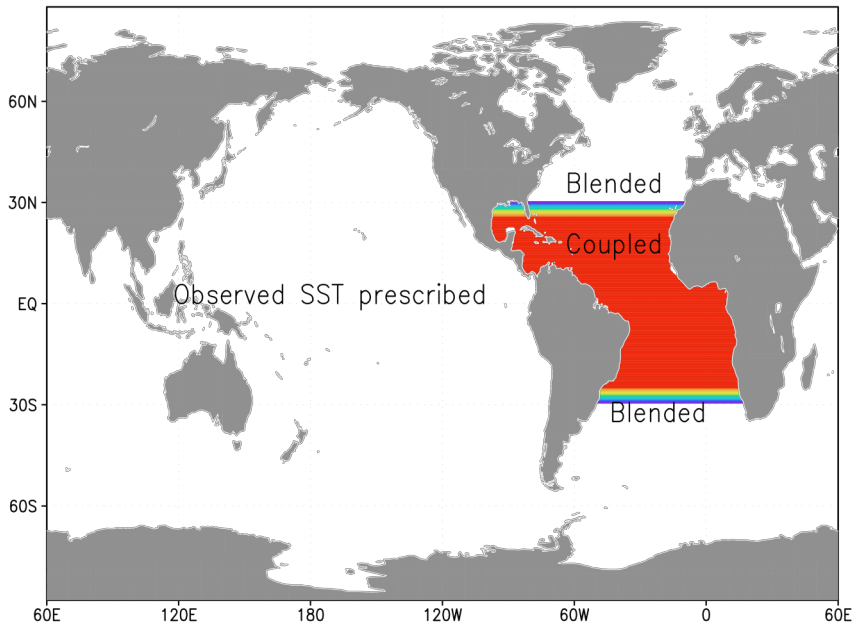

Figure 4.1 The regional coupling strategy over the global domain. The model is fully coupled in red. The rest of the oceanic regions are prescribed by observed SST. Two zonal belts with changing color are blending zones for SST.

4.2 Atlantic RCM and experiment design

The atmospheric component, AGCM, of the RCM used in this study is the Community Climate Model version 3.6.6 (CCM3) developed at the National Center for Atmospheric Research (NCAR). The horizontal resolution of the AGCM used in this study is the standard resolution T42 (triangular spectral truncation at wave number 42, corresponding to a grid resolution of about 2.8° x 2.8° in the Tropics). It has been shown that the CCM3 is able to capture the major global-scale features of atmospheric circulations (Hurrell et al., 1998) and reproduce a fairly realistic atmospheric response to SST variability in tropical Atlantic sector (Saravanan and Chang, 2000; Chang et al., 2008). The oceanic component of the RCM is the RGO model described in Chapter II.

The CCM3 is fully coupled to the RGO within the tropical Atlantic from 30°S to 30°N. The CCM3 exchanges surface fluxes with the RGO once per day, at which the daily mean surface heat fluxes and wind stresses from the CCM3 are provided to the RGO, while the simulated SST from the RGO is supplied to the CCM3. Outside of the tropical Atlantic (30°S to 30°N), observed annual cycle of SST is prescribed for the CCM3 (Figure 4.1).

As aforementioned, the primary objective of this study is to identify the relative contribution of the atmospheric and oceanic processes to the responses of tropical Atlantic to AMOC changes. A way of assessing these contributions from these processes is to conduct a suite of experiments where only one or both teleconnection mechanisms are present. The following is a brief description of the experiments conducted in this Chapter:

Control (CTRL) run: A 14Sv mass transport is specified at the northern open boundary of the oceanic component to mimic the return flow of the AMOC. This run forced by a ‘realistic’ combination of winds and the AMOC represents “the current climate state”. The experiment consists of a 120-yr single integration and approaches to an equilibrium state after about 10-years of integration. The model climatology and variability are derived from the last 80 years of simulation.

Ocean Mechanism Experiment (OME): This simulation is the same as the CTRL run except that the northward mass transport at the open boundaries of the oceanic component is set to zero, representing a climate state when the AMOC is shutdown completely. Since no other external forcing is present in the model, the difference between this and the CTRL run should only be attributed to the shutdown of the AMOC. Thus, this experiment allows us to examine the extent to which the oceanic teleconnection contributes to the TAV response to a shutdown of the AMOC.

Atmospheric Mechanism Experiment (AME): In this experiment, the RGO is forced by a negative surface heat flux anomaly derived from an ensemble of GFDL climate model (GFDL CM2.1) water hosing runs (Zhang and Delworth, 2005) between 10°N and 30°N. The rest of the model configuration is identical to that of the CTRL run. Since the AMOC return flow is kept at the same value as the CTRL run, this experiment allows us to test the effect of AMOC-induced cooling in the North Atlantic on TAV via the atmospheric teleconnection process.

Oceanic-Atmospheric Mechanism Experiment (OAME): In this experiment, the northward mass transport at the open boundaries of the oceanic component is set to zero as in the OME and the heat flux anomaly is applied to the RGO between 10°N and 30°N as in the AME. Since both forcings are used simultaneously, this experiment is designed to assess the combined effect of oceanic and atmospheric teleconnection on the TAV response to AMOC changes.

It is worth pointing out that in a fully-coupled model water hosing experiment, the surface cooling in the high-latitude north Atlantic occurs together with the weakening of the AMOC. Both the surface cooling and the AMOC change can affect TAV. In our experiments, we artificially separate these effects in order to evaluate their relative contribution to TAV. One may argue this separation is dynamically inconsistent, but we believe this is necessary in order to gain dynamical understanding of each process.

The above-described three sensitivity experiments start from the same equilibrium state of the CTRL run at year 10. Each consists of an 80-year integration.

All the analyses shown below are based on the last 65 years of the 80-year integration. Unless stated otherwise, anomalies of each experiment are refered to as the difference between the corresponding sensitivity run and the CTRL run. Before preceding to the discussion of the sensitivity runs, we first evaluate simulated the Atlantic mean climate and climate variability in the model CTRL integration.

4.3 Model validation

Before using the newly developed modeling tool to investigate the underlying mechanisms by which AMOC changes affect tropical Atlantic climate variability, it is necessary to evaluate the performance of the model by comparing the simulated tropical Atlantic climate in the CTRL run with observations. As will be demonstrated below, our RCM captures both the climatology and climate fluctuations ranging from seasonal to interannual time scales.

4.3.1 Annual mean state

Figure 4.2 shows the simulated and observed annual mean state of SST, surface wind stresses and precipitation. The RCM captures the gross features of the observed mean climate state, though with some apparent error in certain areas. Compared with the Reynold SST analysis (Smith et al., 1996), the model underestimates the annual mean SST over most of the tropical Atlantic basin by about 1°C except that excessive warm bias is found along the coast of Angola with a maximum error of 3°C. This warm bias has been identified as a common problem for nearly all fully coupled GCMs (Davey et al., 2002; Breugem et al., 2007). Many hypotheses have been put forward to explain the cause of this warm bias, such as insufficient amount of stratus cloud (Wang et al.1999; Yu and Mechoso, 1999) and inadequate representation of vertical mixing (Hazeleger and Haarsma, 2005). Our analysis suggests that an underestimation of the

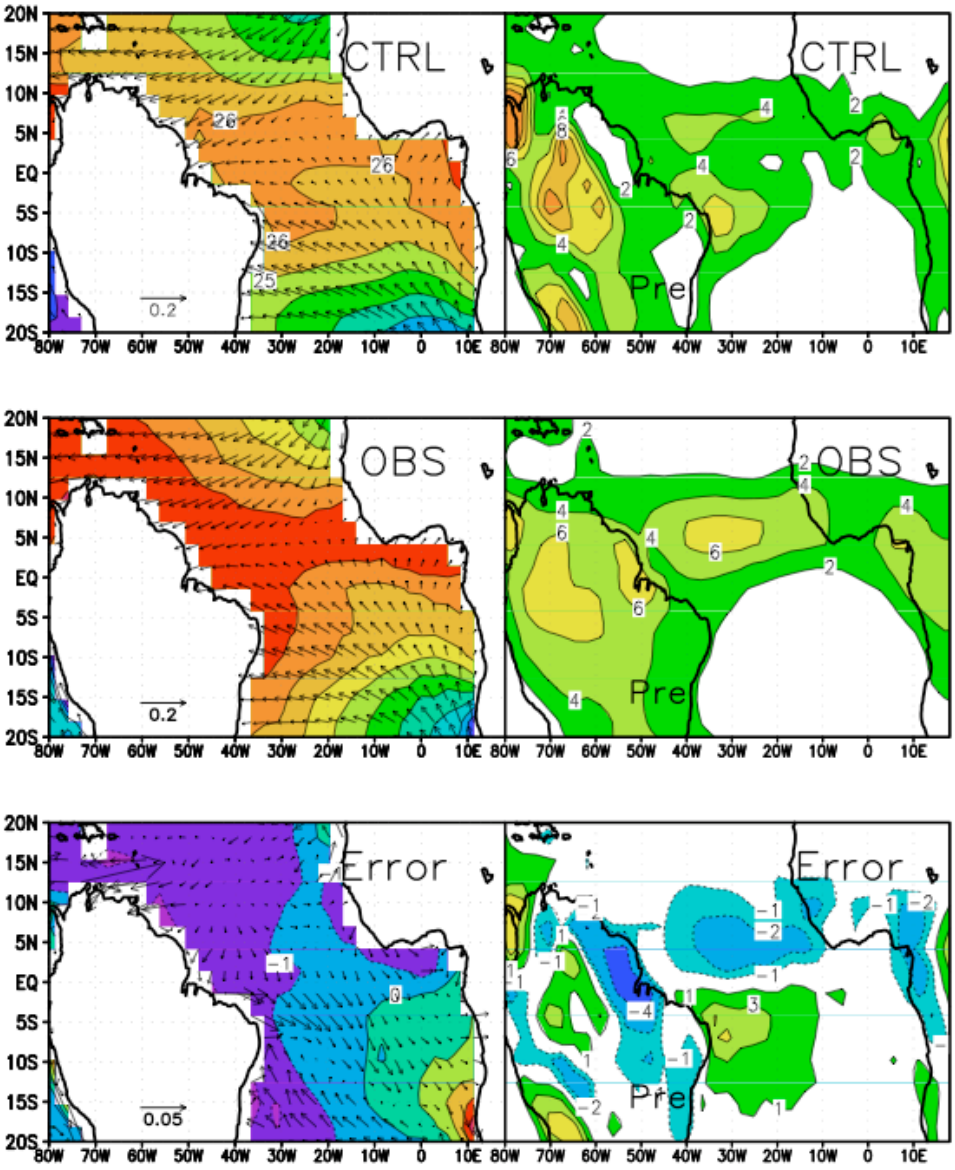

Figure 4.2 The annual mean state of the SST and surface windstress (left panels) and precipitation (right panels). Top panels: CTRL. Middle Panels: Observations. Bottom panels: difference between the CTRL run and observations. The vector unit is in N m^{-2}.

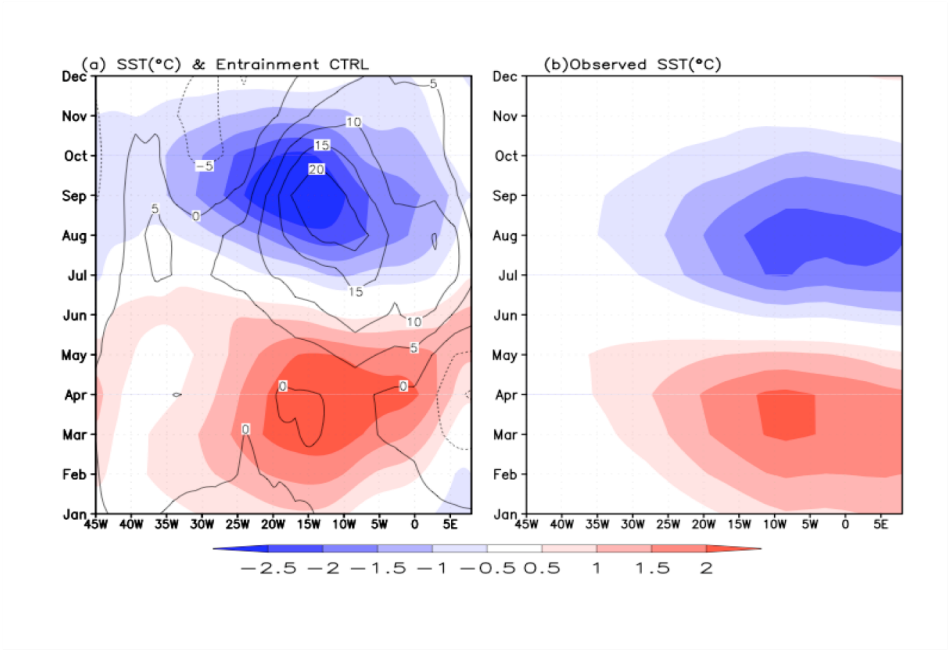

Figure 4.3 (a) Seasonal cycle of simulated SST and entrainment (in 10^{-6} m s^{-1}) from the CTRL run. (b) Seasonal cycle of observed SST (Reynolds et al., 2002).

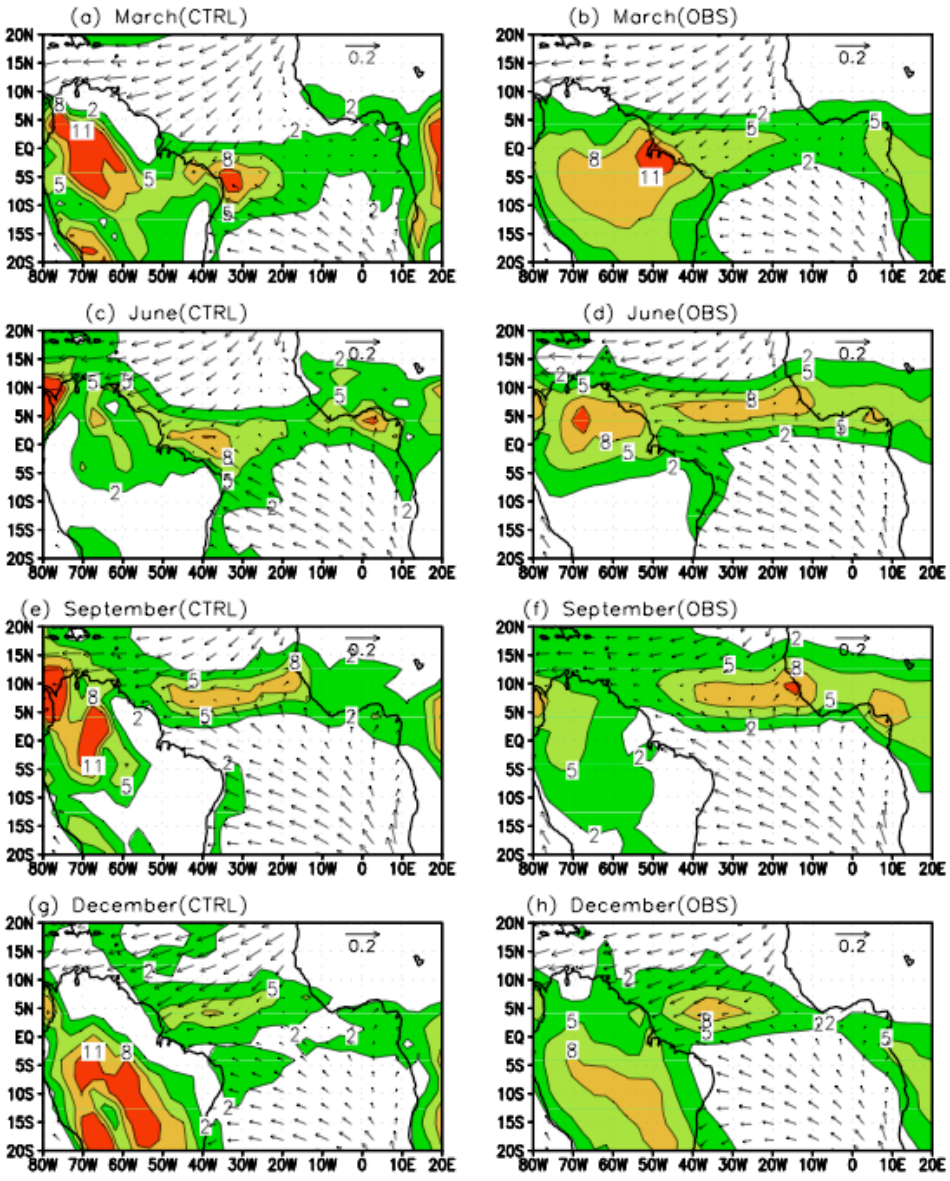

Figure 4.4 Annual cycle of precipitation and surface wind stress(a),(c),(e),(g) in the CTRL run, and (b),(d),(f),(h) in the GPCP data set and NCEP reanalysis respectively. The contour interval of precipitation is 3mm day^{-1} ,starting with 2mm day^{-1}. The vector unit is N m^{-2}.

coastal upwelling may be the major source of the warm bias. The simulated southeasterly trade wind in the model is weaker than the wind in the NCEP reanalysis (Kalnay et al., 1996) from the equator to around 15°S, located north of the warm SST bias. The intensity and location of the ITCZ is reasonably well simulated in comparison with the observation from the Global Precipiation Climatology Project (GPCP) (Huffman et al., 1997), although the heavy precipitation band over the ocean spreads too far southward along the Brazilian coast, giving an appearance of a 'double ITCZ'.

4.3.2 The annual cycle

One of the most prominent features of Atlantic climate variability is the pronounced annual cycle of the cold tongue. Figure 4.3a depicts the seasonal cycle of simulated SST (color) and entrainment velocity at the base of the mixed layer (contour) along the equator. Both the simulated amplitude and phase of SST agree reasonably well with the observation shown in Figure 4.3b, except that the simulated cold tongue variation is located to the west of the observed variation and lags the observation by about 1 month owing to the delayed development of the vertical entrainment at the base of the mixed layer.

Figure 4.4 compares the observed precipitation and NCEP reanalysis surface wind stresses with the simulated precipitation and wind stresses. The observation shows that the ITCZ migrates from the equator in March (Figure 4.4b) to 10°N in August and returns to the equator during winter (Figure 4.4h). This seasonal migration of the ITCZ is well captured by the model, although the phase of the annual cycle in the model during the boreal spring tends to lag the observation by about one month, owing to the delay in SST annual cycle. Over West Africa, the rainy season starts in late spring or early summer (May-June), which marks the onset of the West African Monsoon. During these months, the maximum precipitation is located along the upper Guinea coast (Figure 4.4d). As the season progresses, the maximum precipitation band moves northward to around 10°N at the peak of the monsoon during late boreal summer

(August-September) (Figure 4.4f). This seasonal variation of the monsoon rainfall over West Africa is also reproduced reasonably well by the model.

While the RCM captures many of the observed features, there are noticeable deficiencies in the CTRL simulation that are related to some well-known shortcomings of CCM3 (Chang et al., 2000). For example, the model produces an unrealistically strong precipitation belt located between 5°S and 10°S off the Brazilian coast during boreal spring when the model SST is warmest in this area. The heavy rainfall band over the ocean tends to shift westward compared to the observation and the precipitation is generally overestimated over the land. Also, the precipitation over West Africa is underestimated during the monsoon season, while the Caribbean rainfall is overestimated.

4.3.3 Interannual SST variability

The tropical Atlantic interannual-to-decadal SST variability is dominated by a zonal mode with a strong zonal gradient in the eastern equatorial region and a meridional mode with a cross-equatorial gradient (e.g. Ruiz-Barradas et al., 2000). These two patterns of variability can be described by the first two leading EOFs derived from the NCEP reanalysis SST (Kalnay et al., 1996) anomalies over the period from 1950 to 2007(Figure 4.5c,d). Note that all the principle components (PC) that are associated with EOFs shown in Figure 4.6 have been normalized by their standard deviation, so that the amplitude of each mode is reflected by EOF pattern. As shown in Figure 4.5, the leading SST patterns derived from the observation can be reproduced quite realistically by our

regional coupled model. The zonal mode resembles the observation very well in term of the spatial distribution and amplitude except that the maximum is centered to the west of the cold tongue as shown in the observed counterpart. This discrepancy may be associated with the systematic warm SST bias in the model. The north-south contrast SST anomaly distribution, which is the key feature of the meridional mode, is well captured by the model. However, the anomaly in the southern hemisphere is much weaker than the observation.

One distinctive feature of the two dominant climate fluctuations of tropical interannual climate variability is their seasonal preference. The zonal mode peaks in boreal summer while the meridional mode has peak variability in boreal spring. Figure 4.6 presents standard deviation of PC series associated with these two modes derived from the Ctrl run and observation. It shows that the zonal mode resembles closely the observations with a moderate phase delay (Figure 4.6a). The delay may be attributed to the delay in the development of cold tongue discussed in Section 3.3.1. The simulated meridonal mode agrees well with the observation and has a sharp peak in Mar-Apr-May (Figure 4.6b).

In summary, the RCM reproduces fairly well the mean state and major features of the seasonal cycle of SST and precipitation in the tropical Atlantic. In addition, the RCM successfully reproduces the dominant fluctuations of tropical Atlantic SST variability on interannual time scales. Overall, we conclude that this simple coupled model is suited for our sensitivity studies.

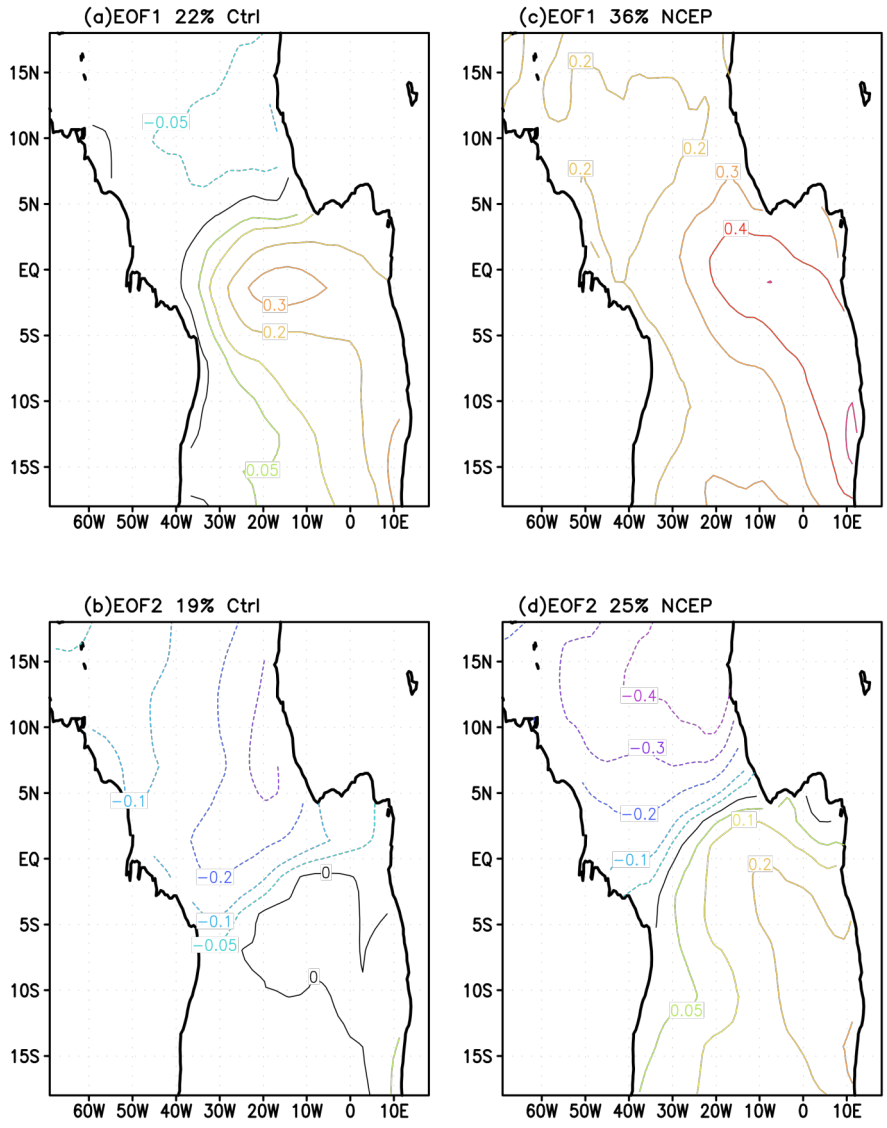

Figure 4.5 The first (top panels) and second(bottom panels) EOFs derived from the 80-yr CTRL simulation(left panels) and from NCEP reanalysis SST over the period 1950-2007. Note that the associated PC time series are normalized by their standard deviations).

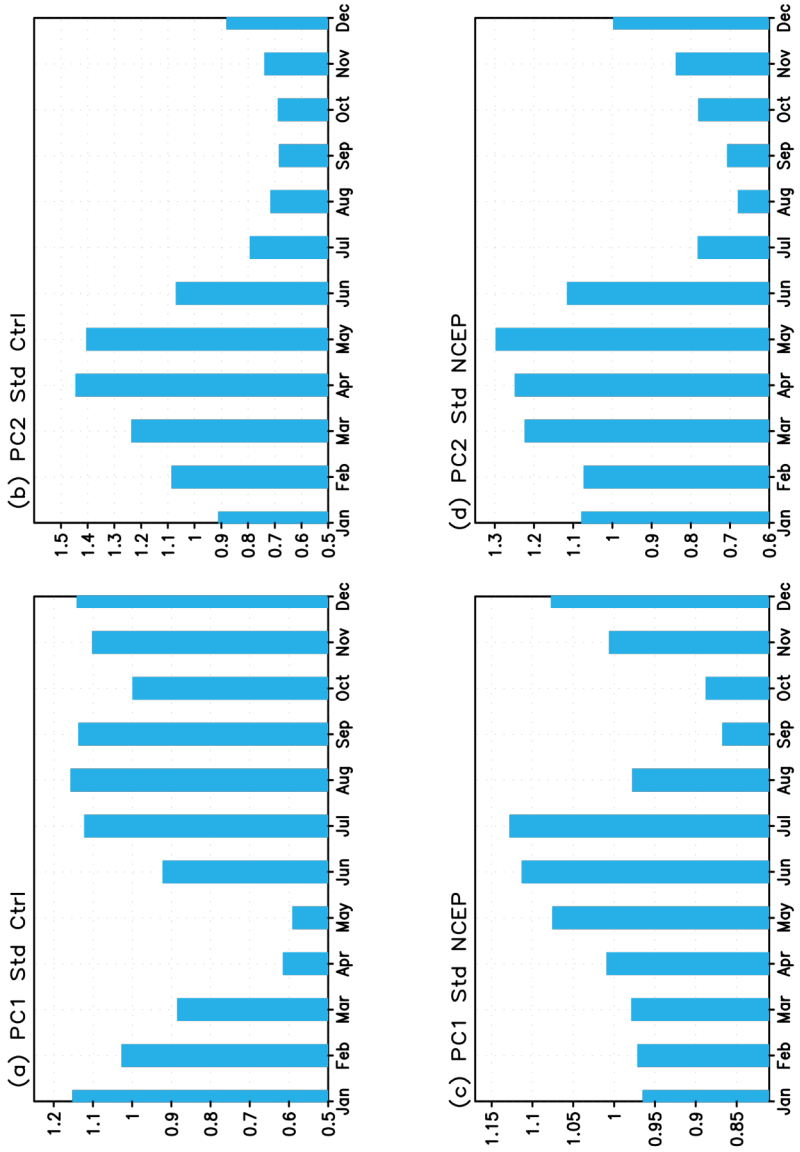

Figure 4.6 Standard deviation of the leading PC time series associated with zonal mode(left panels) and meridional mode(right panels) from the CTRL run(top panels) and NCEP reanalysis SST(bottom panels).

4.4 Impact of AMOC change on TAV

In this section, we will first explore mechanisms through which AMOC influence is progressed to the tropical Atlantic and then assess the impact of the AMOC on tropical Atlantic climate. We will begin our discussion with OAME where both the oceanic and atmospheric forcings are included in the simulation. We will show that the tropical Atlantic response in OAME resembles that of water hosing experiments conducted using fully coupled GCMs (e.g. Stouffer et al. 2006; Timmermann et al. 2007). We will then compare the result of OAME to the results of other experiments to evaluate the relative importance of the oceanic versus atmospheric teleconnection mechanisms. Finally, we will discuss how the changes in the tropical Atlantic SST can have an impact on rainfall variability in the region.

4.4.1 Simulated tropical Atlantic response to the collapse of AMOC

Figure 4.7a and Figure 4.8a show the simulated ocean temperature and circulation anomalies in OAME within the mixed layer and the thermocline layer, respectively. Consistent with fully coupled GCM water hosing simulations, an interhemispheric seesaw pattern in the SST response emerges with a strong cooling in excess of 2.5°C in the North Atlantic and a warming on the order of 0.8°C along the equator and along the upwelling zones of the southeastern tropical Atlantic (Figure 4.7a). Within the model thermocline layer, warm temperature anomaly is seen to emanate from the western boundary region off the coast of upper South America, spreading into the deep tropics. The dominant feature of the ocean circulation change is along the western boundary where the current is substantially weakened in the OAME (Figure 4.8a). Large-scale circulation response of the atmosphere is also consistent with fully coupled GCM water-hosing experiments. The northeast trade winds are strengthened in the OAME, while the southeast trades experience little or no changes. Accompanied with the change in the trade winds, the mean position of the ITCZ shifts

southward as indicated by the southward shift of zero meridional-wind line, resulting in a decrease of precipitation rate to the north of the equator by about 2 mm/day and an increase to the south of the equator by about 1.5mm/day (Figure 4.9a). Over the adjacent continents, there is an increase of precipitation over the Northeast Brazil and along the northern coast of the Gulf of Guinea. This change in the atmospheric circulation is reflected in the Hadley Circulation. As shown in Figure 4.10a, the imposed AMOC forcing gives rise to a southward shift of the Hadley circulation, as clearly indicated by the enhanced (reduced) upward vertical velocity south (north) of the mean ITCZ in the CTRL run.

The fact that the RCM result agrees generally well with the results of fully coupled GCM water hosing simulations (e.g. Stouffer et al.2006; Timmermann et al. 2007) suggests that the RCM contains the essential oceanic and atmospheric teleconnections linking AMOC changes to tropical Atlantic. However, it is noteworthy that the trade wind response in the south Atlantic simulated by the RCM is generally weaker than that found in many fully coupled GCMs experiments, suggesting that not all teleconnection mechanisms may be included. Nevertheless, we assume that major features of tropical Atlantic response to AMOC changes are captured and proceed with further examination of the underlying dynamic mechanism.

4.4.2 Oceanic versus atmospheric teleconnection mechanisms

The OAME run reveals that both the ocean circulation change caused directly by a shutdown of the AMOC and the atmosphere circulation change induced by the surface cooling in the North Atlantic contribute to the interhemispheric SST dipole anomaly and the corresponding southward shift of the ITCZ in the tropical Atlantic. In this subsection, we attempt to address the following questions: Is the interhemispheric SST dipole anomaly caused by the oceanic or by the atmospheric mechanism? Or is it caused by

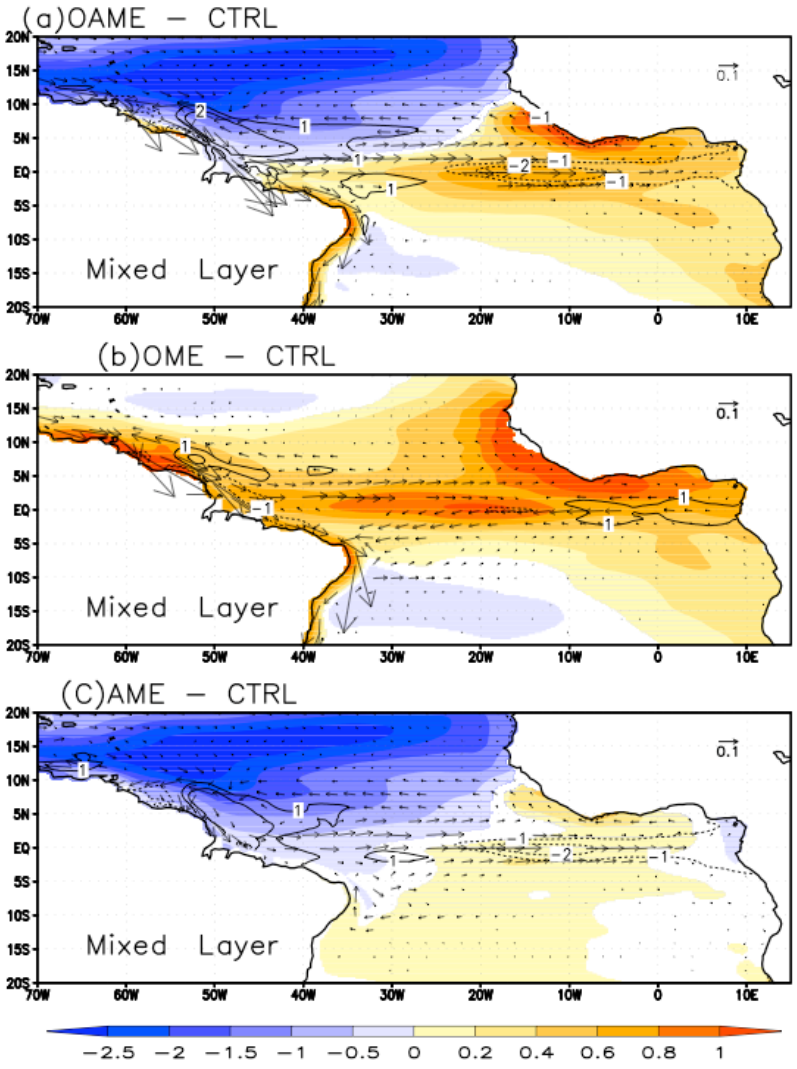

Figure 4.7 SST anomaly(color in °C), velocity anomaly(vector in m s^{-1}) and entrainment anomaly(contour in 10^{-6}m s^{-1}) generated in OAME run (a), OME run(b) and AME run(c) in the mixed layer. Plotted values are significant at the 95% statistical significance level using t-test.

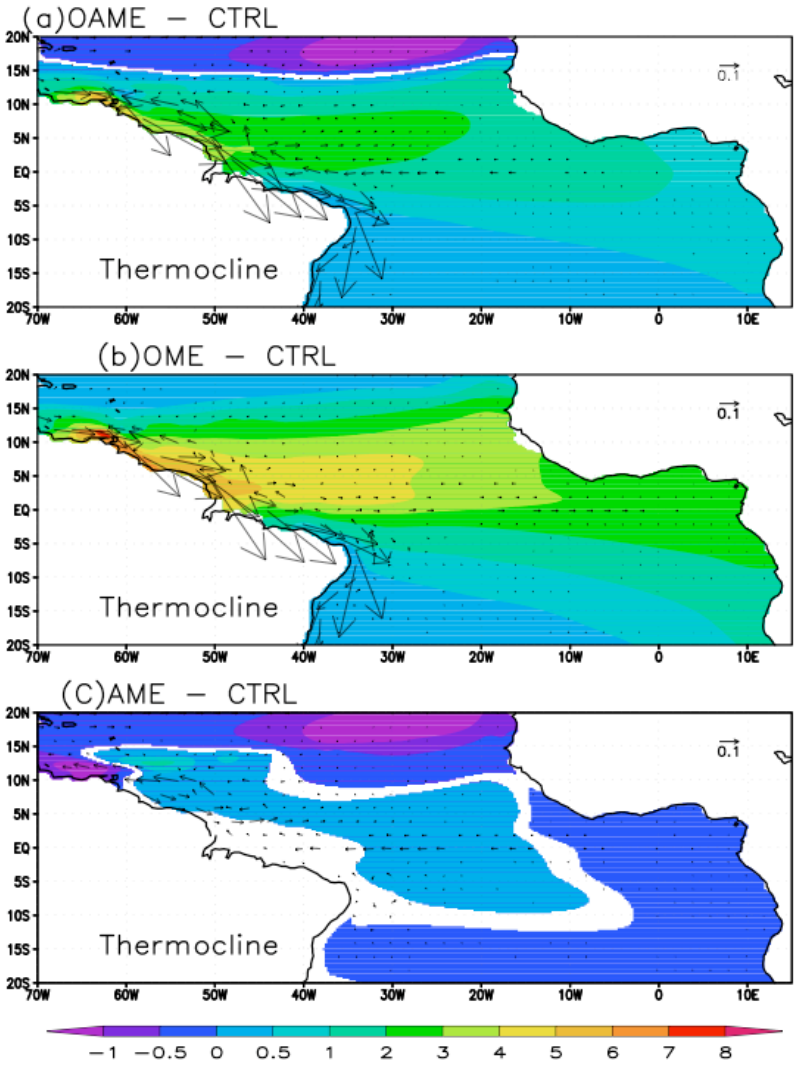

Figure 4.8 The annual mean temperature anomaly (color in °C) and velocity anomaly(vector in m s^{-1}) generated in the OAME run(a), OME run(b) and AME run(c) in the thermocline layer. Plotted values are significant at the 95% statistical significance level using t-test.

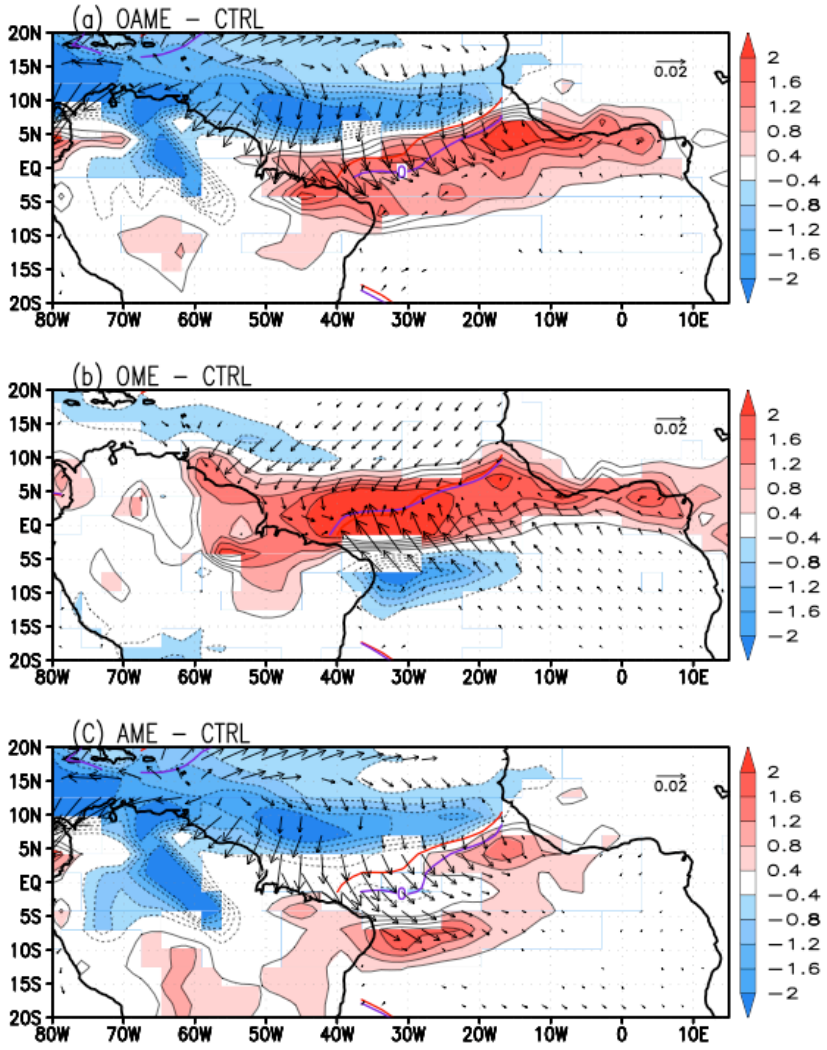

Figure 4.9 The annual mean precipitation anomaly(contour in mm/day) and surface wind stress anomaly(vector in N m^{-2}) generated in OAME run(a), OME run(b) and AME run(c). The red and purple lines represent the annual mean τ_y=0 lines in the CTRL run and experiment, respectively. For windstress anomaly, only values exceeding 95% statistical significance are drawn. For precipitation anomaly, shaded area exceeds the 95% significance level using t-test.

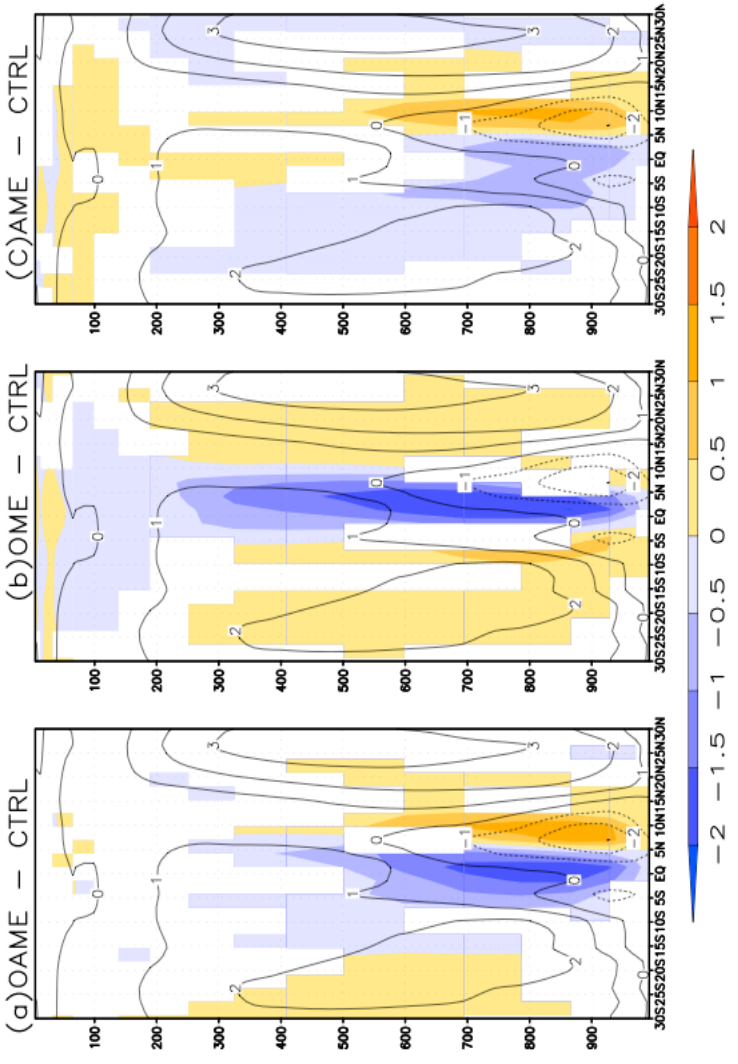

Figure 4.10 Anomalous pressure vertical velocity (color in hPa s^{-1}) averaged over 50°W-10°E in the OAME run(a), OME run(b) and AME run(c). Contour line: CTRL run. Negative values indicate upward motion. Shaded area exceeds the 95% statistical significance level using t-test.

both? Which of the mechanisms is, or are both responsible for the southward displacement of ITCZ?

To answer these questions, we first turn to the OME run where the response in the tropical Atlantic can only be attributed to the ocean circulation change caused directly by the shutdown of the AMOC, because the surface cooling in the North Atlantic is absent. As shown in Figure 4.7b and Figure 4.8b, the coupled model response is similar to that of ocean-alone discussed in Chapter III, where similar experiments were conducted using the RGO model. The most salient circulation change in response to the shutdown of the AMOC occurs in vicinity of the western boundary. Accompanied with the circulation change, a pronounced subsurface warming takes place along the western boundary off the coast of upper South America and spreads into the deep tropics. Without the influence of cooling in the north Atlantic, the subsurface warming in the OME run is stronger than that in the OAME run.

As shown in Chapter III, the removal of the interhemispheric flow in the model causes the NBUC that carries much of the AMOC return flow (Fratantoni et al., 2000) to reverse its direction from north to south. This change of circulation has two major effects on the tropical Atlantic thermocline water: 1) It produces a strong subsurface warming by anomalous heat advection in the region where the strong temperature front between the subtropical and tropical gyres intersects the western boundary; 2) it changes the pathway of the northern STC by allowing the warm northern subtropical gyre water to enter the equatorial region, causing warming in the equatorial thermocline. This subsurface warming gives rise to surface warming in the entire tropical Atlantic with strong warming along the African coast, near the equator in the central Atlantic and along the northern coast of North Brazil, where upwelling is strong (Figure 4.7b). It indicates that the changes in ocean circulation alone do not produce a dipole-like SST anomaly, instead they give rise a warming in the entire tropical Atlantic.

The atmospheric response to this basin-wide warming is different from that in the OAME. The basin-wide warming over the tropical Atlantic mainly enhances the Hadley

circulation (Figure 4.10b), while displacing the maximum vertical velocity slightly southward. Instead of a positive and a negative vertical velocity anomaly that straddle the center of upward motion of the mean Hadley Circulation in the OAME (Figure 4.10), the anomalous vertical velocity in the OME run has a single core situated just south of the center of upward motion (Figure 4.10b). The enhanced Hadley circulation results in an anomalous convergence just north of the equator, which in turn enhances the trade winds in the deep tropics. The ITCZ responds with an increase in precipitation along its mean position. Figure 4.9b shows clearly a positive precipitation anomaly along the mean convergence zone accompanied by two weak negative anomalies in the two subsidence branches of Hadley circulation.

In contrast to the OME run, the AME run produced a strong surface cooling in the north Atlantic, but only a very weak surface warming in the tropical South Atlantic (Figure 4.7c). To the north of 10°N, the cooling is a direct response to the imposed anomalous surface heat flux. South of it, the cooling is a result of the WES feedback where intensification of the northeasterly trades causes an increase in latent heat flux which drives the cold SST anomaly equatorward. In response to the surface cooling, the ITCZ moves southward with strengthened northeasterly (weakened southeasterly) trades (Figure 4.9c). These features appear broadly consistent with the WES feedback, which involves interactions between the SST changes and wind-induced latent heat flux (Xie and Philander, 1994; Chang et al., 1997). Our result supports the CB05 speculation that the WES feedback is particularly effective in transmitting cooling toward the equator and is responsible for the southward displacement of ITCZ.

A comparison of the OAME, OME and AME runs reveals that ocean circulation change are responsible for the surface warming near and to the south of the equator, while the atmospheric processes contribute to the cooling in the northern tropical Atlantic and play only a minor role in the development of surface warming on and south of the equator. Our results indicate that, in terms of the annual mean state, the SST response can be well approximated by a linear superimposition of the responses induced by the oceanic and the atmospheric processes. However, this is not the case for the

precipitation response. In the AME run, the southward shift of the ITCZ induces an increase in the annual mean rainfall over Northeast Brazil by ~1.6mm/day (Figure 4.9c). The oceanic mechanism causes a decrease in precipitation over the same region by as much as 2.5mm/day (Figure 4.9b). A linear superposition of the two would yield a net decrease in the annual mean rainfall in this region. But the OAME produced a positive rainfall anomaly, indicating that precipitation responds nonlinearly. It also suggests that the rainfall response over the Northeast Brazil is mainly attributed to the atmospheric teleconnection. On the other hand, the precipitation response along upper Guinea coast appears to be more controlled by the oceanic processes (Figure 4.9b).

The competing and complementary influences of atmospheric and oceanic teleconnections on the tropical Atlantic response are also clearly seen during the transient state. To filter out the variability internal to the coupled system, we carried out three ensembles of runs with identical forcing of OAME, OME and AME, respectively. Each ensemble consists of five 30-yr integrations. The five ensemble members are initialized with slightly different conditions in the AGCM. All results are averaged over the ensemble members to reduce the effect of internal variability that may make it difficult to identify the coupled model response to the external forcings. Figure 4.11 depicts the evolutions of SST and the atmospheric response in the OAME, OME and AME ensemble runs.

In the AME (Figure 4.11c), the north Atlantic cooling is immediately transmitted toward equator and reaches equilibrium state within the first year. The response in the southern hemisphere is very weak. Associated with the surface cooling is the c-shaped cross-equatorial surface wind anomaly. The wind anomaly follows the cooling closely and quickly reaches equilibrium within a couple of years. In the OME, the positive SST anomaly centered around (0°-5°N) takes longer time to develop and reaches a full equilibrium state after eight years (Figure 4.11b). It is evident that the surface warming has a subsurface origin as the surface response lags subsurface warming (Figure 4.12). As discussed in Chapter III, the circulation change along the western boundary triggers the rapid built up of the subsurface temperature near the strong temperature front. The

warm anomaly is then carried equatorward along the western boundary by the reversed NBUC. Once the warm anomaly enters the equatorial zone, it propagates eastward along the equator by the EUC and equatorial Kelvin waves. These oceanic processes are responsible for the development of the subsurface temperature anomaly shown in Figure 4.8b. In the OAME, the coupled system response is driven by the fast atmosphere processes and the relatively slow oceanic processes (Figure 4.11a). The cooling in the north Atlantic and the wind anomaly rapidly develop within the first couple years. The warm SST anomalies at and to the south of the equator, however, take approximately 8 years to fully develop. This further demonstrates that the oceanic teleconnection is the dominant factor controlling the warming to the south of the equator as discussed above.

4.4.3 Impact of AMOC change on the seasonal cycle

In Section 4.4.1, it is shown that the AMOC changes significantly affect the climatological mean state of the tropical Atlantic. A question immediately arises: Does the tropical Atlantic response exhibit any seasonal dependence? In this subsection, we will discuss the impact of the AMOC change on the seasonal cycle of tropical Atlantic. To facilitate the analysis of the coupled response, we isolate the atmospheric and oceanic processes via comparison among the OAME, OME and AME runs as discussed in Section 4.4.2.

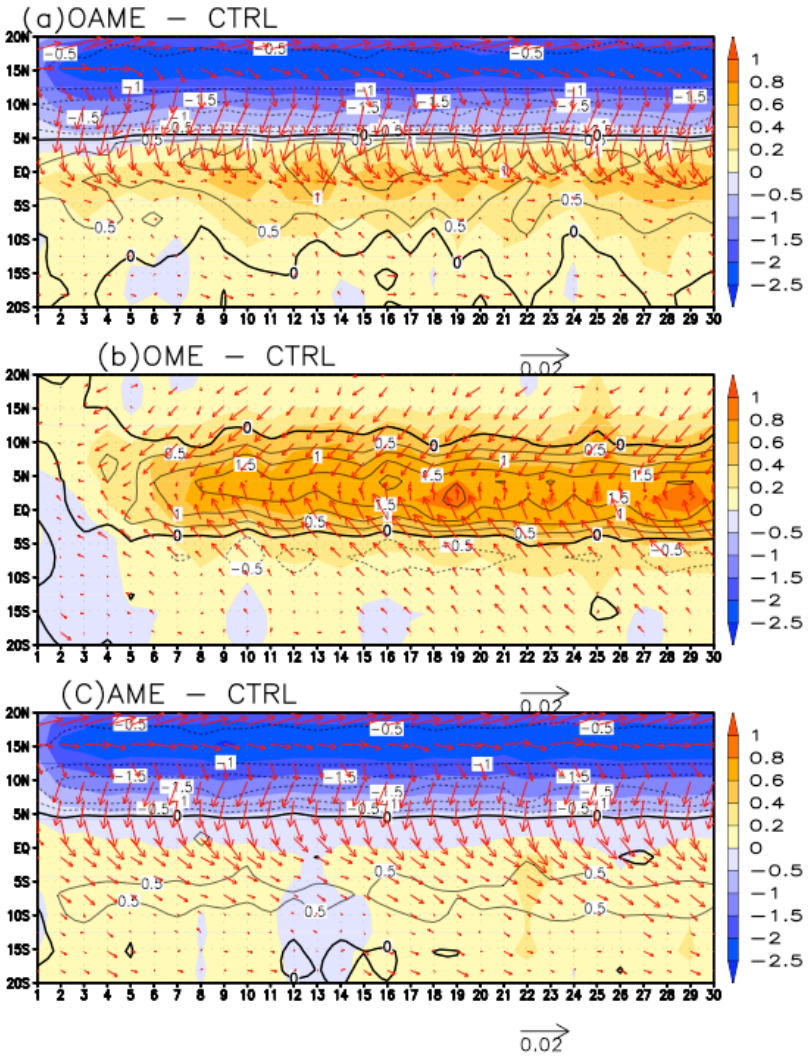

Figure 4.11 Time evolution of zonal averaged SST anomaly (color in °C), wind stress anomaly (vector in N m^{-1}) and precipitation anomaly (contour in mm/day) in a 5-member ensembe of OAME (a), OME (b) and AME(c). All variables are zonally averaged over (60° W-20°E). The anomaly is defined as the difference between ensemble mean and the CTRL run.

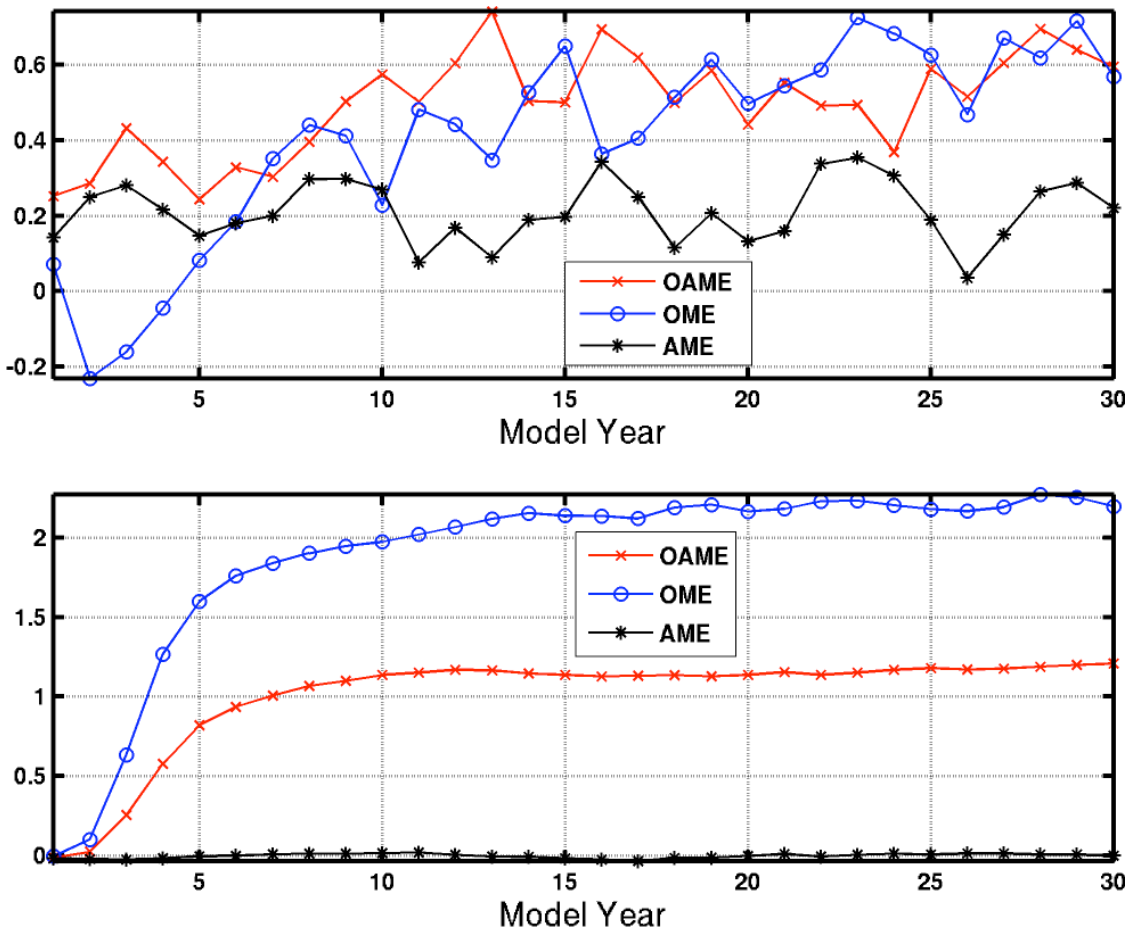

Figure 4.12 Time evolution of temperature anomaly averaged over (25°W-0°,5°S-0°) in the mixed layer(upper panel) and the thermocline layer(bottom panel).

In agreement with other coupled GCM water hosing experiments (e.g., Timmermann et al. 2007), our results show a marked seasonal cycle of tropical Atlantic SST response to the AMOC change. The strongest surface warming of more than 2°C occurs during July to September in the central equatorial Atlantic, whereas the strongest surface cooling of about -1°C occurs during February to May in the western equatorial Atlantic (Figure 4.13a). A comparison among the OAME, OME and AME reveals that both oceanic and atmospheric processes contribute to this seasonality. As shown in Figure 4.13b, the equatorial SST warming in the OME persists year around and peaks in boreal summer. The warming is mainly forced by the mean upwelling acting on the reduced vertical temperature gradient ($\bar{\omega}\frac{\partial T'}{\partial Z}$) and the reduction of upwelling ($\omega'\frac{\partial \bar{T}}{\partial Z}$) as a result of the deepening of the mixed layer (Figure 4.14). Both these terms are most effective during boreal summer and fall. In the AME, except during May to June, the southeasterly trade winds over the central equatorial Atlantic are strengthened most of the year and peak in boreal summer (Figure 4.15d) in response to the anomalous southward displacement of ITCZ. This leads to the deepening of mixed layer and the reduction of upwelling rate. The substantial reduction of entrainment during summer induces strong warming anomaly in this season. It needs to be pointed out that both wind and mixed layer thickness can affect the entrainment rate according to the Kraus-Turner model (Chapter II,Eq. 19). Strong wind tends to enhance entrainment rate, while deeper mixed layer tends to reduce entrainment. During boreal summer, the entrainment is reduced in response to the deepened mixed layer. During fall and winter, enhanced the trade winds increase upwelling, thus leading to cooling in these periods. Our results point to an important role of the oceanic process in causing the strong anomalous warming in summer. On the other hand, the influence of atmospheric processes is twofold: (1) enhancing the summer warming through reducing upwelling; (2) damping warming anomalies during fall/winter. Figure 4.13 also demonstrated that the cooling along the western basin in the OAME is attributed to the atmospheric processes. The

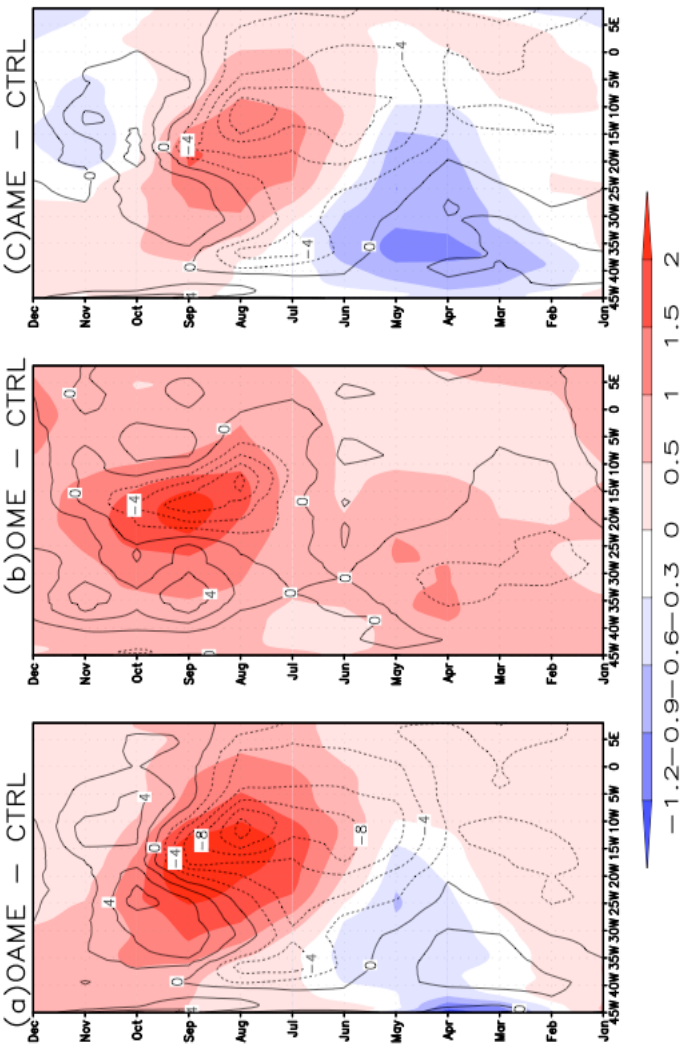

Figure 4.13 Annual cycle of SST anomaly (color in °C) and entrainment anomaly (contour in 10^{-6}m s^{-1}) along the equator in (a) OAME, (b) OME, and (c) AME. Contour interval is $2x10^{-6}$m s^{-1}.

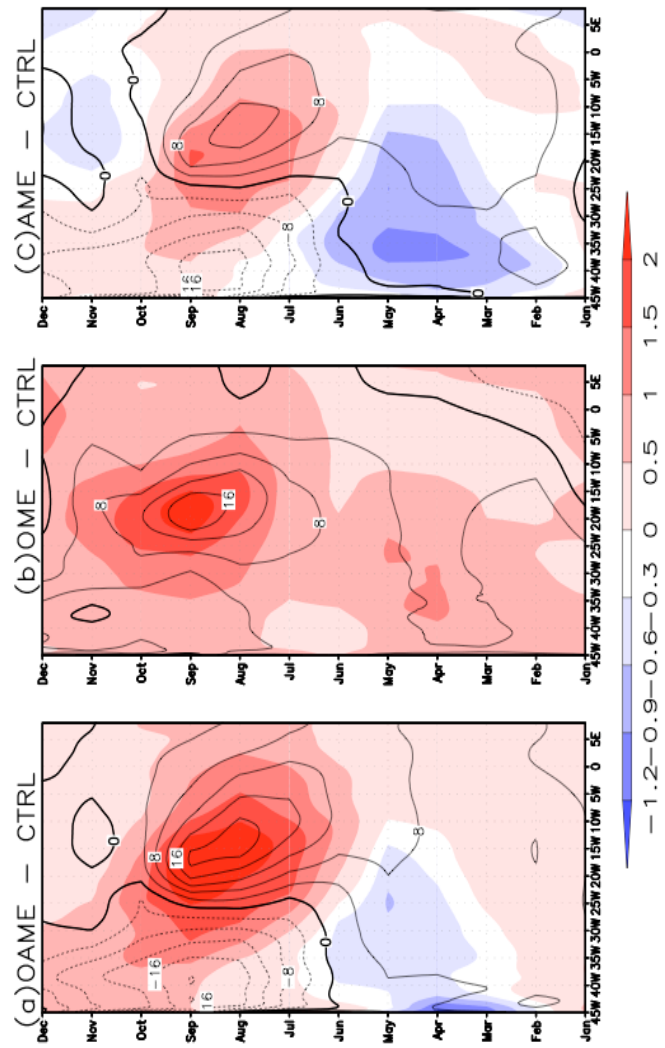

Figure 4.14 Annual cycle SST anomaly (color in °C) and mixed layer thickness anomaly (contour in m) along the equator in (a) OAME, (b) OME, and (c) AME. Contour interval is 4m.

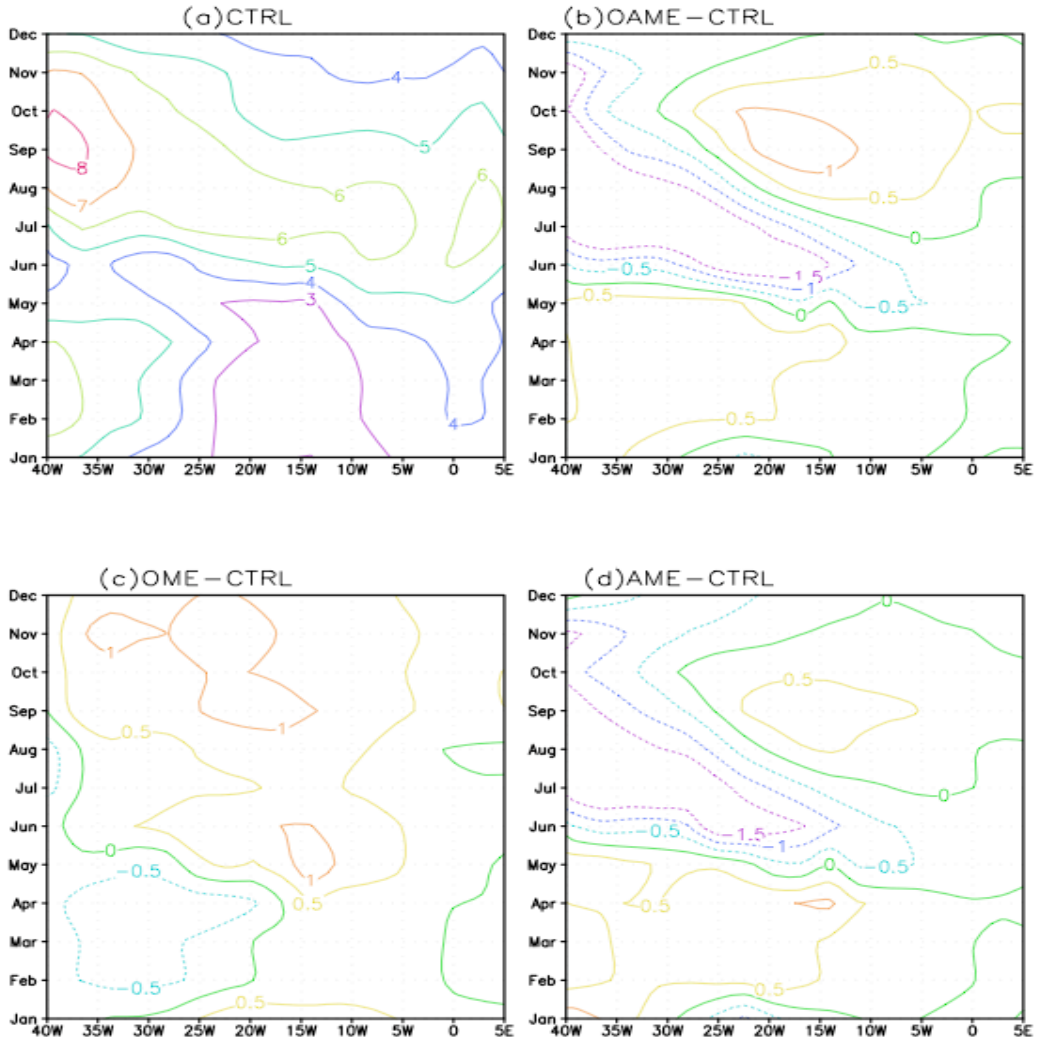

Figure 4.15 Annual cycle of surface wind speed of (a) CTRL run, and wind speed anomaly of (b) OAME, (c) OME,(d)AME along the equator. Unit in m/s.

increase of upwelling, which result from intensified cross-equator winds (Figure 4.15), is responsible for the cooling.

As shown in Section 4.4.1, the precipitation response over the continents adjacent to the AMOC change is most significant over Northeast Brazil and along upper Guinea coast. To evaluate the seasonality of this response, we define the following indices: (1) Northeast Brazil rainfall index (NEB) which is defined as the precipitation change averaged over the region between 42°W-35°W and 12°S-4°S, (2) Gulf of Guinea rainfall index (GGN) which is defined as the precipitation change averaged over the region between 10°W-10°E and 0°N-7°N. Both GGN and NEB show a well-defined seasonal cycle in the CTRL run (Figure 4.16). The pronounced seasonal variations in precipitation over these regions are associated with the seasonal migration of the ITCZ. During spring, the ITCZ approaches its southernmost position and causes rainy season of the Northeast Brazil. As the ITCZ migrates northward, the Northeast Brazil begins its dry season, while the upper Guinea coast enters its rainy season. The simulated annual cycles of these regions are agreed well with observations, except that the phase lags the observation by about one month (Figure 4.17).

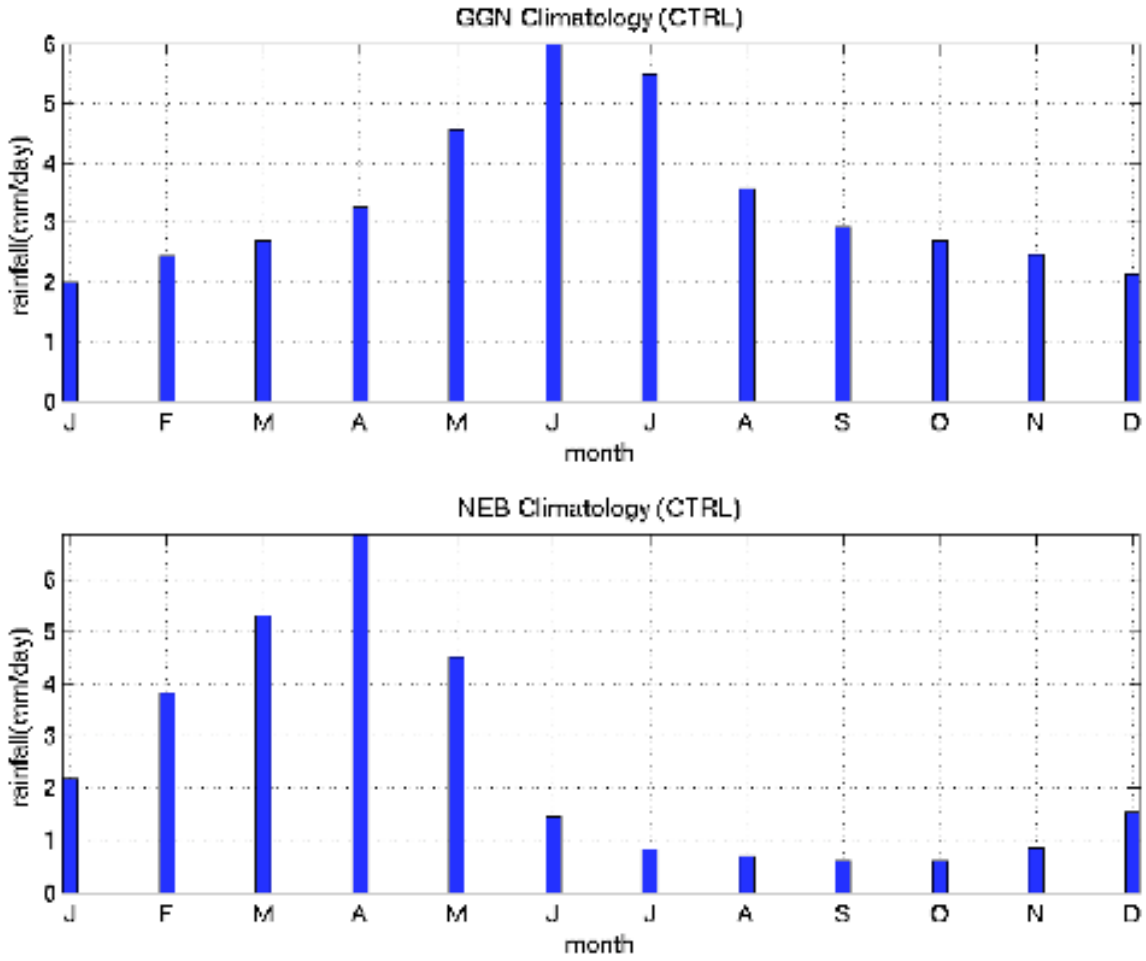

Figure 4.16 Seasonal cycle of GGN index (top panel) and NEB index (bottom panel) from the CTRL run. GGN index is defined as precipitation averaged over the Gulf of Guinea (10°W-10°E, 0°-7°N). NEB index is defined as precipitation averaged over the Northeast Brazil (42°W-35°W, 12°S-4°S).

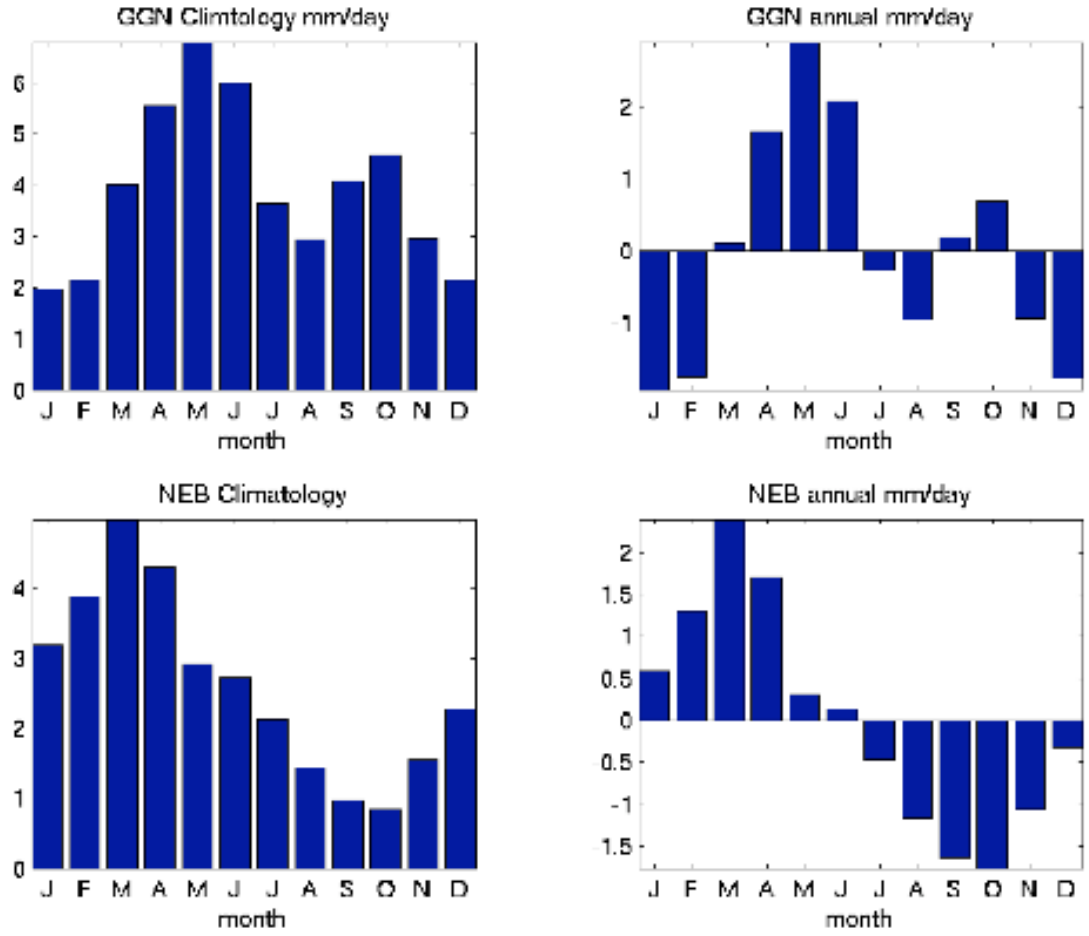

Figure 4.17 Seasonal cycle of GGN index (top panel) and NEB index (bottom panel) from the GPCP data set. GGN index is defined as precipitation averaged over the Gulf of Guinea (10°W-10°E, 0°-7°N). NEB index is defined as precipitation averaged over the Northeast Brazil (42°W-35°W, 12°S-4°S).

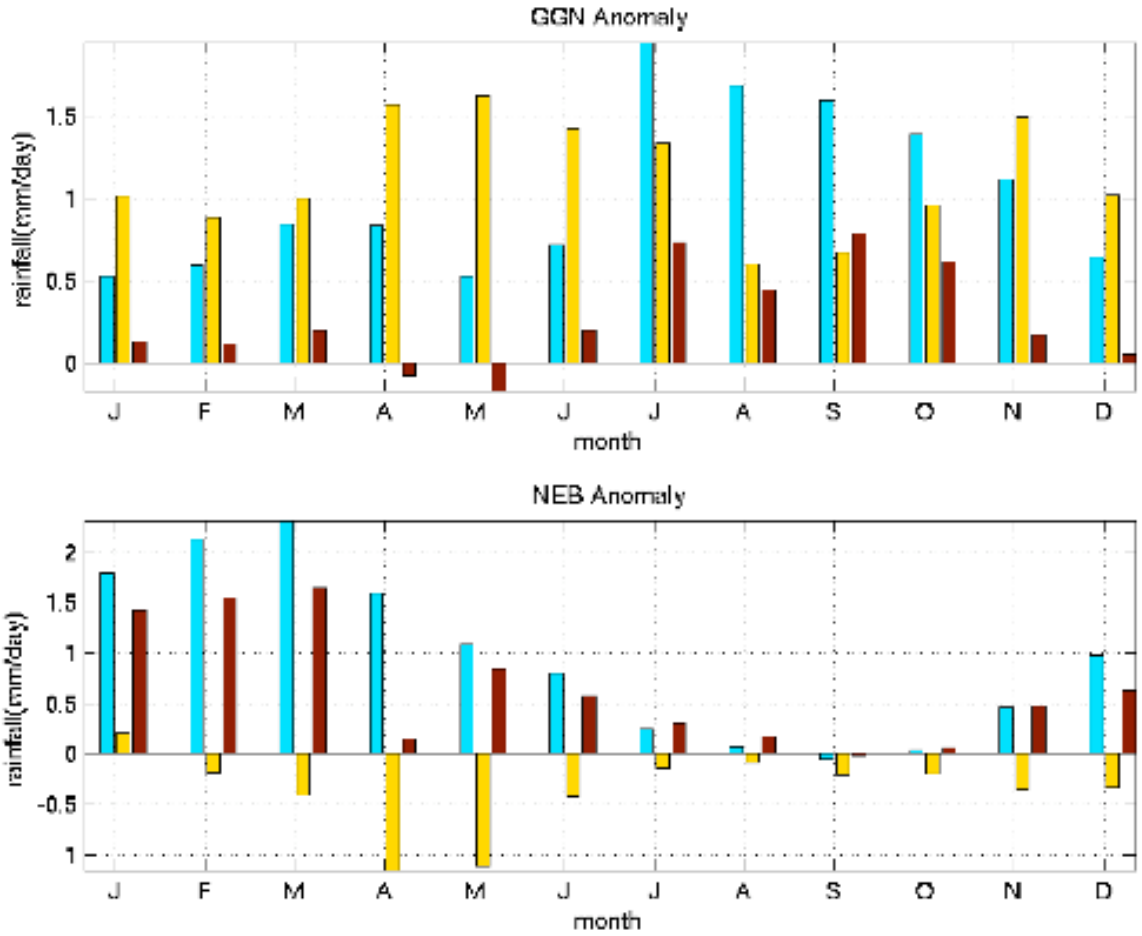

Figure 4.18 Seasonal cycle of rainfall anomaly of (a) GNN index and (b) NEB index in the OAME (cyan), OME(yellow), AME(red). The definitions of GNN index and NEB index are the same as those in Fig.4.16.

In the OAME, the precipitation over the upper Guinea coast increases over the entire year, in response to the AMOC change with a strong seasonal variation. The precipitation change from January to June is in the range of 0.5mm/day to 1.0mm/day, but increases drastically in July to 2mm/day (Figure 4.18 top panel). As shown in Figure 4.16, the onset date of the West African Monsoon in the model occurs around June, the rapid change of precipitation response indicates change in Monsoon circulation. Our analysis suggests that the oceanic and atmospheric processes interact in a complex manner to produce the rainfall response over the Gulf of Guinea. The surface warming produced by the ocean circulation change alone generally gives rise to a positive rainfall anomaly throughout the year and it also gives rise to a semiannual response with the first maximum in May and the second in November. Arguments used to explain the equatorial annual cycle of the Pacific and the Atlantic ocean may offer one possible explanation of this semiannual response. Li and Philander (Li and Philander, 1996) and other studies suggest that air-sea interactions are one of the major factors contributing to the maintenance of the cold tongue/ITCZ complex in the eastern equatorial Pacific and Atlantic and the pronounced equatorial annual cycle. If the cold tongue disappears, the air-sea interactions will weaken and the seasonal response of the coupled system to seasonal change in solar radiation will behave in a manner similar to that of the Pacific warm pool region, which is dominated by a semiannual cycle of the ITCZ movement near the equator, because of the semiannual variation of solar radiation over the equator. In the AME, the precipitation change in the region is generally small except for the months from July to October. The precipitation response in this case may be due to the fact that during the summer and fall, the cooling in the northern tropical Atlantic makes it difficult for the ITCZ to move northward. As a result, more precipitation occurs over the Gulf of Guinea, while drier conditions prevail over the Sahel. Overall, the oceanic process appears to have a stronger influence on the precipitation change in this region. However, the strong rainfall response from July to October in the OAME clearly requires both the oceanic and atmospheric processes.

In contrast to the precipitation change over the Gulf of Guinea, the atmospheric and oceanic processes act as two competing influences over the Northeast Brazil. In the OAME, the wet season during boreal spring becomes significantly wetter with little change during the dry season (Figure 4.18 bottom panel). A comparison between the OME and AME suggests that the atmospheric processes tend to generally increase the precipitation, whereas the oceanic processes tend to reduce the precipitation. However, the total precipitation change in the OAME cannot be simply explained as a linear superposition of precipitation changes in the OME and AME.

4.5 Sensitivity of tropical Atlantic response to changes in AMOC strength

It is demonstrated in Chapter III that the equatorial SST responds nonlinearly to changes in AMOC strength in the RGO model simulation. A prominent equatorial warming occurs when AMOC is weakened below a threshold value. In this section, we will examine whether similar nonlinear behavior can be found in the coupled system and explore how it is manifested in the atmosphere.

For this purpose, we performed a set of coupled simulations, where the forcing configurations are the same as those in the OAME except that the imposed northward mass transport at the open boundary is decreased systematically from 14Sv to 0Sv. The CTRL run with the imposed 14Sv interhemispheric flow serves as a reference for all sensitive experiments.

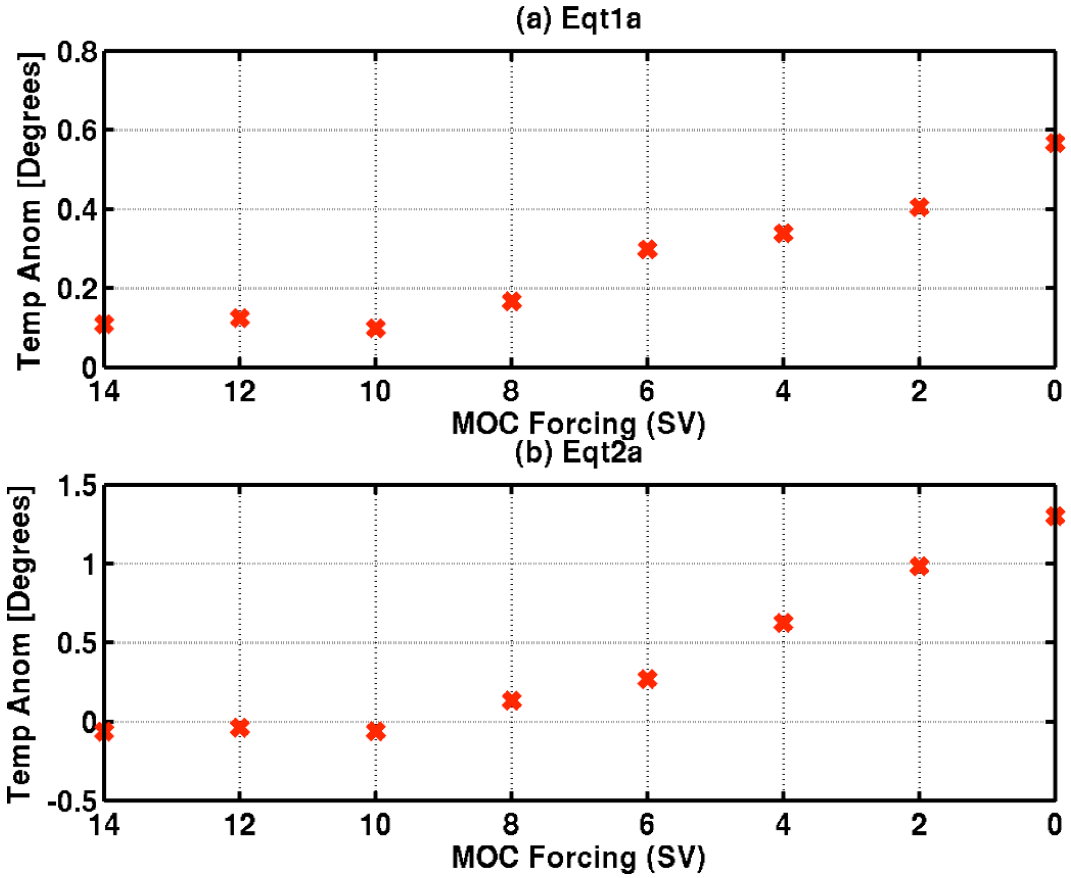

Figure 4.19 Changes in SST index (a) Eqt1a, and thermocline temperature index (b)Eqt2a, as a function of AMOC strength. Eqt1a, Eqt2a are defined as SST anomaly and thermocline anomaly averaged over an equatorial box (25°W-5°E, 4°S-5°N).

Similar to the ocean-only experiment, we define two temperature indices to assess the SST response sensitivity. Eqt1a is defined as the SST anomaly from each experiment averaged over an equatorial box of 25°W to 5°E and 4°S to 5°N and then subtracted by the SST from the control run; Eqt2a is the same as Eqt1a except that it is taken from the thermocline layer. Figure 4.19 shows these indices as a function of AMOC strength. Evidently, both Eqt1a and Eqt2a exhibit nonlinear behavior. The rate of equatorial temperature change increases rapidly when AMOC decreases below 10Sv. This nonlinear behavior holds for all seasons (not shown). As pointed out in Chapter III, the nonlinear SST response over the equatorial zone is associated with the interplay

between the wind-driven northern STC and the AMOC. As shown in Figure 4.8, the return flow of the AMOC interacts with the wind-driven circulation mainly via western boundary currents (Fontaine et al., 1999; Wen et al., 2009). In the presence of a strong AMOC, the NBUC of the southern hemisphere origin penetrates into the northern Hemisphere and effectively blocks the return branch of the northern STC. As the AMOC weakens, the strength of the northward western boundary current decreases. When the imposed AMOC strength is below 10Sv, the equatorward branch of the northern STC becomes dominant, causing the NBUC to reverse its direction (Figure 4.20). As a result, the subsurface temperature anomaly near the subsurface thermal front generated by AMOC changes is able to enter the equator zone and propagate eastward along the equatorial zone. This in turn leads to substantial equatorial warming.

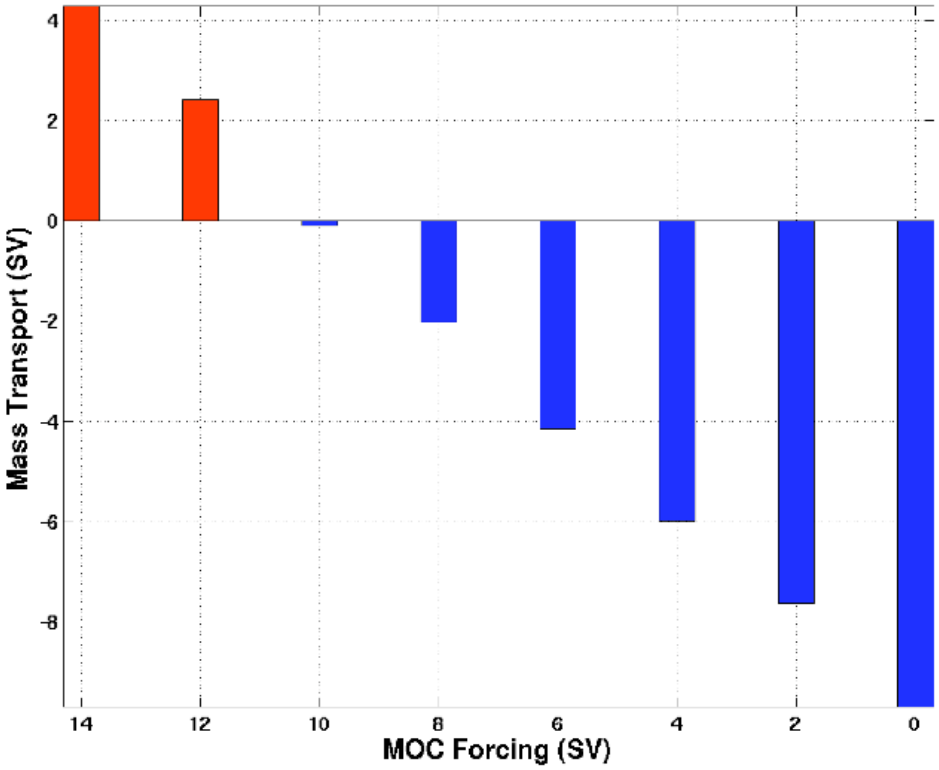

Figure 4.20 The western boundary current transport across 5°N in the thermocline layer as a function of AMOC strength. A positive value means northward transport.

The response of the SST in the coupled system is slightly differently from that in the RGO model-alone simulation (Figure 3.12). It is likely attributed to the influence of air-sea interactions. As shown in Figure 4.7c, cooling over the North Atlantic enhances the northeasterly trade winds, which in turn strengthens the northern STC. As a result, the NBUC reverses its direction from northward to southward when the AMOC strength is below 10Sv, instead of 8Sv in the RGO model alone simulation (Figure 3.12c). It means that the northern STC outweighs the AMOC return flow when the imposed mass transport decreases below 10Sv in the coupled system instead of 8Sv in the uncoupled system. The anomaly generated near the subsurface thermal front, therefore, is easier to propagate into the equatorial zone, resulting in a lower threshold for the nonlinear SST response behavior.

Does the precipitation response show a similar behavior? We assess the sensitivity of precipitation response along upper Guinea coast and over the Northeast Brazil using the GGN and NEB index. As shown in Figure 4.21, the precipitation response along upper Guinea coast also shows a clear nonlinear response for most of seasons. In contrast, the relation between the precipitation response and AMOC strength over the Northeast Brazil is ambiguous (Figure 4.22). It should be noted that our results are based on a single simulation, so the results may be contaminated by the internal atmospheric variability.

An interesting phenomena revealed in Figure 4.7a is that a narrow strip of warmer water, surrounded by wide-spread surface cooling in the north Atlantic, appears off the coast of north Brazil. This area has received extensive attention in paleo climate studies, as the Caribbean current is a main conduit for the water mass to transport from south Atlantic to high-latitude North Atlantic. Although paleo-temperature reconstruction over a broad geographic scale reveals a SST dipole with cooling in the north Atlantic and warming in the south Atlantic during the Younger Dryas (e.g. Zhao et al., 1995; Mulitza and Rühlemann, 2000), there are some inconsistent findings about the temperature changes in the southern Caribbean region. Some studies indicate a surface

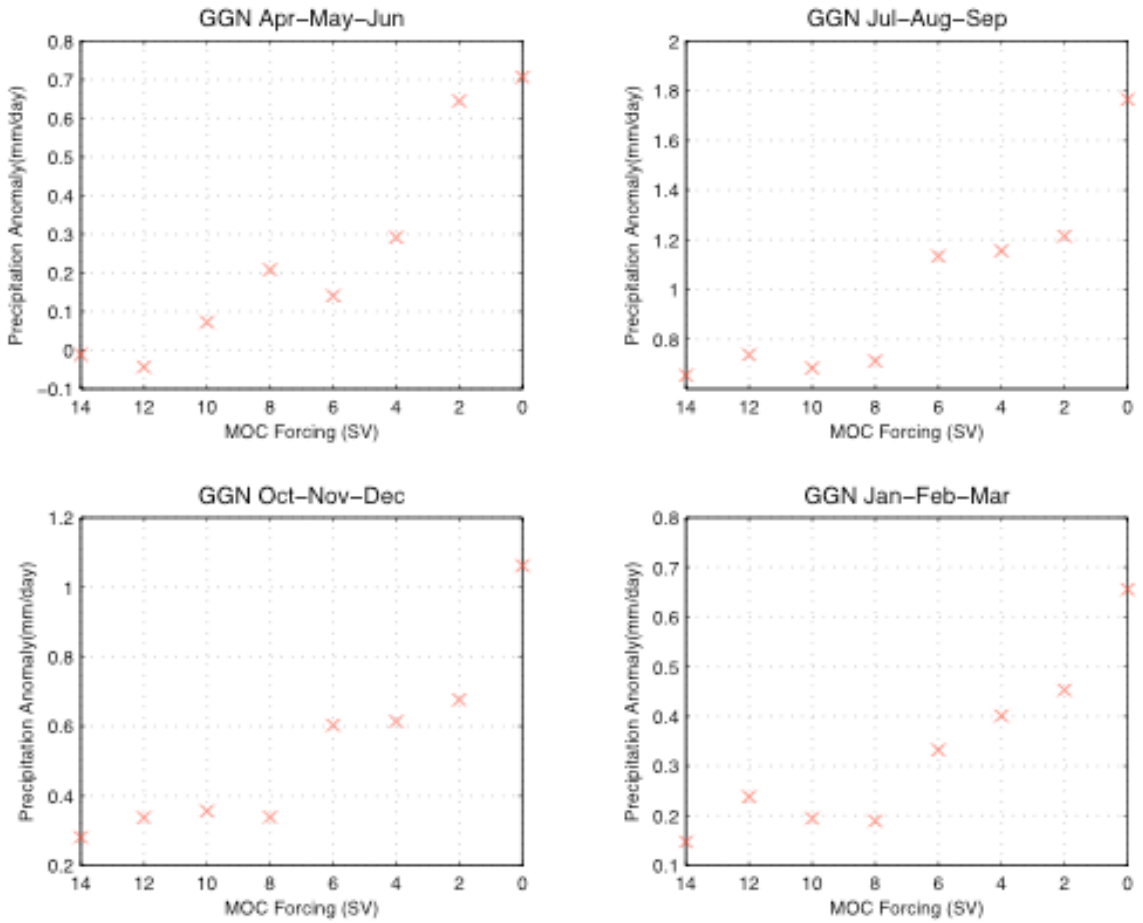

Figure 4.21 Change in GGN index as a function of AMOC strength. GGN index is defined as precipitation averaged over the Gulf of Guinea (10°W-10°E, 0°-7°N).

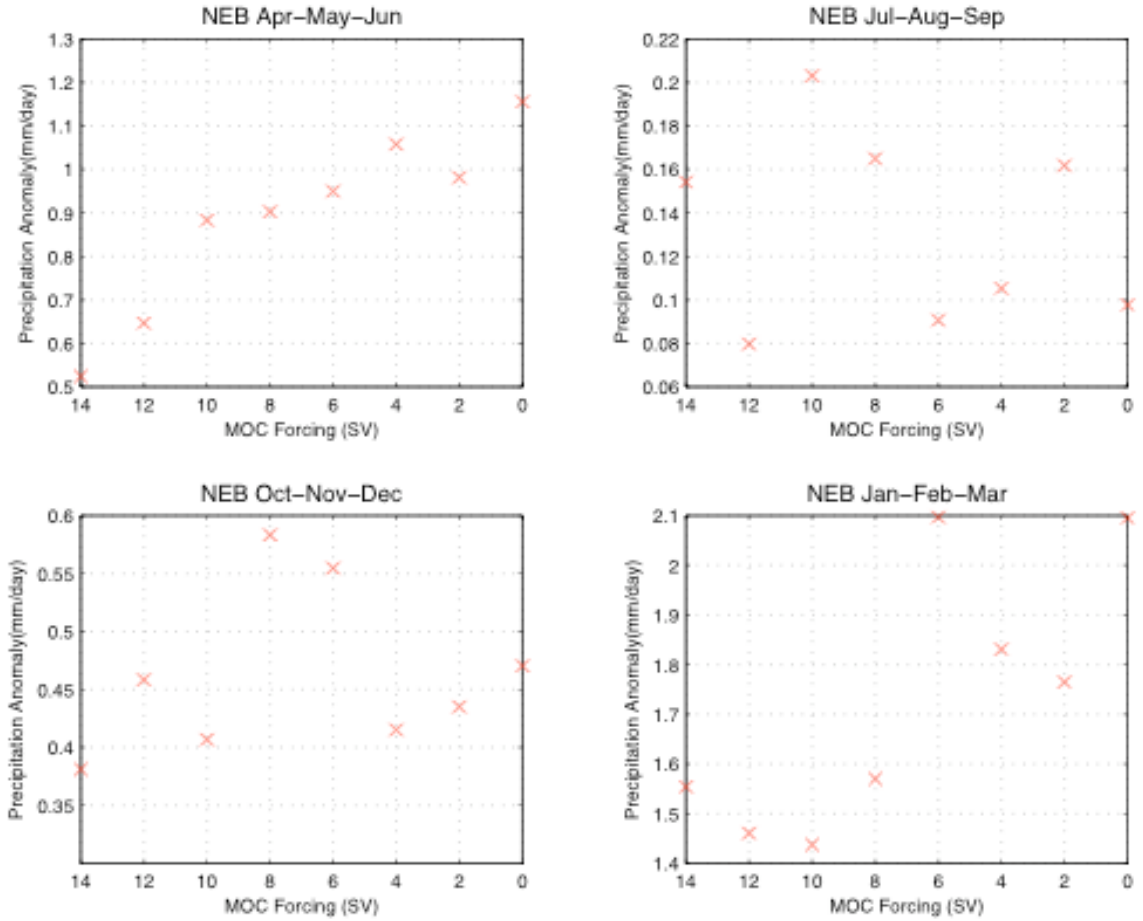

Figure 4.22 Changes of NEB index as a function of AMOC strength. NEB index is defined as precipitation averaged over the Northeast Brazil (42°W-35°W, 12°S-4°S).

cooling during the Younger Dryas (e.g. Lea et al., 2003), while others indicate a surface warming (e.g. Schmidt et al., 2004). In a more sophisticated coupled ocean-atmosphere model, Wan et al.,(2009) found that the atmospheric processes alone give rise to cooling over southern Caribbean region while oceanic processes alone induce warming response. They hypothesized that the paradoxical surface temperature response constructed from paleoproxy records may be as result of the competition between different physical processes.

Figure 4.7 indicates that the narrow warming near the coast of north Brazil has an oceanic origin. This raises some interesting questions: Can different strengths of the oceanic influence lead to opposite sign of SST response as suggested by Wan et al.(2009)? Can the SST response be approximated by a linear superposition of the response of oceanic and atmospheric processes as discussed in Section 4.4.1? To address these questions, we define two indices: NBt1a is taken as the SST anomaly from over a box where warm temperature anomaly occurs near the coast of North Brazil (58°W-53°W, 5°N-6.5°N); NBt2a is the same as NBt1a except that it is taken from the thermocline layer. Note that the box coincides with the location where the subsurface temperature front along the subtropical and tropical gyre intersects the western boundary. As shown in Figure 4.23, the response of NBt1a varies almost linearly with changes in AMOC strength. This is because subsurface temperature anomales near the strong temperature gradient zone are mainly attributed to the horizontal heat advection associated anomalous current, which is proportional to the changes of the AMOC strength. Figure 4.23 shows that the opposite sign of temperature response is attributed to the competition between atmospheric and oceanic processes. For a weakly reduced AMOC, a cooling response prevails, as the surface cooling associated with atmospheric processes is more dominant than the subsurface warming. When the AMOC weakens substantially, a warming occurs in response to enhanced subsurface warming. Our results presented here may offer an explanation of the paradoxical temperature response during past abrupt climatic event, such as the Younger Dryas.

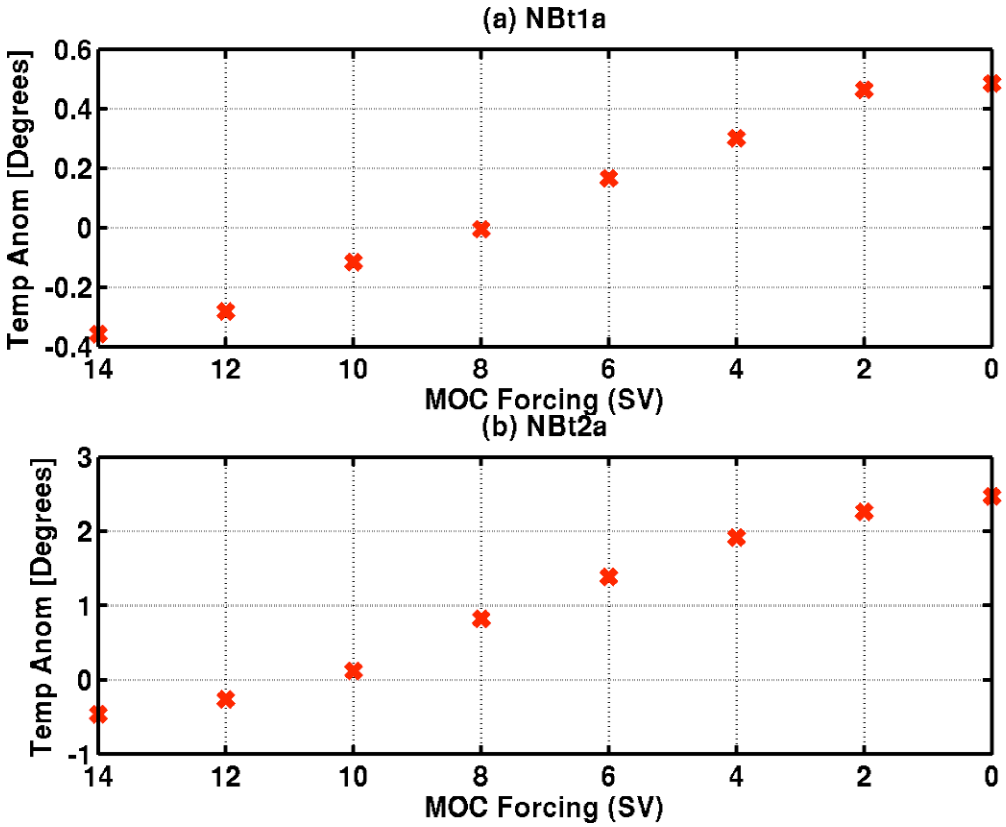

Figure 4.23 Changes in SST index (a) NBt1a, and thermocline temperature index (b) NBt2a as a function of AMOC strength. NBt1a, NBt2a are defined as SST anomaly and thermocline anomaly averaged over a box (58°W-52°W, 5°N-6.5°N).

4.6 Conclusion and discussion

In this study, we investigate the impact of AMOC changes on tropical Atlantic climate in the framework of a RCM consisting of an AGCM (CCM3) coupled to a tropical Atlantic RGO model. We demonstrate that the RCM is capable of simulating many key features of both mean climate and climate variability in the tropical Atlantic sector and it presents perhaps one of the simplest coupled climate models that can be used to explore the underlying dynamical processes linking AMOC changes to TAV.

We conduct extensive numerical experiments with the RCM to examine the relative importance of oceanic versus atmospheric processes in linking AMOC changes to the tropics. We find that ocean circulation changes directly induced by AMOC

changes and atmosphere circulation changes driven by surface cooling in the north Atlantic work in concert to generate the dipole-like SST pattern and a southward shift of the ITCZ. From a set of sensitivity experiments, we identify that the oceanic mechanism is the primary factor contributing to the warming near and to the south of equator and much of the precipitation changes over the Gulf of Guinea. When the AMOC is absent, the NBUC flows equatorward and the STCs become more symmetric about the equator. These circulation changes cause a significant subsurface warming which leads to surface warming in the Gulf of Guinea and along the African coast. This finding supports the hypothesis put forward by Chang et al. (2008). Meanwhile, a reduction of entrainment induced by weakened southeasterly trade wind enhances the surface warming on the equator. On the other hand, the atmospheric processes are largely responsible for establishing the surface cooling in the tropical north Atlantic and the southward displacement of ITCZ, lending support to CB04.

The response of tropical Atlantic to AMOC changes exhibits a pronounced seasonality. The surface warming is strongest during the boreal summer and fall when the seasonal equatorial upwelling is at its peak. Both the reduced vertical temperature gradient and weakened entrainment contribute the surface warming during these seasons. A seasonal preference is also shown in the precipitation response. AMOC changes can lead to excessive rainfall over the Northeast Brazil with a peak during spring and along upper Guinea coast with a peak during boreal summer. The seasonal precipitation response over the Northeast Brazil is consistent with the southward shift of the ITCZ, suggesting the importance of atmospheric processes. Along the upper Guinea coast, however, the oceanic processes induced surface warming over the Gulf contributes significantly to both the mean and the seasonal cycle of precipitation change.

To assess the sensitivity of tropical Atlantic coupled system to changes in AMOC strength, a set of sensitivity experiment is conducted where the imposed northward transport at the open boundaries is systematically decreased from 14Sv to 0Sv. We find that the cold tongue SST responds nonlinearly to AMOC changes. The sensitivity of the SST response to AMOC changes increases rapidly when AMOC

strength decreases below a threshold value of about 10Sv. Such a nonlinear behavior is also found in precipitation change over the Gulf of Guinea. The nonlinear behavior is attributed to the reversal of the NBUC when the western boundary current carrying AMOC return flow becomes weaker than the northern STC return flow. This behavior, however, is weaker in the coupled system than that in the stand-alone RGO experiments as shown in Chapter III. The reason is that the intensified northeasterly trade winds in response to the surface cooling in the north Atlantic produce a stronger northern STC in the coupled simulation, which lowers the reversal threshold of the NBUC.

Our results suggest that the SST anomaly in the northern tropical Atlantic is controlled by a set of competing atmospheric and oceanic processes that tend to cancel each other. The ocean circulation changes tend to produce a surface warming, counteracting the surface cooling that is brought down to the tropics by atmospheric processes. The competing nature of these processes may give rise to a complex pattern of SST response to AMOC changes in certain areas. For example, SSTs off the coast of north Brazil show a cooling response to a slightly weakened AMOC, but a warming to a substantially weakened AMOC. In fact, some paleo proxy records suggest that a cooling over the Caribbean region occurs during the Younger Dryas event (e.g. Lea et al., 2003), while others suggest the opposite (e.g. Hüls and Zahn, 2000). Our results may offer an explanation of this complexity. The same argument has been presented in a recent study using a more sophisticated GCM (Wan et al., 2009). The competing nature of atmospheric and oceanic processes also manifests itself in precipitation response over the Northeast Brazil.

The 2-1/2-layer model used in this study might be the simplest model that is capable of resolving interactions between the return flow of the AMOC and the wind-driven circulation. Owing to the simple physics of the model, there are three important caveats that should accompany the results of this simple coupled model. The first one is the neglection of salinity in this model. In reality, the distribution of the salinity field will be modified owing to the precipitation and ocean circulation changes, which in turn may affect SST pattern. The second one is that the upper tropical Atlantic is crudely

represented by two active layers of uniform initial depth, neglecting the water exchange between thermocline layer and intermediate layer. However, the thickness of the thermocline layer will adjust to a new equilibrium state in real ocean when the stratification changes in response to AMOC changes. The third is that an idealized thermal front is prescribed in this simple model. Admittedly, such idealized setting is unrealistic because changes of thermal structure, in reality, are associated with changes in circulation structures as the two are dynamically linked through geotropic constraints. Despite these shortcomings, our simple couple model provides an effective tool to shed light on the impact of the AMOC on the tropical Atlantic climate.

CHAPTER V
IMPACT OF ATLANTIC MERIDIONAL OVERTURNING CIRCULATION CHANGES ON TROPICAL INSTABILITY WAVE – A REGIONAL COUPLED MODEL STUDY

5.1 Introduction

Tropical instability waves (TIWs) are a commonly observed phenomena in both the Atlantic and the Pacific oceans, where they appear as westward-propagating wavelike oscillations of the temperature front between cold upwelling equatorial water and warmer water to the north (Duing et al., 1975; Legeckis et al., 1983). Figure 5.1 shows an example of cusp-shaped TIWs as observed by the satellite. The typical zonal wavelength, period and phase speed of TIWs are about 600-1000 km, 20-40days and 0.3-0.6 m/s (Qiao and Weisberg, 1995; Katz, 1997). TIWs have a distinct seasonal cycle, appearing in June and decaying in January of the following year.

Numerous studies have discussed the generation mechanisms of TIWs. The cause of TIWs is generally attributed to the barotropic instability of shears associated with equatorial current flowing in alternative directions (e.g. Philander, 1978; Cox, 1980) and the baroclinic instability of the sea surface temperature front immediately north of the equator (Hansen and Paul, 1984; Yu et al., 1995).

As introduced in previous chapters, both paleoproxy evidence and numerical studies reveals that a substantially weakened AMOC induces a dipole like SST pattern with cooler (warmer) temperature over the northern (southern) tropical Atlantic (e.g. Broecker et al., 1985; Stouffer et al., 2006; Timmermann et al., 2007). Such pattern reduces meridional temperature gradient of the climatological mean state over the equatorial Atlantic. Such scenario is particularly pronounced during boreal summer and fall (Haarsma and Hazeleger, 2007; Chang et al., 2008; Wu et al., 2008) when TIWs are most active. It raises a question: Does the change of the AMOC affect TIWs activity by modulating background climate state? This issue is important as TIWs are potentially

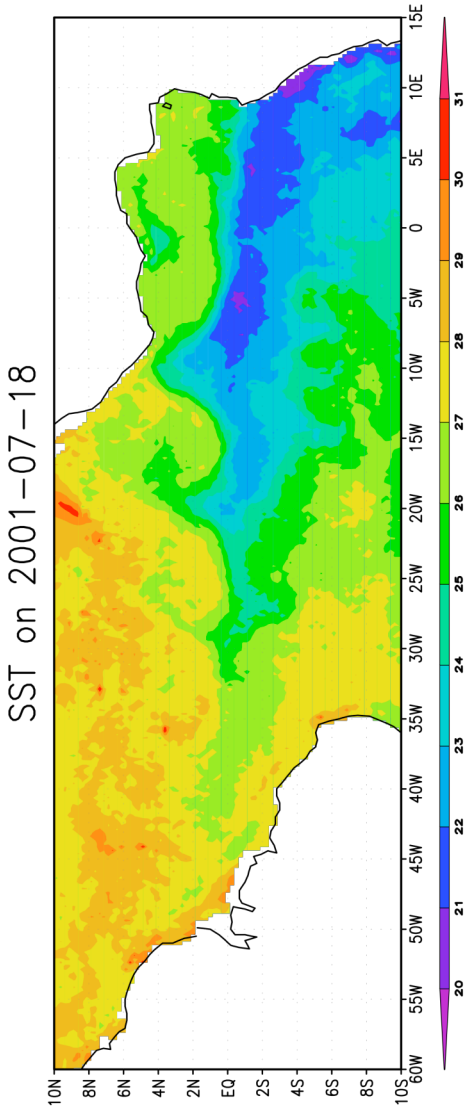

Figure 5.1 TIWs as seen in TMI SST for a 3-day average on 2001-07-21. Note the cups shape along 4°S and 4°N.

important to climate. TIWs are a key element in the momentum balance (Weisberg, 1984) and the ocean mixed layer heat budget (Hansen and Paul, 1984; Jochum and Murtugudde, 2006). TIWs also play an important role in atmosphere-ocean coupling as some observational studies have presented evidence that the SST variations associated with TIWs can induce a significant response in the atmospheric boundary layer (Hashizume et al., 2001; Wu and Bowman, 2007).

This chapter aims to investigate the impact of AMOC change on TIWs activity and the potential mechanisms throuth which the AMOC may modulate TIWs. The chapter is structured in the following way. Section 5.2 introduces data and analysis method. Characteristics of simulated TIWs are evaluated in Section 5.3. The impact of AMOC changes on TIWs activities are presented in Section 5.4. Section 5.5 summarizes and discusses the major results.

5.2 Data and analysis methodology

5.2.1 Model and experiments

In this study, we continue to employ our RCM introduced in Chapter IV to investigate the impact of the AMOC change on the tropical instability waves in the Atlantic. In this coupled system, the 2-1/2-layer RGO is fully coupled to an AGCM (CCM3). The RGO has a 1/4° horizontal resolution and two vertical active layers. Similar 2-1/2-layer models have been used to study generation mechanisms of TIWs in many studies (i.e. Philander, 1978; Yu et al., 1995).

We conduct three sets of experiment to evaluate the relative importance of the atmospheric versus oceanic teleconnection mechanisms. The results have been discussed in Chapter IV. For the purposes of this chapter, we only recall some salient results here:

OME: the AMOC is completely disabled by setting the northward mass transport to zero. The intent of this experiment is to test the effect of oceanic teleconnection mechanism. In this experiment, surface warming occurs in the entire tropical Atlantic

with strong warming along the African coast, near the equator in the central Atlantic and along the coast of North Brazil where upwelling is strong. (Figure 5.2c).

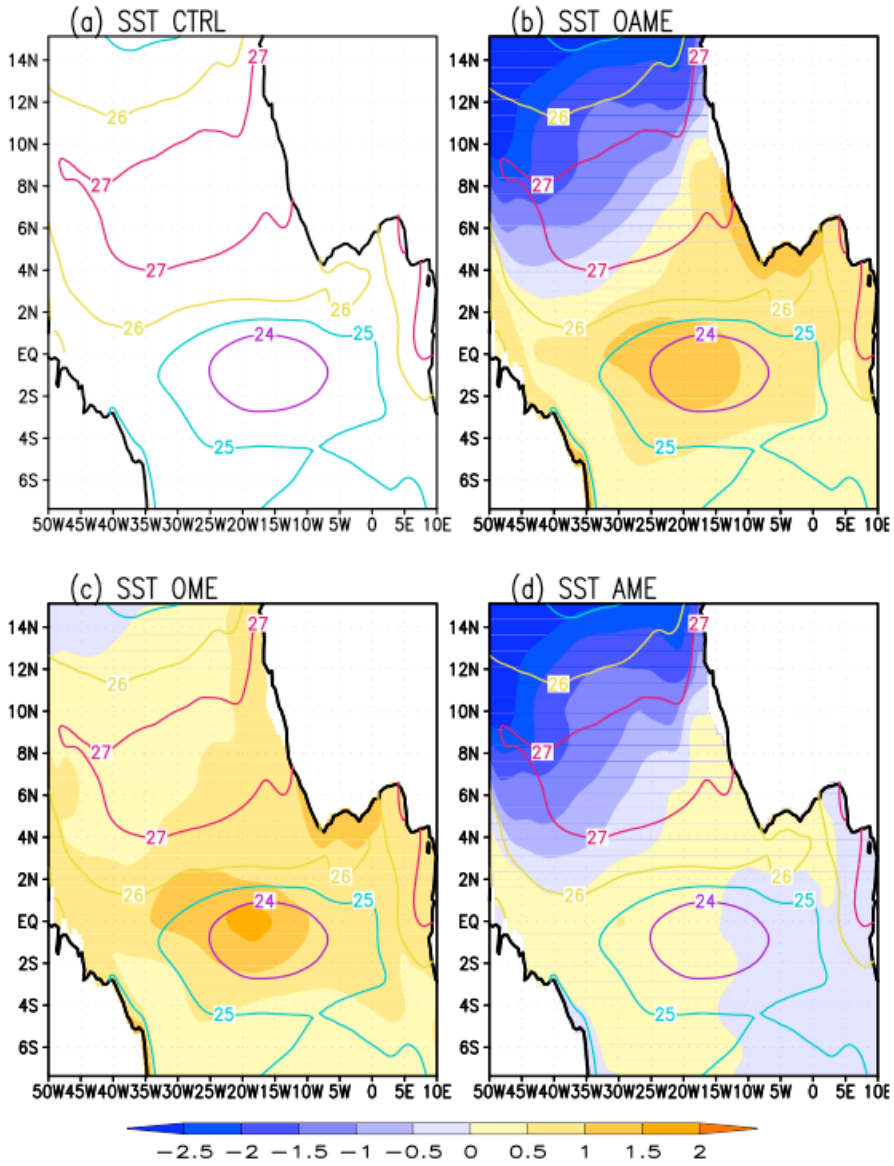

Figure 5.2 Mean SST of the CTRL run(contour) and response(shaded area) in the sensitive experiments during the July-November season.

AME: the model is forced by an anomalous heat flux in the off-equatorial North Atlantic. This experiment is designed to examine the effect of atmospheric processes on tropical Atlantic response. This run produced a strong surface cooling in the north Atlantic, but only a very weak surface warming in the tropical South Atlantic (Figure 5.2d).

OAME: the model is forced by both the surface heat flux in the North Atlantic and mass transport at the open boundaries of the ocean model. This experiment is designed to test the combined effect of oceanic and atmospheric processes. This run produces a dipole like SST response with strong cooling in the north Atlantic and warming along the equator and along the upwelling zones of the southeastern tropical Atlantic. (Figure 5.2b).

In Chapter IV, an 80-year simulation of each sensitive experiment and a 100-year simulation of CTRL run were performed to study the impact of the AMOC on tropical Atlantic variability. In this chapter, only 12-year (years 30-41) daily output of each run is used. Such period is long enough to establish a climatological view of the influence of the AMOC on TIWs. Since this chapter focuses on the effect of the AMOC on TIWs, the domain analyzed here is limited to the region close to the equator where TIWs is most active.

5.2.2 Analysis methodology

a. Wavenumber-frequency spectra analysis

To study the impact of the AMOC on TIWs, the first step is to identify TIWs' signal from model simulations. Wheeler and Kiladis (Wheeler and Kiladis, 1999) demonstrated that wavenumber-frequency spectra analysis is particularly useful for the study of zonally propagating waves as it decomposes a field of data as a function of longitude and time into frequency and wavenumber components of eastward and westward propagating waves. The technique was also recently used to identify oceanic equatorial waves (Shinoda et al., 2008). We will apply this technique to obtain typical

wavelength and period of TIWs in our CTRL simulation. Specifically, a complex FFT is first done on a field of data in longitude to obtain the Fourier coefficients (in zonal planetary wavenumber space) for each time and for each latitude. A second complex FFT is applied to these coefficients to determine the spectral power of each resolved wavenumber in frequency at each latitude. Finally, the obtained power is averaged over the whole time series and over the latitudes.

b. Linear regression

The covariability of SST and atmospheric fields is assessed using the linear regression technique demonstrated in Hashizume et al. (Hashizume et al., 2001). In this technique, the grid point with maximum variance of TIW SST variability serves as a reference point (x0,y0) and the regression coefficient between a variable(T(x,y)) and the SST index (x0,y0) is obtained by a least-square fitting.

5.3 Simulated TIWs in the CTRL run

Before proceeding to the results of abovementioned experiments, we first examine the skill of our CRM in terms of resolving and reproducing the major characteristic features of the observed TIWs in the Atlantic. Following Wheller and Kiladis (1999), we first identify TIWs signal by the wavenumber-frequency spectral analysis. Since TIWs have strong interannual variation (Wu and Bowman, 2007), we conduct the spectral analysis for each year. Figure 5.3 displays the latitudinal mean base-10 logarithm power spectra of SST between 0° and 4°N on the wavenumber-frequency domain. A spectrum center is located between frequency of 0.025 day^{-1}(period of 40 day) and 0.05 day^{-1}(period of 20day) and between wavenumber of 70 (wavelength of 572 km) and 27 (wavelength of 1500km). The opposite signs of frequencies and wavenumbers in the center indicate the westward propagation features of waves. These frequencies and wavenumbers are consistent with those associated with observed TIWs (e.g., Qiao and Weisberg, 1995).

In order to extract characteristics of TIWs from other signals, such as the seasonal cycle, we apply a bandpass filter to the data at periods 20-40 days and then at zonal wavelengths 600-1500km. Sensitivity studies suggest that the results are not sensitive to small changes of this filter box. Figure 5.4 gives an example of how the filter scheme works. The left panel shows a snapshot of TIW-SST overlaid with surface current from the original data in the OAME. The wave structures are blended into the background field, whereas the wave structures are much clearer (right panel) after the filter. Hereafter, unless state otherwise, all the variables discussed are filtered anomalies.

The observed TIWs show large seasonal and interannual variations. Figure 5.5 illustrates some of those variations by showing 2000-2006 TMI (TRMM Microwave Imager) SST anomalies along 1°N. The simulated TIWs also exhibit strong seasonal and interannual variations (Figure 5.6). However, the simulated TIWs peak during July-December, while observation is generally during Jun-Jan. This delay may be due to one-month lag of development of cold tongue in our model (Chapter IV). In order to focus on TIW activity, the analyses performed in the rest of study only use data from July to December.

Figure 5.7 shows the spatial distribution of SST variance calculated from the 12-year of simulation. Maximum SST variance is found to the north of the equator (0° and 4°N) where the meridional SST gradient is high. This asymmetry of TIWs in the Atlantic is consistent with previous observation studies (e.g. Wu and Bowman 2007).

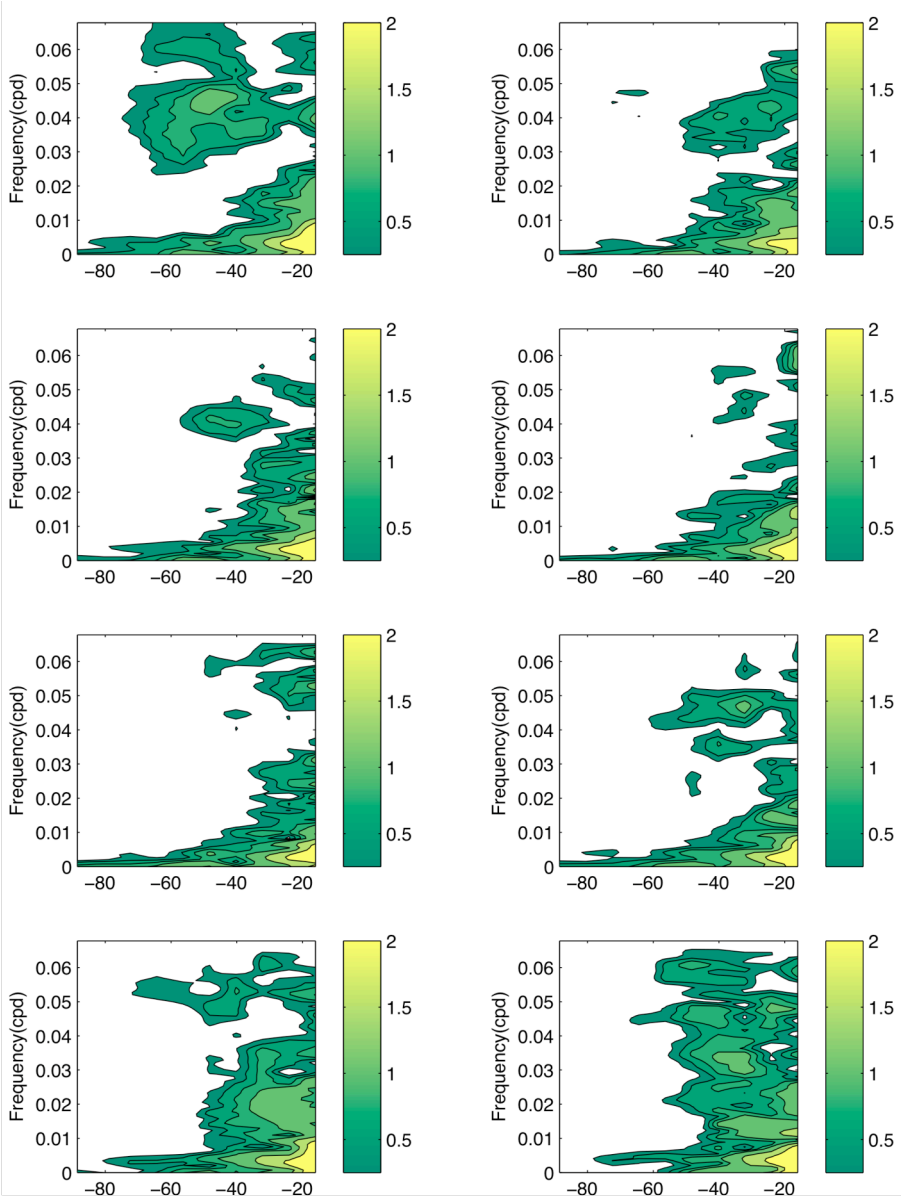

Figure 5.3 Zonal wavenumber-frequency power spectra of SST from the CTRL simulation. The number of the color bar indicates the base-10 logarithm.

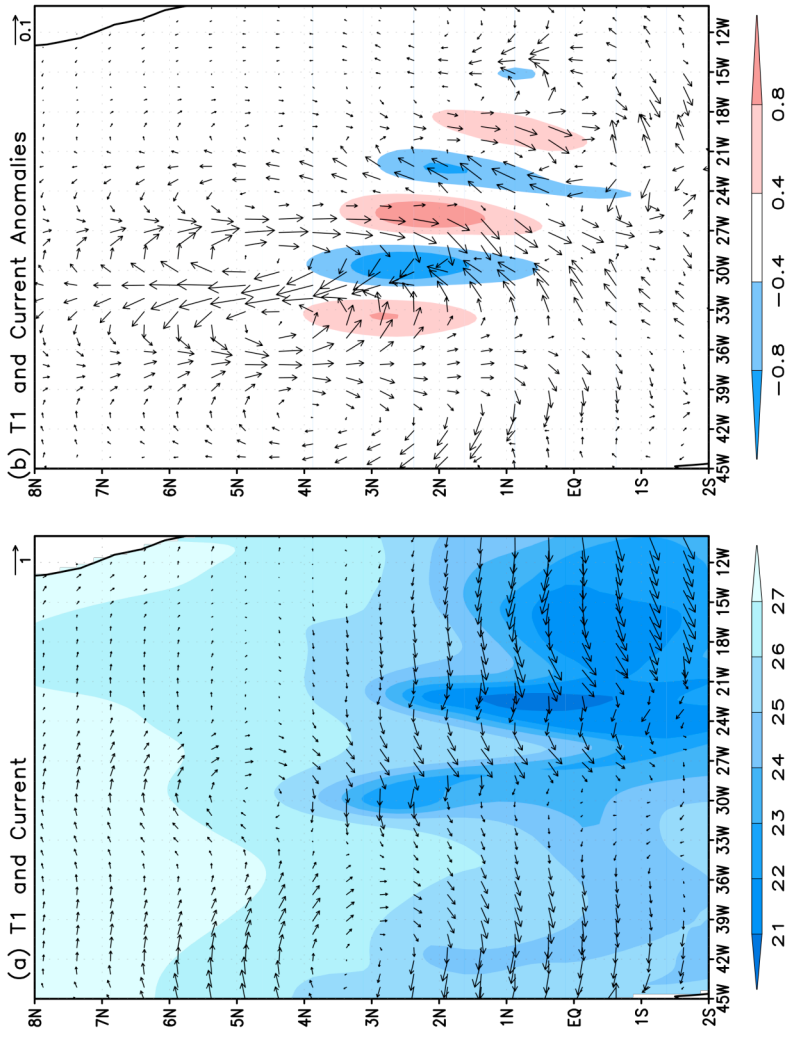

Figure 5.4 Snapshot of TIWs as seen from original daily- mean of SST and mixed layer current (a) and from the filtered SST anomaly and current anomaly (b). Note that TIWs are much clearer after applying the bandpass filter.

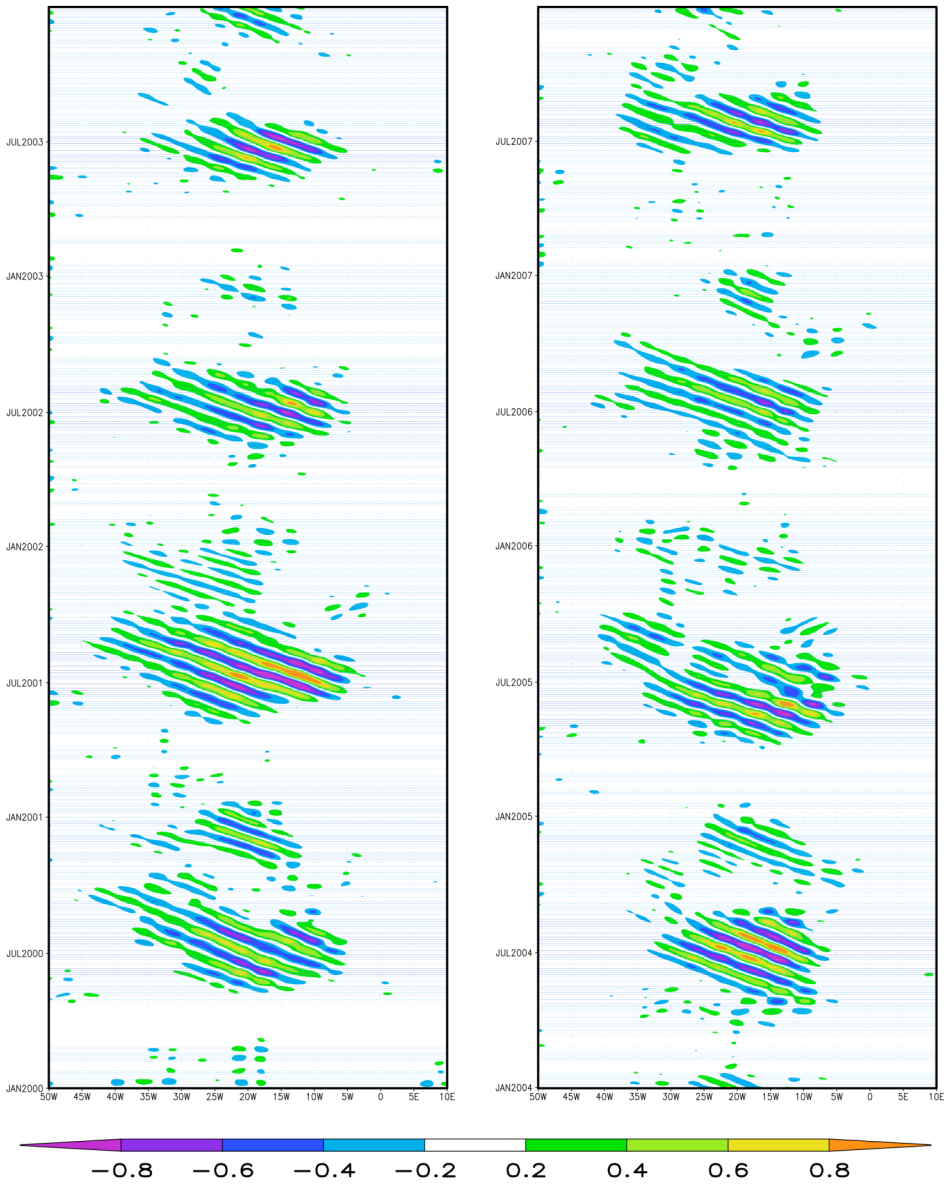

Figure 5.5 Time-longitude section of the TMI SST anomalies along 1°N from 2000-2006.

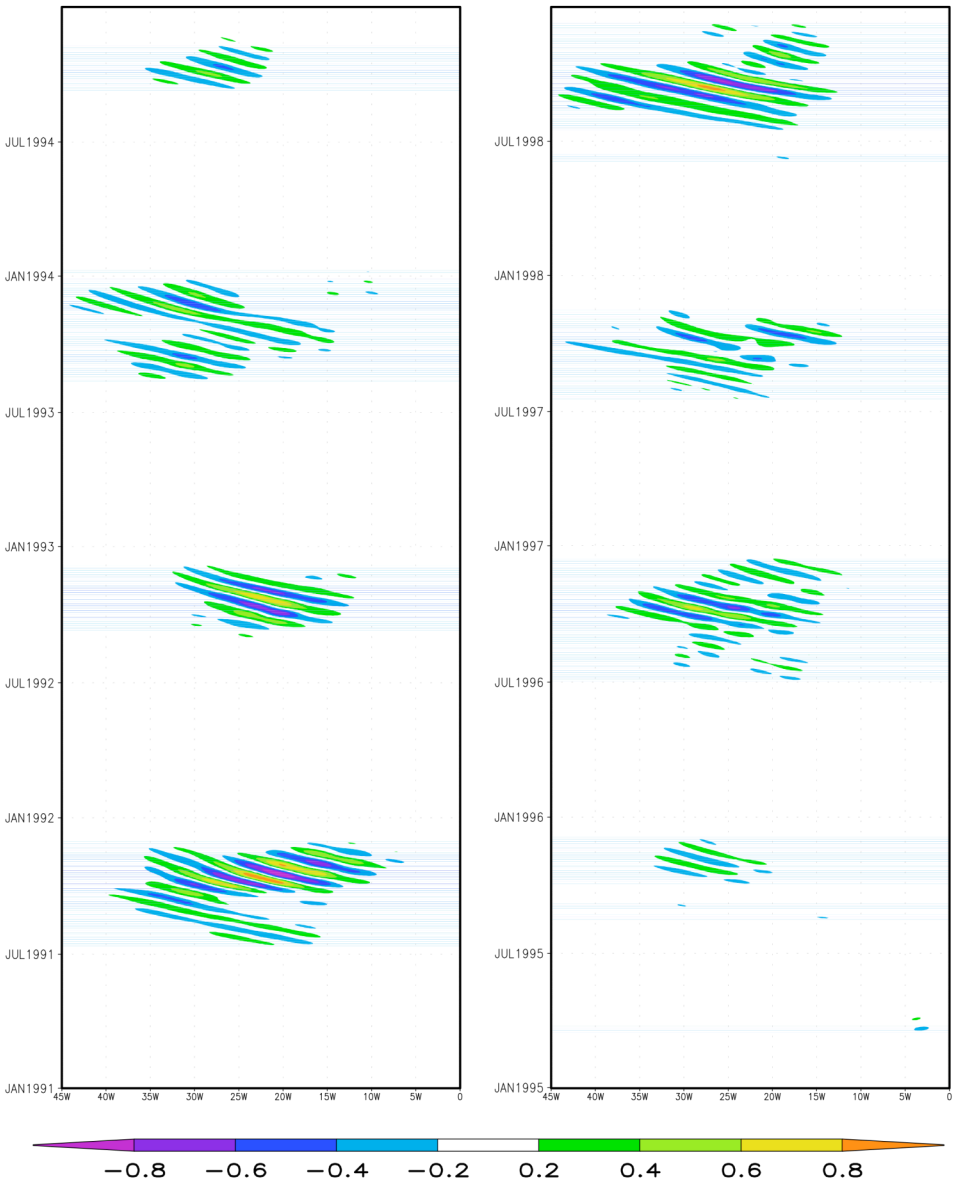

Figure 5.6 Time-longitude section of simulated SST anomalies along 1°N. Note year number represent model year.

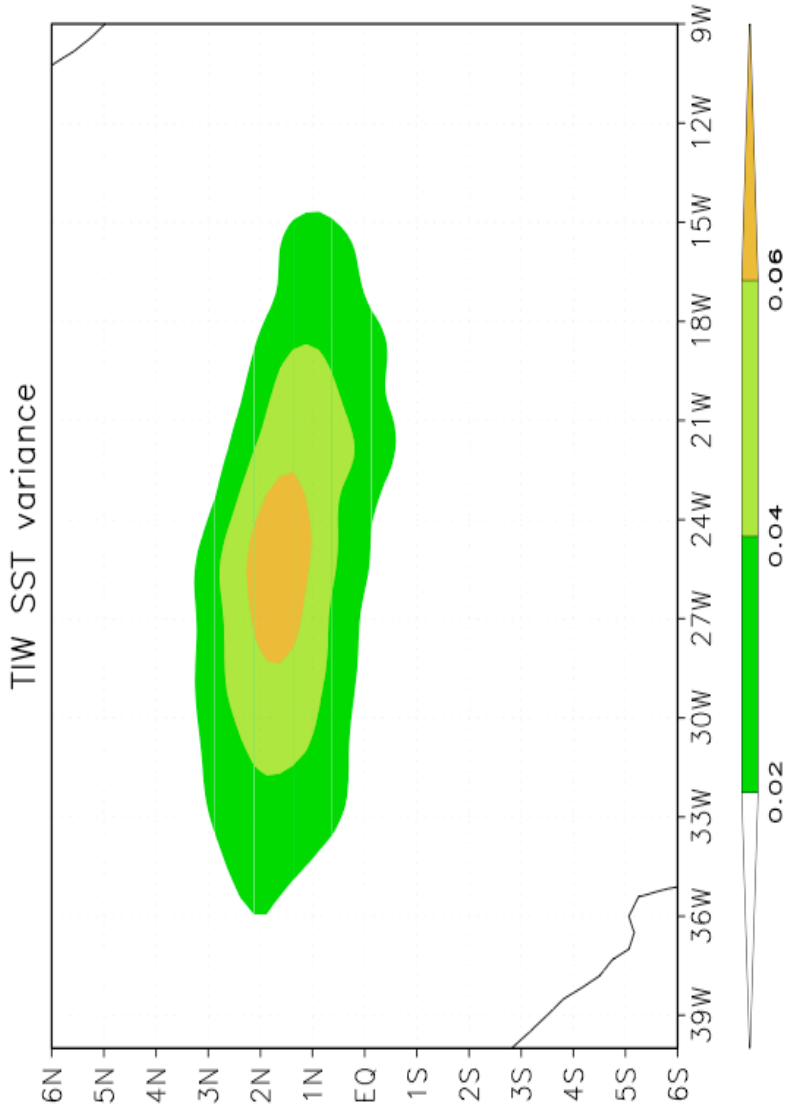

Figure 5.7 TIW SST variance during July to November averaged over 12-year CTRL simulation.

Previous studies suggest that TIWs are generally associated with SST and surface current (e.g. Chelton et al., 2003). The phase relation between SST and surface current are described statistically by regression analysis following Hashizume et al. (Hashizume et al., 2001). Time series of filtered SST and surface current anomalies are regressed against the filtered SST at a reference point where the SST variance is maximum (Figure 5.7). As shown in Figure 5.8, the most active TIW-SST anomalies are from 15°W to 35°W and from the equator to 4°N with a wavelength about 8°. Compared with satellite observations (Wu and Bowman, 2007), our TIWs active region is relatively narrow and displaced somewhat westward. It may result from the westward shift of cold tongue of our model. The current anomalies consist of alternating anticyclones and cyclones just to the north and south of the equator. Northward (southward) current anomalies are found at the coldest (warmest) anomalies around 1.5°N, suggesting a net meridional heat transport by TIWs. Apparently, the TIWs induce an entrainment response. The entrainment anomalies are located slightly at the eastern side of SST anomalies. These patterns are consistent with the westward wave propagation as the enhanced(reduced) entrainment cooling tends to damp the warm(cold) anomalies.Noted that this analysis is based on a 12-year simulation, the pattern revealed here may vary from year to year.

Overall, the above results indicate that our model is able to capture most of the observed statistical features of the TIWs. Thus, this simple coupled model is suitable to investigate the impact of the AMOC on TIWs.

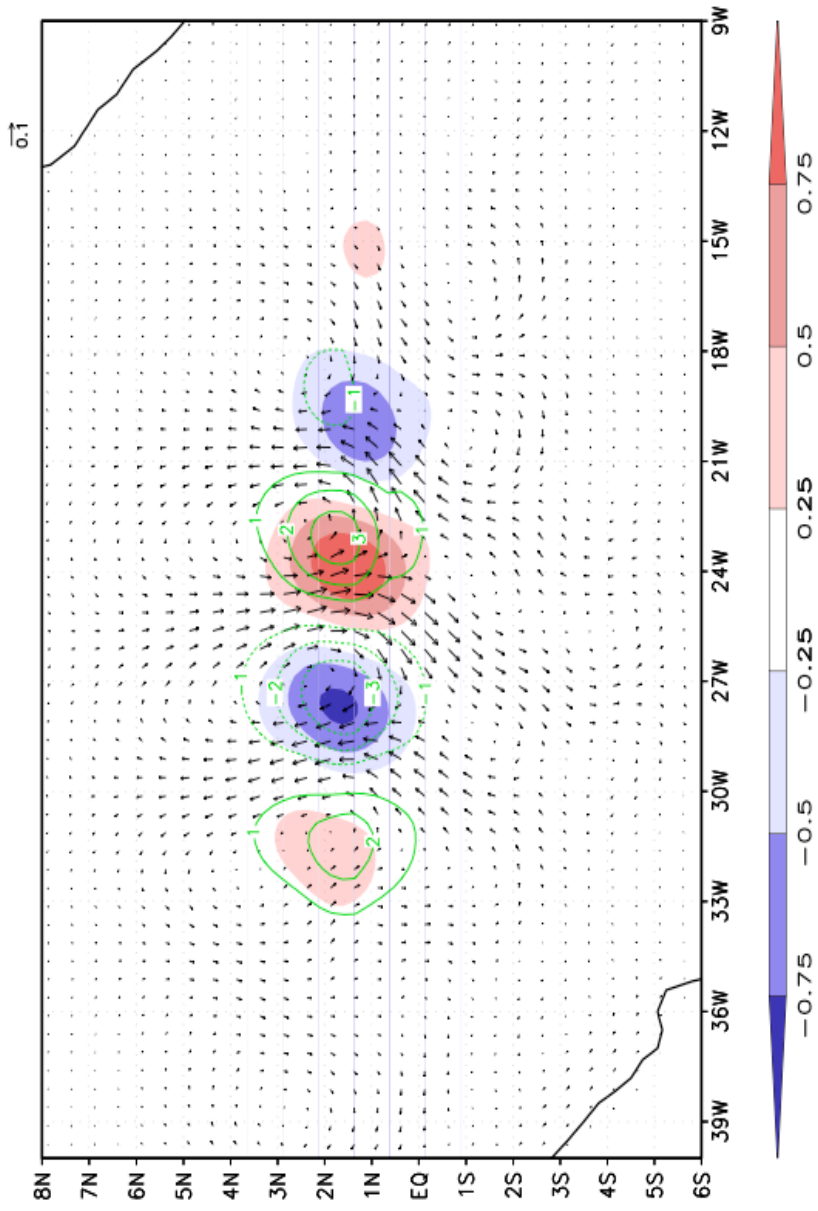

Figure 5.8 SST(shaded), surface current (arrows, unit in m/s) and entrainment (contour, unit in 10^{-5} m/s) anomalies regressed onto filtered SST anomalies at reference point (25°W, 1.6°N) .

5.4 Effect of the AMOC on TIW activity

As shown in Figure 5.2, the shutdown of AMOC induces a substantial warming in the equatorial region mainly caused by the oceanic processes (the OME run) and also, to a lesser extent, by the atmospheric processes (AME run). As a result, the equatorial cold tongue is weakened to different extents in the three experiments. As the warming region coincides with the TIWs active region, it is important to know how the change of background state affects the TIW activity.

Figure 5.9 displays the variance of TIW SST anomalies in the CTRL run and the three experiments. The spatial structure of TIWs is presented by the regression map created by regressing the SST time series at each location against a reference point with the largest variance in each run. To make the regression map comparable among experiments, the SST time series at the reference point is normalized by its standard deviation. A striking feature in Figure 5.9 is that the TIW variances in the OME run and AOME run are strongly reduced. The variance in the AME run is also slightly reduced. SST anomalies are confined between the equator and 2°N in all runs. The TIW SST pattern in the CTRL run has the broadest meridional and zonal scales, which is consistent with variance analysis.

One may argue that substantial weakened TIWs activities in the OAME run and the OME run may not be real as the same bandpass filter is applied in each run. It is possible that the frequency and the wavenumber band of TIWs may be modified after the climatological states are changed. To exclude this possibility, we conduct the wavenumber-frequency spectrum analysis for the OAME run. It is evident that no significant spectrum center is observed (Figure 5.10), suggesting our results based on the same bandpass filter are robust.

Figure 5.11 shows the regression maps of SST, velocity in the mixed layer and the entrainment. Unlike the SST anomalies, current anomalies can extend from 4°S to 6°N and the wave structure is quite different between the experiments. In the OAME run, current anomalies are more dominant to the north of the equator. The asymmetric structure of the wave is clearly observed in the OME run, though the magnitude of wave

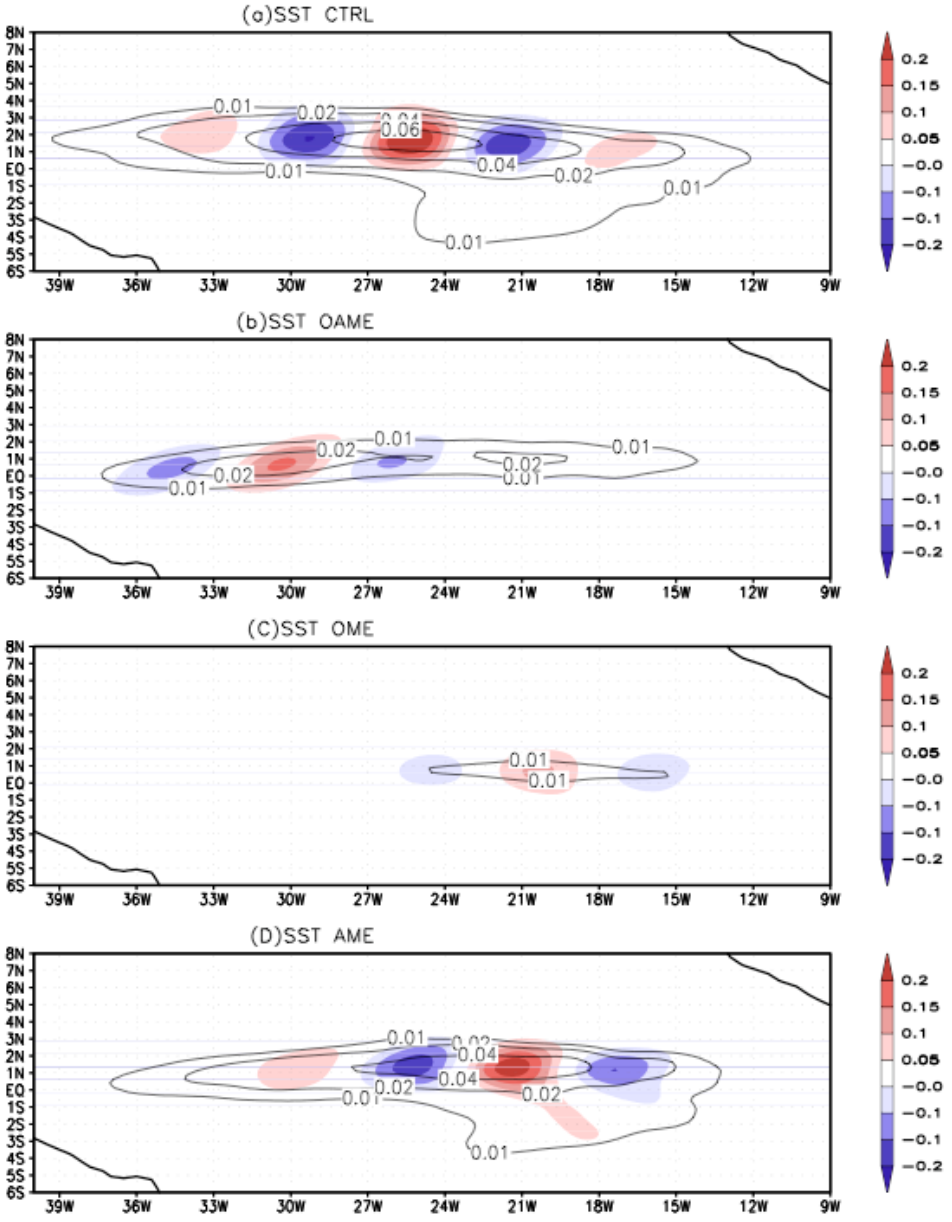

Figure 5.9 TIW SST variance (contour) and regression map(shaded) of (a) CTRL run, (b) OAME run, (c) OME run and (d) AME run. Grid points where the SST variance is maximum in each run. Note that the reference time series are normalized by their own standard deviation in each run.

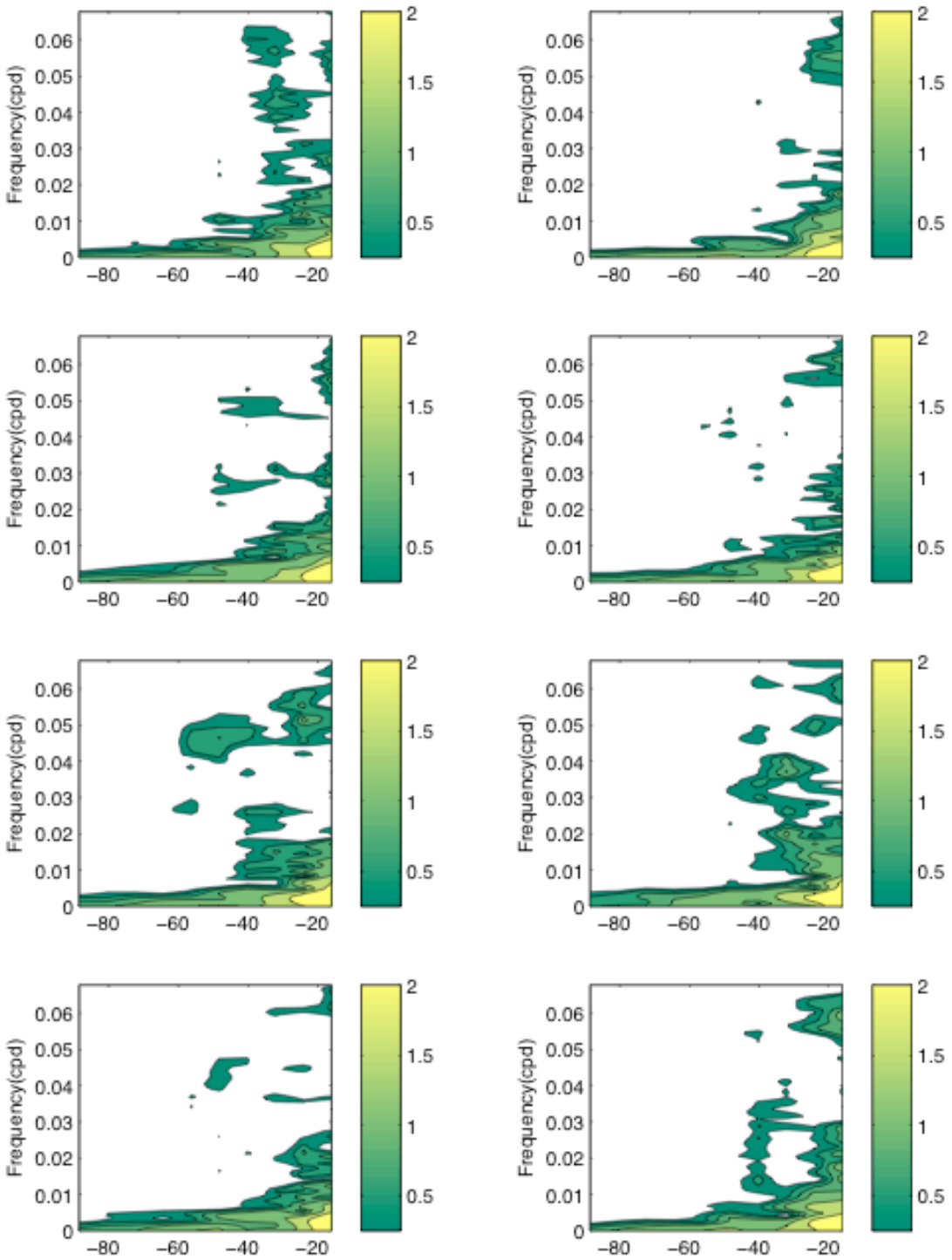

Figure 5.10 Zonal wavenumber-frequency power spectra of SST from the OAME run. The number of the color bar indicates the base-10 logarithm.

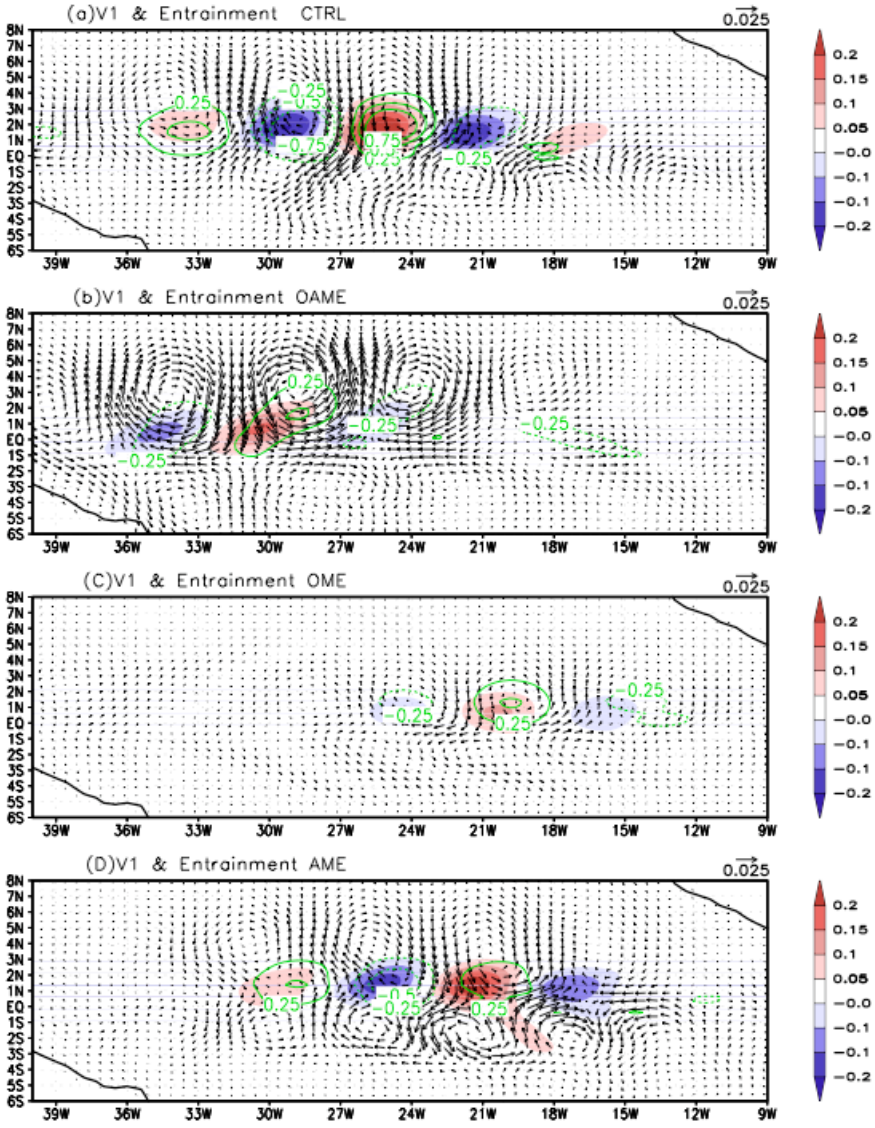

Figure 5.11 Regression map of SST(shaded), surface current (arrows, unit in m/s) and entrainment (contour, unit in 10^{-5} m/s) anomalies in (a) CTRL run, (b) OAME run, (c) OME run and (d) AME run. In each run, reference point is where the SST variance is maximum. Note that the reference time series are normalized by their own standard deviation in each run.

is weak,. The wave structure becomes more symmetric about the equator in the AME run. In fact, the TIWs structure in the CTRL run and the AME run are very similar to those presented in study of Yu et al.(1995) (See Figure 5.12). Using a linearized 2-1/2-layer ocean model, Yu et al. (1995) identified two prominent unstable waves: the first type has a period of 23.3 day and a wavelength of 785 km; the second type has a period of 47 days and a wavelength of 1571 km. The structure and energy of these two waves are determined by the background state of South Equatorial Current (SEC) and temperature. Yu et al. 1995 demonstrated that a weakened the southern branch of SEC or an asymmetric SST front can lead to an asymmetric unstable wave structure. As our ocean model has similar dynamics with theirs, their studies may offer explanations for our results here.

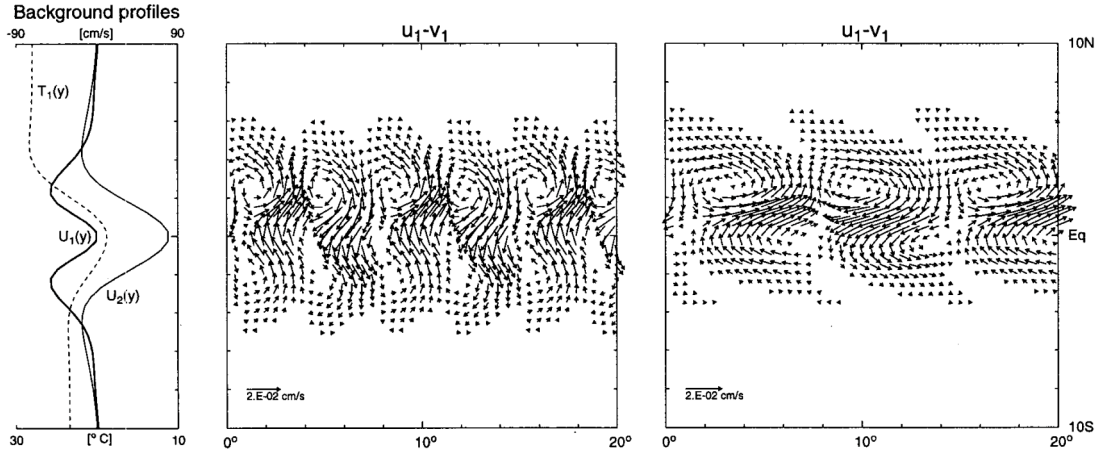

Figure 5.12 Structures of upper-layer perturbation velocity fields for wave 1(middle panel) and wave 2(right panel). Profiles of background current and temperature are provided in the left panel. Both waves, especially wave 2, are apparently weaker south of the equator due to the weaker SST front.(From Yu et al.1995)

Figure 5.9 shows that the TIW activity is substantially weakened in response to a slowdown of the AMOC. How does the AMOC change modulate TIWs activities? Our results suggest the following mechanisms. As aforementioned, the baroclinic instability

associated with the SST front can trigger the development of TIWs, and so does the barotropic instability associated with the ocean current shears between the SEC and the EUC or the NECC. Therefore, we examined the relation between the meridional gradient of average temperature ($\partial\overline{T}/\partial y$) and zonal current shear in the mixed layer ($\partial\overline{U}/\partial y$). Figure 5.13 displays 12-year meridional gradient of temperature overlaid by TIWs variance. It shows that TIWs are generally located at the region where the largest temperature gradient exhibits, whereas the relation between the zonal shear and the TIWs activities are relative vague (Figure 5.14). To make the relation between TIWs and gradient of temperature and current more clear, we construct three indices: TIW index, defined as standard deviation averaged over an northern equatorial box (40°W-0°,0°-4°N); SST gradient index, defined as mean meridional temperature gradient over the same box as TIW index; Zonal shear index, defines as mean zonal current shear over the same box as TIW index. Figure 5.15 shows the year-to-year relation among the three indices (blue dots). The points in red, magenta, yellow, green correspond to the 12-year averaged relation in the CTRL, OAME, OME, AME run, respectively. The TIW activity generally increases with increasing temperature gradient. The relation between the three indices in the OME and AME run is very close to the least square fit. It indicates that the AMOC change may affect TIW activity by modulation the equatorial SST front. However, the large deviation of OAME run from the fitting line suggests that oceanic processes and atmospheric process affect the TIWs in a nonlinear manner. Our results do not show a clear dependency of TIW activity on the zonal shear. Note that the strength of SEC in our model is much weaker than the observation, indicating a possible underestimate of barotropic instability in our model.

5.5 Conclusion and discussion

This Chapter stems from our study discussed in Chapter IV, which focus on the impact of AMOC on the large-scale tropical Atlantic climate. In this Chapter, we focus on the influence of the AMOC change on mesoscale ocean variability.

Using frequency-wavenumber spectral analysis, we identified the typical frequency and wavenumber of the simulated TIWs. Bandpass filter and linear regression analysis are used to extract the characteristics of TIWs. Our RCM is shown to be able to simulate temporal and spatial characteristics, as well as seasonality of the observed TIWs.

Three sensitivity experiments are conducted to investigate the impact of the AMOC on the TIWs. We found that the TIW activity is reduced in all three experiments. The extent to which the activity is reduced depends on the anomalous surface warming over the equatorial region. The TIWs are greatly reduced when the AMOC-induced warming over the equatorial region is strong.

To explore the possible mechanisms through which the AMOC affect TIW activities, we analyze the relation between the TIWs and meridional SST gradient and zonal shear from a 12-year CTRL simulation. Our correlation analysis suggests that AMOC changes modulate TIW activities mainly by modifying SST gradient north of the equator. It is also noted that the strength of the simulated equatorial currents are weaker than observed. This may prevent the barotropic instability mechanism to become more dominant in the generation of TIWs in our model.

The implication of this study is that AMOC changes can modulate TIW activities through modifying large scale SST distribution. The dynamical explanation lies in the fact that baroclinic instability associated with the northern SST front is a major generation mechanism of TIWs in our RCM. How changes in TIWs affect the mixed layer heat transport and air-sea interactions deserves further study.

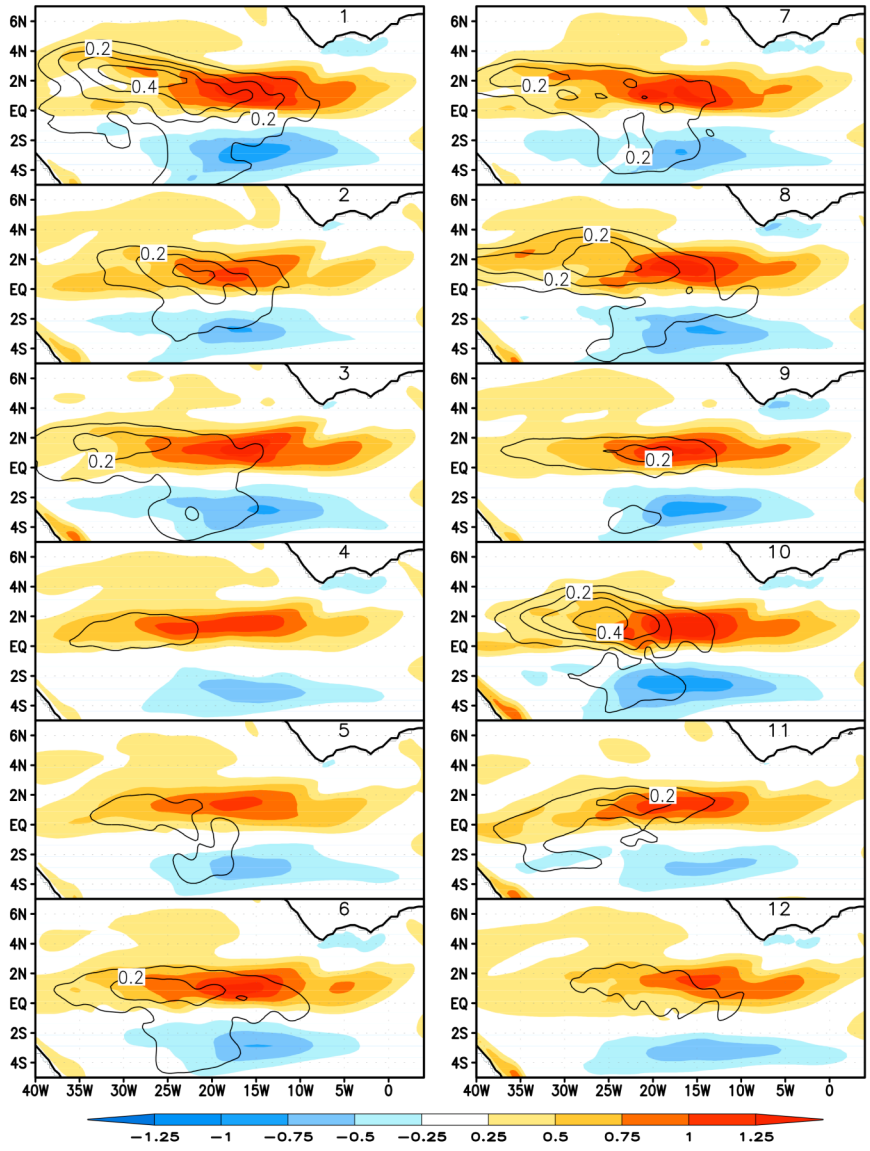

Figure 5.13 The meridional gradient of averaged SST(shaded, unit in C°/100 km) and variance of filtered SST(contour) of the CTRL run in each model year.

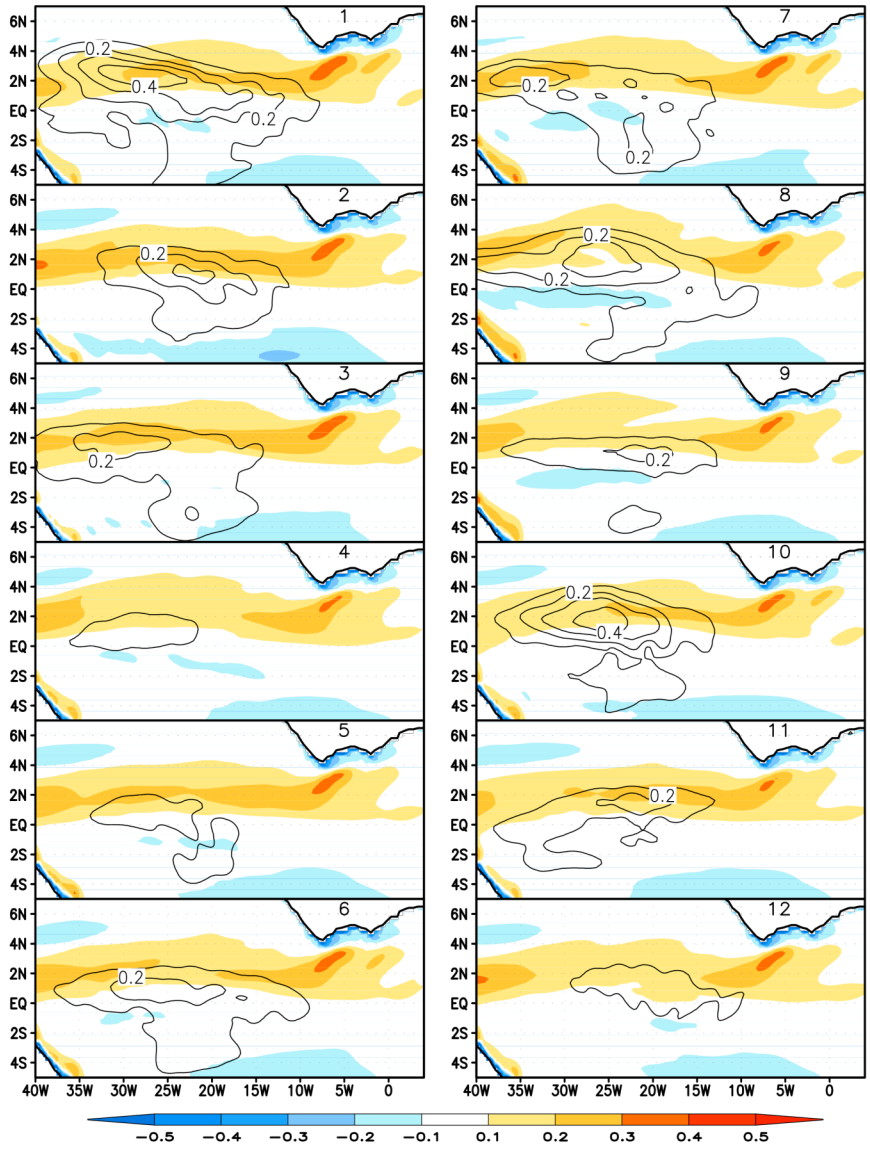

Figure 5.14 The zonal current shear (shaded, unit in m/s/100 km) and variance of filtered SST(contour) of the CTRL run in each model year.

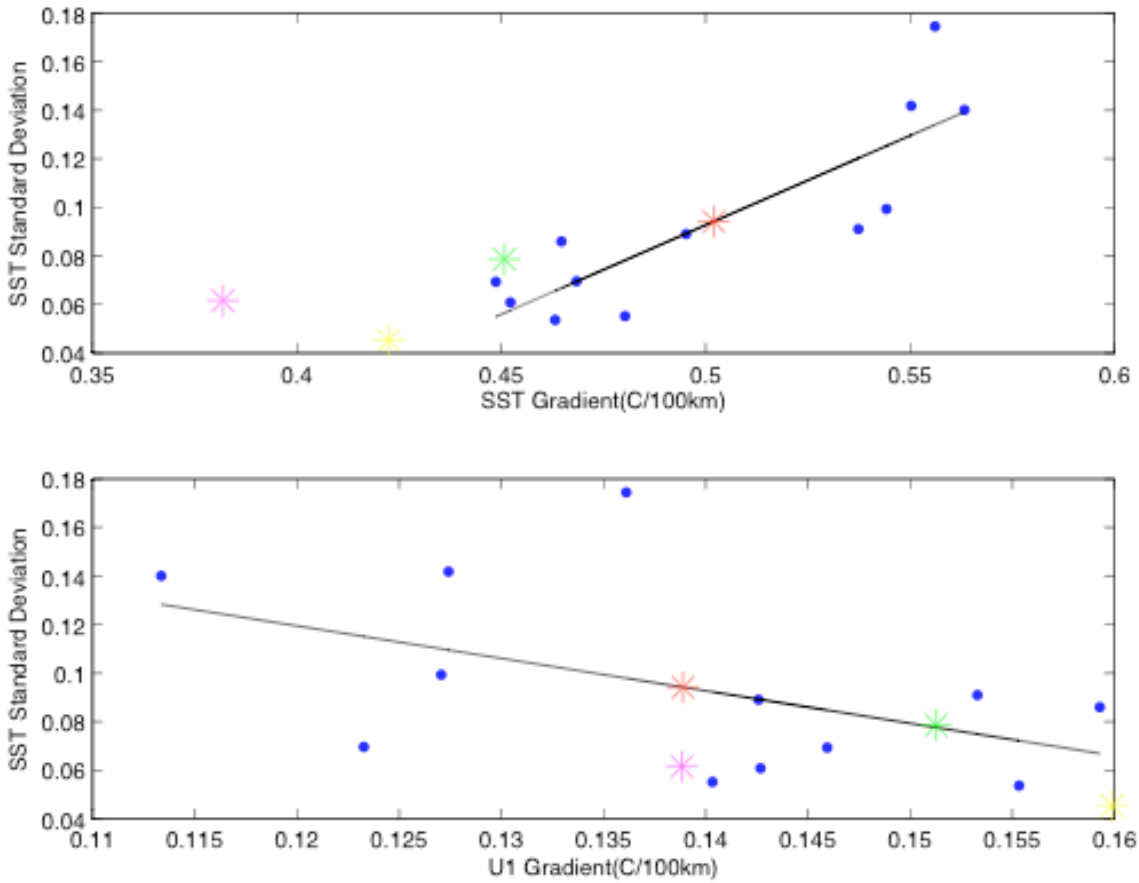

Figure 5.15 Standard deviation of SST index as a function of SST gradient index (a), and zonal current shear index (b). The indices are defined as the averaged values for the region (40°W-0°,0°-4°N). Blue dots represent year-to-year relation in 12-year CTRL simulation. The points in red, magenta, yellow, green correspond to the 12-year averaged relation in the CTRL, OAME, OME, AME run respectively.

CHAPTER VI
SUMMARY AND DISCUSSION

6.1 Highlights

A 2-1/2-layer reduced gravity ocean circulation model with open boundary conditions has been developed and coupled with an AGCM model to form a regional fully coupled climate model. The coupled model is able to capture the observed tropical Atlantic climate variability and simulate the AMOC influence on the tropical Atlantic coupled system that are consistent with paleo observations and CGCM sumulations. The simplicity and computational efficiency of the ocean model make it an ideal tool for climate variability and climate change, air-sea interaction and ocean circulation studies. Using this coupled model as the framework, we studied the impact of the AMOC changes on the tropical Atlantic climate. The results have greatly improved our understanding of the tropical Atlantic climate system and the influence of high-latitude climate change on this system. Several findings from this study may have far-reaching implications for modeling and predicting abrupt climate prediction.

6.2 Summary

The conventional 2-1/2-layer reduced gravity ocean model has the following limitations: (1) subduction or detrainment process is not included; (2) subsurface temperature is assumed to be constant; (3) impact of the AMOC on the tropical Atlantic is ignored. Substantial efforts of this thesis have been made to extend the capability of the conventional 2-1/2-layer reduced gravity ocean model. Specifically, the following improvements have been introduced to a 2-1/2-layer reduced gravity ocean model originally developed by Lee and Csanady (1999): (1) Implementation of a new open boundary condition (OBC) developed by Marchesiello et al. (Marchesiello et al., 2001). With the OBC, the strength of the AMOC can be modulated by the prescribed mass transport at the northern and southern boundaries of the model domain. (2) Adoption of a

new vertical mixing scheme. Both entrainment and detrainment processes are included. The former is estimated using a modified version of KT (Krauss and Turner, 1967) model. The latter is parameterized following McCreary et al. (1993). (3) Implementation of subsurface temperature physics. A flux correction scheme is introduced in the thermocline layer to maintain an idealized temperature front.

Using the new 21/2-layer reduced gravity ocean model, we have conducted a systematic investigation of the role of oceanic processes in controlling the tropical Atlantic sea-surface temperature (SST) response to AMOC changes. The basic methodology is similar to that of Fratantoni et al. (2000) where a northward interhemispheric flow is specified at the northern and southern open boundaries of the model, mimicking the return flow of the upper limb of the AMOC. It was found that the North Brazil Undercurrent (NBUC) reverses its direction in response to a shut-down of AMOC. Such circulation change causes the upper equatorial ocean stratification to decrease and leads to warmer conditions in the Gulf of Guinea and off the coast of Africa. These findings indicate that oceanic processes play an important role in triggering and modulating the response of SST to AMOC changes. Sensitivity experiments further show that the SST responds nonlinearly to AMOC changes. A sudden increase of the rate of SST changes is observed when the AMOC strength decreases to a threshold value. This nonlinear threshold behavior depends on the position of subsurface temperature gradient forming along the boundary between the northern subtropical gyre and tropical gyre that interacts with the western boundary current. Our analysis suggests that the following two are the necessary conditions for the oceanic dynamics to have a dominant influence on the response of the tropical Atlantic SST to AMOC changes: (1) the AMOC must weaken substantially so that the NBUC flows equatorward, permitting water mass exchange between the northern subtropical and tropical gyres; (2) the subsurface temperature front must be located in an optimal location where subsurface temperature anomalies induced by AMOC change are able to enter the equatorial zone.

The third part of this thesis is to elucidate the relative importance of the atmospheric processes versus the oceanic processes in AMOC-induced TAV change. For this purpose, a fully coupled climate model consisting of an AGCM (CCM3) and the abovementioned ocean model is developed. The coupled model successfully simulated the major features of the tropical Atlantic climate variability. We designed a series of numerical experiments with different combinations of oceanic and atmospheric processes to investigate the annual cycle response of the tropical Atlantic SST to a shutdown of the AMOC. Also investigated are the rainfall response and the relative role of atmospheric and oceanic processes in this response. We found that the oceanic processes are the primary factor contributing to the warming on and south of the equator and much of the precipitation changes over the Gulf of Guinea. The atmospheric processes are responsible for the surface cooling in the tropical north Atlantic and the southward displacement of the ITCZ. Furthermore, the sensitivity of tropical Atlantic coupled system to changes in the AMOC strength is assessed. It is found that the sensitivity increases rapidly when AMOC strength decreases below a threshold value of about 10Sv. Such a nonlinear behavior is also found in precipitation change over the Gulf of Guinea. The nonlinear behavior, however, is weaker in the coupled system than that in the stand-alone RGO experiments.

Finally, we investigated the impact of the AMOC change on oceanic mesoscale activities in the tropical Atlantic. In this part, we first demonstrated that the statistical features of simulated TIWs are generally consistent with observations. We then assessed the impact of the AMOC on the activity of TIWs in three sensitivity experiments, where only one or both teleconnection mechanisms are present. We found that TIWs are greatly reduced when oceanic processes are present while slightly reduced in case only atmospheric processes are present. We also found that the extent to which the activity is reduced is related to the strength of the induced surface warming over the equatorial region. To explore the possible mechanisms behind the influences of AMOC change on TIW activity, we examine the generation mechanisms by analyzing the relation between TIWs and meridional SST gradient and zonal shear from a 12-year CTRL simulation.

Our correlation analysis suggests that the AMOC changes modulate TIW activities mainly by modifying SST gradient north of the equator.

6.3 Discussion and Future work

6.3.1 Model limitations

The RCM presented here might be the simplest model suitable for studying the effect of the AMOC on tropical Atlantic to a reasonable extent. However, owing to the simple physics of the model, some caveats may affect the results of this simple coupled model. One of the major deficiencies of the present RCM is the lack of salinity controlled process. Our results show that the ITCZ shift southward in response to a shutdown of the AMOC. In the real ocean, such large-scale precipitation perturbation is likely to modify the distribution of salinity and alter the circulation of the upper ocean. Thus, the response to the AMOC changes might be underestimated by the present model. Another limitation of our model is that an idealized thermal front is prescribed in the thermocline layer. Admittedly, such setting may be over simplified because changes of thermal structure, in reality, are associated with changes in circulation structures as the two are dynamically linked through geostropic constraints.

6.3.2 Future work

The current work has focused on the impact of the AMOC on the mean state and seasonal cycle of tropical Atlantic climate. Beyond the seasonal time scale, the interannual variability in the tropical Atlantic is dominated by two modes: the cold tongue mode (or zonal mode) and the meridional mode. The Atlantic cold tongue mode is tied to the seasonal cycle and has its maximum amplitude during the boreal summer. The meridional mode is strongly connected to the seasonal cycle of ITCZ. Our results showed that AMOC changes have a significant impact on the annual cycle of the

Atlantic cold tongue complex. Further investigation is needed to elucidate how seasonal response affects the interannual variability.

In addition, we found that AMOC changes can have a significant impact on TIW activities. The mechanisms behind this impact remain unclear and are worth of further investigation as TIWs play an important role in the mixed layer budget and can induce significant response in the atmospheric boundary layer.

REFERENCES

Barreiro, M., A. Fedorov, R. Pacanowski, and S. G. Philander, 2008: Abrupt climate changes: How freshening of the Northern Atlantic affects the thermohaline and wind-driven oceanic circulations. *Annual Review of Earth and Planetary Sciences*, **36**.

Boyle, E. A., 2000: Is ocean thermohaline circulation linked to abrupt stadial/interstadial transitions? *Quaternary Science Reviews*, **19,** 255-272.

Breugem, W. P., W. Hazeleger, and R. J. Haarsma, 2007: Mechanisms of Northern tropical Atlantic variability and response to CO2 doubling. *Journal of Climate*, **20,** 2691-2705.

Broecker, W. S., D. M. Peteet, and D. Rind, 1985: Does the ocean-atmosphere system have more than one stable state of operation? *Nature*, **54,** 21-26.

Chang, P., 1994: A study of the seasonal cycle of sea surface temperature in the tropical Pacific Ocean using reduced gravity models. *Journal of Geophysical Research*, **99**,7725-7741

Chang, P., L. Ji, and H. Li, 19 97: A decadal climate variation in the tropical Atlantic Ocean from thermodynamic air-sea interactions. *Nature*, **385,** 516-518.

Chang, P., R. Saravanan, L. Ji, and G. C. Hegerl, 2000: The effect of local sea surface temperatures on atmospheric circulation over the tropical Atlantic sector. *Journal of Climate*, **13,** 2195-2216.

Chang, P., R. Zhang, W. Hazeleger, C. Wen, X. Wan, L. Ji, R. J. Haarsma, W. P. Breugem, and H. Seidel, 2008: Oceanic link between abrupt changes in the North Atlantic Ocean and the African monsoon. Nature Geoscience, **1**, 444.

Chelton, D. B., M. G. Schlax, J. M. Lyman, and G. C. Johnson, 2003: Equatorially trapped Rossby waves in the presence of meridionally sheared baroclinic flow in the Pacific Ocean. *Progress in Oceanography*, **56,** 323-380.

Chepurin, G. and J. A. Carton, 1996: Hydrographic data of the Soviet SECTIONS tropical Atlantic Program and the circulation of the upper 1200 meters. *J. Mar. Res*, **55,** 633–670.

Chiang, J. C. H. and C. M. Bitz, 2005: Influence of high latitude ice cover on the marine intertropical convergence zone. *Climate Dynamics*, **25,** 477-496.

Chiang, J. C. H., M. Biasutti, and D. S. Battisti, 2003: Sensitivity of the Atlantic intertropical convergence zone to last glacial maximum boundary conditions. *Paleoceanography*, **18,** 1094.

Chiang, J. C. H., W. Cheng, and C. M. Bitz, 2008: Fast teleconnections to the tropical Atlantic sector from Atlantic thermohaline adjustment. *Geophysical Research Letters*, **35,**7704.

Cox, M. D., 1980: Generation and propagation of 30-day waves in a numerical model of the Pacific. *Journal of Physical Oceanography*, **10,** 1168-1186.

Dahl, K. A., A. J. Broccoli, and R. J. Stouffer, 2005: Assessing the role of North Atlantic freshwater forcing in millennial scale climate variability: A tropical Atlantic perspective. *Climate Dynamics*, **24,** 325-346.

Davey, M. K., M. Huddleston, K. R. Sperber, P. Braconnot, and F. Bryan, 2002: STOIC: A study of coupled model climatology and variability in tropical ocean regions. *Climate Dyn*, **18,** 403–420.

Duing, W., P. Hisard, E. Katz, J. Meincke, L. Miller, K. V. Moroshkin, G. Philander, A. A. Ribnikov, K. Voigt, and R. Weisberg, 1975: Meanders and long waves in the equatorial Atlantic. *Nature*, **257,** 280-284.

Fedorov, A. V., P. S. Dekens, M. McCarthy, A. C. Ravelo, P. B. deMenocal, M. Barreiro, R. C. Pacanowski, and S. G. Philander, 2006: The Pliocene Paradox (mechanisms for a permanent El Nino). *Science*, **312,** 1485-1489.

Fontaine, B., S. Janicot, and P. Roucou, 1999: Coupled ocean-atmosphere surface variability and its climate impacts in the tropical Atlantic region. *Climate Dynamics*, **15,** 451-473.

Fratantoni, D. M., W. E. Johns, T. L. Townsend, and H. E. Hurlburt, 2000: Low-latitude circulation and mass transport pathways in a model of the tropical Atlantic Ocean. *Journal of Physical Oceanography*, **30,** 1944-1966.

Ganachaud, A. and C. Wunsch, 2003: Large-scale ocean heat and freshwater transports during the world ocean circulation experiment. *Journal of Climate*, **16,** 696-705.

Haarsma, R. J. and W. Hazeleger, 2007: Extratropical atmospheric response to equatorial Atlantic cold tongue anomalies. *Journal of Climate*, **20,** 2076-2091.

Hansen, D. V. and C. A. Paul, 1984: Genesis and effects of long waves in the equatorial Pacific. *Journal of Geophysical Research-Oceans*, **89,**3379-3393.

Hashizume, H., K. Takeuchi, S. P. Xie, and W. T. Liu, 2001: Local and remote atmospheric response to tropical instability waves- A global view from space. *Journal of Geophysical Research*, **106,** 10173-10185.

Hastenrath, S., 1984: Interannual variability and annual cycle: Mechanisms of circulation and climate in the tropical Atlantic sector. *Monthly Weather Review*, **112,** 1097-1107.

Haug, G. H., K. A. Hughen, D. M. Sigman, L. C. Peterson, and U. Rohl, 2001: Southward migration of the intertropical convergence zone through the Holocene. Science, **293**, 1304-1308.

Hazeleger, W. and R. J. Haarsma, 2005: Sensitivity of tropical Atlantic climate to mixing in a coupled ocean–atmosphere model. *Climate Dynamics*, **25,** 387-399.

Huffman, G. J., R. F. Adler, P. Arkin, A. Chang, R. Ferraro, A. Gruber, J. Janowiak, A. McNab, B. Rudolf, and U. Schneider, 1997: The global precipitation climatology project (GPCP) combined precipitation dataset. *Bulletin of the American Meteorological Society*, **78,** 5-20.

Hughen, K. A., T. I. Eglinton, L. Xu, and M. Makou, 2004: Abrupt tropical vegetation response to rapid climate changes. *Science*,**304,**1955-1959.

Hüls, M. and R. Zahn, 2000: Millennial-scale sea surface temperature variability in the western tropical North Atlantic from planktonic foraminiferal census counts. *Paleoceanography*, **15**.

Hurrell, J. W., J. J. Hack, B. A. Boville, D. L. Williamson, and J. T. Kiehl, 1998: The dynamical simulation of the NCAR Community Climate Model version 3 (CCM3). *Journal of Climate*, **11**.

Jochum, M. and P. Malanotte-Rizzoli, 2001: Influence of the meridional overturning circulation on tropical–subtropical pathways. *Journal of Physical Oceanography*, **31,** 1313-1323.

Jochum, M. and R. Murtugudde, 2006: Temperature advection by tropical instability waves. *Journal of Physical Oceanography*, **36,** 592-605.

Johnson, H. L. and D. P. Marshall, 2002: A theory for the surface Atlantic response to thermohaline variability. *Journal of Physical Oceanography*, **32,** 1121-1132.

Josey, S. A., E. C. Kent, and P. K. Taylor, 1998: The Southampton oceanography centre (SOC) ocean-atmosphere heat, momentum and freshwater flux atlas. Southampton Oceanography Centre Rep. , 6, 55 pp.

——, 1999: New insights into the ocean heat budget closure problem from analysis of the SOC air–sea flux climatology. *Journal of Climate*, **12,** 2856-2880.

Kalnay, E., M. Kanamitsu, R. Kistler, W. Collins, D. Deaven, L. Gandin, M. Iredell, S. Saha, G. White, and J. Woollen, 1996: The NCEP/NCAR 40-Year Reanalysis Project. *Bull. American Meteo. Soc*, **77,** 437-471.

Katz, E. J., 1997: Waves along the equator in the Atlantic. *Journal of Physical Oceanography*, **27,** 2536-2544.

Kawase, M., 1987: Establishment of deep ocean circulation driven by deep-water production. *Journal of Physical Oceanography*, **17,** 2294-2317.

Krauss, E. B. and J. S. Turner, 1967: A one-dimensional model of the seasonal thermocline. II: The general theory and its consequences. *Tellus*, **19,** 98–105.

Lea, D. W., D. K. Pak, L. C. Peterson, and K. A. Hughen, 2003: Synchroneity of tropical and high-latitude Atlantic temperatures over the last glacial termination. *Science*, **301,**1361-1364.

Lee, S. K. and G. T. Csanady, 1999: Warm water formation and escape in the upper tropical Atlantic Ocean. 2. A numerical model study. *Journal of Geophysical Research*, **104,** 29573-29590.

Legeckis, R., W. Pichel, and G. Nesterczuk, 1983: Equatorial long waves in geostationary satellite observations and in a multichannel sea surface temperature analysis. *Bull. American Meteo Soc*, **64,** 133-139.

Levitus, S., 1994: World Ocean Atlas 1994. U. S. Department of Commerce, 552-560.

Li, T. and S. G. H. Philander, 1996: On the annual cycle of the eastern equatorial Pacific. *Journal of Climate*, **9,** 2986-2998.

Marchesiello, P., J. C. McWilliams, and A. Shchepetkin, 2001: Open boundary conditions for long-term integration of regional oceanic models. *Ocean Modelling*, **3,** 20.

McCreary, J. P. and Z. Yu, 1992: Equatorial dynamics in a 2.5-layer model. *Progress in Oceanography*, **29,** 61–132.

McCreary, J. P., P. K. Kundu, and R. L. Molinari, 1993: A numerical investigation of dynamics, thermodynamics and mixed-layer processes in the Indian Ocean. *Progress in Oceanography*, **31,** 181-244.

McManus, J. F., R. Francois, J. M. Gherardi, L. D. Keigwin, and S. Brown-Leger, 2004: Collapse and rapid resumption of Atlantic meridional circulation linked to deglacial climate changes. *Nature*, **428,** 834-837.

Mitchell, T. P. and J. M. Wallace, 1992: The annual cycle in equatorial convection and sea surface temperature. *Journal of Climate*, **5,** 1140-1156.

Molinari, R. L. and E. Johns, 1994: Upper layer temperature structure of the western tropical Atlantic. *Journal of Geophysical Research*, **99,**18225-18233.

Moura, A. D. and J. Shukla, 1981: On the dynamics of droughts in northeast Brazil: Observations, theory and numerical experiments with a general circulation model. *Journal of the Atmospheric Sciences*, **38,** 2653-2675.

Mulitza, S. and C. Rühlemann, 2000: African monsoonal precipitation modulated by interhemispheric temperature gradients. *Quaternary Research*, **53,** 270-274.

Nobre, P. and J. Srukla, 1996: Variations of sea surface temperature, wind stress, and rainfall over the tropical Atlantic and South America. *Journal of Climate*, **9,** 2464-2479.

Philander, S. G., 1990: *El Nino, La Nina, and the southern oscillation*. Academic Press, 100-156.

Philander, S. G. H., 1978: Forced ocean waves. *Rev. Geophys. Space Phys*, **16,**15-46.

Qiao, L. and R. H. Weisberg, 1995: Tropical instability wave kinematics: Observations from the Tropical Instability Wave Experiment (Paper 95JC00305). *Journal of Geophysical Research-Part C-Oceans-Printed Edition*, **100,** 8677-8694.

Richardson, P. L. and T. K. McKee, 1984: Average Seasonal Variation of the Atlantic Equatorial Currents from Historical Ship Drifts. *Journal of Physical Oceanography*, **14,** 1226-1238.

Richardson, P. L. and D. Walsh, 1986: Mapping climatological seasonal variations of surface currents in the tropical Atlantic using ship drifts. *Journal of Geophysical Research*, **91,**10537-10550.

Ruiz-Barradas, A., J. A. Carton, and S. Nigam, 2000: Structure of interannual-to-decadal climate variability in the tropical Atlantic sector. *Journal of Climate*, **13,** 3285-3297.

Saravanan, R. and P. Chang, 2000: Interaction between tropical Atlantic variability and El Niño–Southern oscillation. *Journal of Climate*, **13,** 2177-2194.

Schmidt, M. W., H. J. Spero, and D. W. Lea, 2004: Links between salinity variation in the Caribbean and North Atlantic thermohaline circulation. *Nature*, **428,** 160-163.

Schmitz, W. J. and P. L. Richardson, 1991: On the sources of the Florida current. *Deep-sea Research. Part A. Oceanographic Research Papers*, **38,** 379-409.

Schopf, P. S. and M. A. Cane, 1983: On equatorial dynamics, mixed layer physics and sea surface temperature. *Journal of Physical Oceanography*, **13,**917-935.

——, 1983: On equatorial dynamics, mixed layer physics and sea surface temperature. *Journal of Physical Oceanography*, **13,** 917-935.

Seager, R., Y. Kushnir, P. Chang, N. Naik, J. Miller, and W. Hazeleger, 2001: Looking for the role of the ocean in tropical Atlantic decadal climate variability. *Journal of Climate*, **14,** 638-655.

Shinoda, T., G. N. Kiladis, and P. E. Roundy, 2008: Statistical representation of equatorial waves and tropical instability waves in the Pacific Ocean. *Atmos Res.* (in press).

Shuman, F. G., 1957: Numerical methods in weather prediction: II. smoothing and filtering. *Monthly Weather Review*, **85,** 357-361.

Smagorinsky, J., 1963: General circulation experiments with the premitive equations. *Monthly Weather Review*, **91,** 99-164.

——, 1993: Some historical remarks on the use of nonlinear viscosities. *Large Eddy Simulation of Complex Engineering and Geophysical Flows*, **1,** 69-106.

Smith, T. M., R. W. Reynolds, R. E. Livezey, and D. C. Stokes, 1996: Reconstruction of historical sea surface temperatures using empirical orthogonal functions. *Journal of Climate*, **9,** 1403-1420.

Stouffer, R. J., J. Yin, J. M. Gregory, K. W. Dixon, M. J. Spelman, W. Hurlin, A. J. Weaver, M. Eby, G. M. Flato, and H. Hasumi, 2006: Investigating the causes of the response of the thermohaline circulation to past and future climate changes. *Journal of Climate*, **19,** 1365-1387.

Timmermann, A., H. Goosse, and Coauthors, 2007: The influence of a weakening of the Atlantic meridional overturning circulation on ENSO. *J. Climate*, **20,** 4899–4919.

Trenberth, K. E. and J. M. Caron, 2001: Estimates of meridional atmosphere and ocean heat transports. *Journal of Climate*, **14,** 3433-3443.

Uppala, S. M., P. W. Kållberg, A. J. Simmons, U. Andrae, V. Da Costa Bechtold, M. Fiorino, J. K. Gibson, J. Haseler, A. Hernandez, and G. A. Kelly, 2005: The ERA-40 re-analysis. *Quarterly Journal of the Royal Meteorological Society*, **131,** 2961-3012.

Vellinga, M. and R. A. Wood, 2002: Global climatic impacts of a collapse of the Atlantic thermohaline circulation. *Climatic Change*, **54,** 251-267.

Vizy, E. K. and K. H. Cook, 2002: Development and application of a mesoscale climate model for the tropics: Influence of sea surface temperature anomalies on the West African monsoon. *J. Geophys. Res*, **107,**4023-4025.

Wajsowicz, R. C., 1993: A consistent formulation of the anisotropic stress tensor for use in models of the large-scale ocean circulation. *Journal of Computational Physics*, **105,** 333-333.

Wallcraft, A. J., A. B. Kara, H. E. Hurlburt, and P. A. Rochford, 2003: The NRL Layered Global Ocean Model (NLOM) with an embedded mixed layer submodel: Formulation and tuning. *Journal of Atmospheric and Oceanic Technology*, **20,** 1601-1615.

Wan, X., P. Chang, R. Saravanan, R. Zhang, and M. W. Schmidt, 2009: On the interpretation of Caribbean paleo-temperature reconstructions during the Younger Dryas. *Geophysical Research Letters*, **36,** 2701-2705.

Wang, X., A. S. Auler, R. L. Edwards, H. Cheng, P. S. Cristalli, P. L. Smart, D. A. Richards, and C. C. Shen, 2004: Wet periods in northeastern Brazil over the past 210 kyr linked to distant climate anomalies. *Nature*, **432,** 740-743.

Weisberg, R. H., 1984: Instability waves observed on the equator in the Atlantic Ocean during 1983. *Geophys. Res. Lett*, **11,** 753-756.

Wen, C., P. Chang, and R. Saravanan, 2009: Effect of atlantic meridional overturning circulation changes on tropical Atlantic sea-surface temperature variability: A 2-1/2 layer reduced gravity ocean model study. *Journal of Climate*, **(Submitted)**.

Wheeler, M. and G. N. Kiladis, 1999: Convectively coupled equatorial waves: Analysis of clouds and temperature in the wavenumber–frequency domain. *Journal of the Atmospheric Sciences*, **56,** 374-399.

Wu, L., C. Li, C. Yang, and S. P. Xie, 2008: Global teleconnections in response to a shutdown of the Atlantic meridional overturning circulation. *Journal of Climate*, **21,** 3002-3019.

Wu, Q. and K. P. Bowman, 2007: Interannual variations of tropical instability waves observed by the tropical rainfall measuring mission. *Geophysical Research Letters*, **34,** 9701.

Xie, S.-P., 1999: A dynamic ocean-atmosphere Model of the tropical Atlantic decadal variability. *Journal of Climate*, **12,** 64-70.

Xie, S. P. and S. G. H. Philander, 1994: A coupled ocean-atmosphere model of relevance to the ITCZ in the eastern Pacific. *Tellus A*, **46,** 340-350.

Yang, J., 1999: A linkage between decadal climate variations in the Labrador Sea and the tropical Atlantic Ocean. *Geophysical Research Letters*, **26**.

Yu, J. Y. and C. R. Mechoso, 1999: Links between annual variations of Peruvian stratocumulus clouds and of SST in the eastern equatorial Pacific. *Journal of Climate*, **12,** 3305-3318.

Yu, Z., J. P. McCreary Jr, and J. A. Proehl, 1995: Meridional asymmetry and energetics of tropical instability waves. *Journal of Physical Oceanography*, **25,** 2997-3007.

Zhang, D., M. J. McPhaden, and W. E. Johns, 2003: Observational evidence for flow between the subtropical and tropical Atlantic: The Atlantic subtropical cells. *Journal of Physical Oceanography*, **33,** 1783-1797.

Zhang, R., 2008: Coherent surface-subsurface fingerprint of the Atlantic meridional overturning circulation. *Geophysical Research Letters*, **35,** 20705-20708.

Zhang, R. and T. L. Delworth, 2005: Simulated tropical response to a substantial seakening of the Atlantic thermohaline circulation. *Journal of Climate*, **18,** 1853-1860.

Zhao, M., N. A. S. Beveridge, N. J. Shackleton, M. Sarnthein, and G. Eglinton, 1995: Molecular stratigraphy of cores off northwest Africa: Sea surface temperature history over the last 80 ka. *Paleoceanography*, **10,**661-675.

VITA

Name: Caihong Wen

Address: Department of Oceanography
MS 3146, Texas A&M University
College Station, TX, 77840-3146

Email Address: Caihong@neo.tamu.edu

Education: B.S.,Atmospheric Sciences, Nanjing University, Nanjing, China, August, 2001
M.S.,Atmospheric Sciences, Nanjing University, Nanjing, China, August, 2003
Ph.D., Oceanography,Texas A&M University, TX, U.S.A, August, 2009